International School for Advanced Studies
(SISSA/ISAS)

Nicola Lanatà

PhD Thesis:

The Gutzwiller variational approach to correlated systems

study of three significant cases

Supervisor: Prof.Michele Fabrizio

October 2009

Contents

Chapter 1

Introduction and Overview of the main results

Since the discovery twenty years ago of high temperature superconductivity in cuprates doped Mott insulators, *strong correlations* in electronic systems have progressively become synonymous of striking physical phenomena. Following the impressive experimental progress in synthetizing novel correlated materials and even designing artificial correlated models, e.g. cold atoms trapped in optical lattices, as well as in improving old or creating new investigating tools, there has been a great theoretical effort in developing reliable and efficient schemes for treating strong electronic correlations, like for instance dynamical mean field theory (DMFT) [1] or improved density functional calculations in the local density approximation, e.g. LDA+U [2] or LDA+U+DMFT [3]. At the meantime, old theoretical tools developed long time before the discovery of high T_c superconductors have been improved and adapted to better describe realistic correlated materials, among those particularly the Gutzwiller variational approach, which is actually the subject of this thesis. In fact, it is not exaggerated claiming that most important concepts in strongly correlated systems originated from Gutzwiller variational calculations or, equivalently, slave-boson mean-field results, as for instance the famous Brinkmann-Rice scenario [4] of the Mott transition or the slave-boson mean-field phase diagram of the $t-J$ model for cuprates [5], which remains so far the most promising, although still controversial, explanation of high-temperature superconductivity.

In a series of three papers [6, 7, 8] Martin Gutzwiller introduced in the 60th's a variational wavefunction for studying ferromagnetism in transition metals, which has the general expression

$$|\Psi_G\rangle = \prod_{\mathbf{R}}^{\text{sites}} \mathcal{P}_{\mathbf{R}} \, |\Psi_0\rangle, \tag{1.1}$$

where $|\Psi_0\rangle$ is an uncorrelated wavefunction that satisfies Wick's theorem, and the operator $\mathcal{P}_{\mathbf{R}}$ has the role of modifying the relative weights of the electronic configurations at site $\mathbf{R}$ with respect to their uncorrelated values in order to improve local correlations. Both $|\Psi_0\rangle$ and $\mathcal{P}_{\mathbf{R}}$ are to be variationally determined by minimizing the average energy. In spite of its simplicity, the average values of any operator on $|\Psi_G\rangle$ can not be computed but numerically in realistic lattice models. For this reason, Gutzwiller also introduced an approximate scheme to compute those average values analytically. Both the wavefunction and the approximation were named after him. Since then, the Gutzwiller wavefunction and approximation became very popular tools to attach theoretically strongly correlated systems. We previously mentioned the famous Gutzwiller scenario of a paramagnetic Mott transition that was found by Brinkmann and Rice in the attempt of describing the prototypical Mott insulator V_2O_3, but the list of interesting results that were obtained by this variational technique is impressively long, hence impossible to cite in an exhaustive way. Because it is closely related to this thesis and help the following discussion, we just mention the Gutzwiller approaches to the physics of heavy fermion materials [9, 10], which were quite popular just before high T_c era, and, among them, the seminal works by Rice and Ueda [11] and Brandow and Fazekas [12, 13, 14], which, at the same time, showed qualities and defects of the method. In the context of heavy fermions, the Gutzwiller approach was actually in competition with another approximate analytical tool that was developing in early 80s, the so-called *slave-boson* technique [15, 16, 17, 18]. In reality, both the Gutzwiller approximation and the slave-boson mean field theories applied to models for heavy fermions gave almost coincident results and in accord with most experiments. This coincidence motivated the attempt by Kotliar and Ruckenstein [19] for building a bridge between the two approaches. Essentially these authors found a novel version of a slave-boson path integral action

for a single band Hubbard that, at the saddle point, reproduces exactly the Gutzwiller results of Brinkmann and Rice. In principle, slave-boson mean field theory can be improved going beyond the mean field approximation [20, 21, 22], which is an advantage with respect to the Gutzwiller approximation but is in fact quite an hard task. Conversely, the Gutzwiller approach can be improved with respect to the Gutzwiller approximation by direct numerical evaluation of average values on the Gutzwiller wavefunction, see Refs. [23] and [24], and references therein, which has the advantage to be a consistent variational approach. In spite of these differences, the Gutzwiller approximation and the slave-boson mean field theory has become somehow synonymous, in the sense that they lead to equivalent results.

After the discovery of cuprate superconductors and the consequent explosion of research activity in strongly correlated materials, there has been a revival of interest in the Gutzwiller variational approach as well as in the slave-boson technique. In fact, many popular theoretical concepts born in the context of high T_c materials, like the spin liquids, i.e. lattice models of spins whose ground state does not break any symmetry [25], or the so-called RVB superconductivity [26] that may arise when doping a liquid of valence bonds (spin-singlet pairs), a particular case of a spin-liquid, have been originally formulated through a Gutzwiller approximation or a slave-boson approach to models for cuprate materials. [26, 27, 28, 5] Just to face the need for broader applicability and greater reliability, both the Gutzwiller variational approach and the slave-boson technique have been considerably improved during years and along several directions. Sophisticated algorithms have been developed to increase accuracy and variational freedom in the Gutzwiller wavefunctions, see e.g. [29], and applied to several models [30, 31, 32, 33]. On the other side, multi-orbital effects have been included in the simpler Gutzwiller approximation [34, 35] as well as in the slave-boson mean field theory [36], in the attempt of describing realistic correlated materials beyond simple single-band ones and of including inter-site correlations absent in the original wavefunction (1.1).

In addition, the development of DMFT has brought novel insights in the physical meaning of the Gutzwiller approximation. Metzner and Vollhardt showed [37, 38] that the Gutzwiller approximation is actually exact in the limit of infinite coordination lattices, where the single-particle self-energy becomes

purely local in space [39]. In this limit, where also DMFT becomes exact, the Gutzwiller approach seems to provide a variational prescription to determine an approximate low-frequency behavior of the self-energy, unlike DMFT that can access the whole frequency range. Hence the Gutzwiller approximation can be regarded also as a tool to extract Fermi-liquid parameters, or, more generally, renormalized band-structure parameters, within the assumption that spatial correlations are not important [40], justifying what was done by Vollhardt for ^{3}He [41] and opening a promising route towards combining the Gutzwiller approach with *ab-initio* calculations [42].

All novel perspectives that one can foresee in the future of the Gutzwiller variational method require however a number of preliminary steps to be undertaken in order to make this technique really flexible and able to cope with more complicated cases than the simple single band Hubbard model. This is what motivated the work presented in this thesis. Specifically, by facing three problems of current interest, the Fermi surface evolution in heavy fermion systems, the emergence of superconductivity upon doping a simple spin-liquid and finally the quantum transport across a correlated microscopic object, we ended up in a series of novel developments in the method that allowed us to access physical properties previously unaccessible unless by more involved numerical simulations. Therefore this thesis has a dual nature: first there are few interesting physics questions that we have addressed and solved; secondly, their solution has brought us to improve, in our opinion significantly, the method.

After this brief digression, we briefly list the three problems that we attached and our main results.

1.1 Fermi-surface evolution across the magnetic phase transition in the Kondo lattice model

The physics of heavy fermion materials has a long history that enriched along the years with more and more interesting aspects [9, 10]. The name *heavy fermions* is commonly refereed to compounds where the electrons occupying narrowly localized partially filled f-shells get promoted to the Fermi level forming very narrow, hence the adjective *heavy*, paramagnetic bands, lead-

ing e.g. to a specific heat coefficient γ orders of magnitude bigger than in conventional metals. This behavior is conventionally interpreted by invoking the Kondo effect [43], i.e. the many-body phenomenon by which the localized moments of magnetic impurities get screened when diluted in metals. From this viewpoint, the heavy-fermion behavior corresponds to the on-set of coherence of the different Kondo clouds that form around each magnetic ion, apart from subtleties as for instance the Nozières exhaustion principle [44]. A more traditional approach, which is nevertheless deeply related to the essence of the Kondo effect, is that, if the strong correlations active on the f-orbitals could be hypothetically switched off without encountering any phase transition, then the heavy-fermion state should be adiabatically connected with a non-interacting state, e.g. the state obtained by a non-magnetic electronic structure LDA calculation. Since the latter is characterized by a Fermi surface that encloses a volume counting the f electrons besides the more itinerant *s-p-d* ones, also the fully interacting Fermi surface of the heavy-fermion state must have the same property, a consequence of the so-called Luttinger's theorem [45]. It then follows that the f electrons must contribute to the metallic behavior, i.e. to the linear in temperature specific heat, to the Pauli paramagnetic susceptibility, etc..

In reality, not all f-electron systems display a paramagnetic heavy-fermion behavior. There are in fact materials where the local moments of the f-shells order magnetically, thus inducing magnetic ordering also in the itinerant bands, leading to SDW metals usually with a complicated magnetic structure. Because of the spin-symmetry breaking, there is no more guarantee by Luttinger's theorem that the f electrons do partecipate to the metallic behavior. Indeed, there are evidences that the Fermi volume in the SDW metal does not include f electrons, which is supported also by the more conventional metallic properties with respect to heavy-fermion paramagnets [9, 10]. Quite interestingly, there are compounds where, by means of external agents, like physical or chemical pressure, it is possible to cross the transition from a SDW metal to heavy-fermion paramagnetic metal. This transition has attracted a lot of interest since, besides obvious topological changes of the Fermi surface [46, 47, 48, 49, 50], it is usually accompanied by an anomalous behavior of various transport and thermodynamic quantities. [10, 51] The Fermi surface change and the magnetism

can be explained in a conservative scheme as simply the consequence of the additional Bragg scattering due to the static magnetism, assumed to arise predominantly by an instability of the itinerant phase [52, 53]. Correspondingly, the observed anomalous behavior is thought to arise by critical magnetic quantum fluctuations. [54] This explanation is contrasted by a different one that ascribes the changes of the Fermi surface to an f-electron Mott localization [55], which is assumed to occur concomitantly with magnetism [56, 57, 58, 59]. In this case the anomalous behavior is believed to arise from the singular local magnetic fluctuations accompanying the f-localization, hence the death of the Kondo effect. On the contrary, in the former scenario, what matters are the singular magnetic scattering localized around the q-vector of the contiguous magnetic order.

In order to shed some light in this debated issue, we have decided to study the prototypical Kondo lattice model, i.e. a lattice of localized spin-1/2 antiferromagnetically coupled to conducting electrons, by an extension of the standard Gutzwiller variational approach. While in the past a Gutzwiller wavefunction as in (1.1) was studied in which $\mathcal{P}_{\mathbf{R}}$ was assumed to act only within the f-shell, here we consider a more general $\mathcal{P}_{\mathbf{R}}$ that acts on all local configurations including f and conduction electrons. The novelty is the possibility to variationally control the strength of the singlet-coupling between localized spins and conduction electrons, which otherwise is dictated only by the uncorrelated wavefunction $|\Psi_0\rangle$. The additional variational freedom leads however to several technical difficulties to extend the Gutzwiller approximation, that we have successfully overcome.

The variational phase diagram as function of the Kondo exchange has been found to depend non-trivially on the conduction electron density. Very close to the compensated regime (one conduction electron per impurity-spin), upon decreasing the Kondo exchange there is first a second-order paramagnetic-to-antiferromagnetic phase transition, followed by a first-order transition between two magnetic phases with completely different Fermi surfaces. Moving away from the compensated regime, the second order phase transition disappears and we find a single first order line separating a paramagnetic phase from an antiferromagnetic one with different Fermi surfaces. Our results suggest that the magnetic transition and the topological change of the Fermi surface are

not necessarily coincident, which has been also observed in a very recent experiment [60, 61]. In order to understand if the abrupt change in the Fermi surface is due to a Mott localization rather than to magnetism, we have studied the model in the paramagnetic sector by preventing any magnetic ordering. Although our optimal uncorrelated wavefunction $|\Psi_0\rangle$ is forced to have always a finite, although small, weight of f-electrons at the Fermi energy – this is the only allowed way to gain Kondo exchange energy within the simplest Gutzwiller scheme – yet this weight undergoes a sharp discontinuity, corresponding to an abrupt transfer away from the chemical potential, at what seems to be variationally a weakly first order phase transition. Indeed, visualizing the shape of the Fermi surface at finite temperature, this transition seems to be accompanied by a topological change of the Fermi surface. Finally, we have analyzed the role of a uniform magnetic field in the paramagnetic phase and found a metamagnetic instability near the above phase transition, suggestive of the metamagnetism observed experimentally. [62]

In conclusion, our results show that the f-localization is indeed close to the on-set of magnetism but is not necessarily coincident, hence that the two points of view previously mentioned do not necessarily exclude each other. However, it remains opened the question whether the anomalous behavior observed is caused by magnetism or rather by the Mott localization. Our finding about the metamagnetic behavior of the paramagnetic phase seem to favour the Mott localization mechanism, but this is only a speculation.

1.2 Superconductivity in a liquefied valence-bond crystal

Just after the discovery of high temperature superconductivity in doped cuprates, Anderson [26] came out with an original proposal that remains till now one of the most convincing one, apart from minor changes intervened along with the experimental developments, e.g. d-wave symmetry instead of the originally proposed extended-s. Without pretending to be exhaustive, Anderson's idea can be summarized as follows. All cuprate superconductors can be regarded as doped Mott insulators. The undoped insulating phase, when accessible, is

antiferromagnetic. Once holes are injected by doping, long range antiferromagnetism dies out, but it is conceivable, given the strength of the magnetic exchange, that short range magnetic correlations survive. Instead of attempting to describe such a phenomenon starting from the ordered antiferromagnet, it is tempting to undertake a different point of view and start from a spin liquid phase, actually a liquid of spin-singlet pairs, so-called resonating valence bond (RVB), which is already lacking long range order, and dope it. Indeed, at short range an antiferromagnet and a RVB are hardly distinguishable. Furthermore, a RVB state can be adiabatically turned into a long range antiferromagnet [63]. If one accepts to start from an RVB phase and dope it, i.e. remove spins that leave behind holes, then the spin-singlet pairs will start moving around and it is not difficult to believe that they could become superfluid at low temperature, hence, being charged, actually superconduct. This very crude picture of the RVB superconductivity, has been elaborated in much detail during the years, especially by numerical studying variational wavefunctions for the t-J model of the type (1.1) with $|\Psi_0\rangle$ a a d-wave BCS wavefunction [30, 32, 33] and $\mathbf{P_R}$ projecting out doubly occupied sites, leading to very promising results.

In reality, one may generalize Anderson's point of view and ask whether melting a non-magnetic Mott insulator formed by spin-singlet pairs is generally accompanied by the emergence of superconductivity. In the RVB scenario, the spin-paired sites can be at any distance and in any direction, but one can imagine a simpler case of a crystalline short-range RVB, or valence-bond solid, with pairs with fixed length and orientation, which is no more a liquid but remains non-magnetic. Such an insulating crystal can be melt either by reducing the repulsion, the pairs can overlap and eventually liquefy, or, similarly to the RVB case above, by doping. In order to investigate this extreme case of a valence-bond solid, in Ref. [35] a Gutzwiller approximation was used to study a model of two Hubbard planes at half-filling coupled by an inter-plane hopping. The latter was assumed to be strong enough to make the Mott insulator at large on-site repulsion U non-magnetic, a collection of inter-plane singlet bonds, but weak enough that the uncorrelated phase at $U = 0$ is metallic. Upon increasing U from the metal to the valence-bond Mott insulator, it was shown that the Gutzwiller wavefunction stabilizes a superconducting dome that intrudes between the two phases. To further extend this analysis, here we have

decided to look at the same problem but upon doping the valence-bond insulator. As we hoped, we find that liquefying the valence-bond crystal by doping also leads to a superconducting dome that counter-intuitively exists only close to the half-filled Mott insulator; a striking similarity to cuprates and in accord with existing speculations [64]. This result suggests that indeed Anderson's speculation is generalizable to a larger class of non-magnetic insulators [65], even though it remains open the question of its relevance to cuprates.

Technically, in order to describe accurately the valence-bond insulator, we had to to use an operator $\mathcal{P}_{\mathbf{R}}$ in (1.1) that acts on all electronic configurations of the two sites, one on top of the other, connected by the inter-plane hopping. The allowance of superconductivity and the absence of particle-hole symmetry away from half-filling made the variational problem quite complicated, hence, in order to simplify it, we had to enforce symmetries. Their inclusion within the Gutzwiller scheme is the technical novelty of the work.

1.3 Transport in quantum dots

The physics of the Kondo effect has become recently quite popular also in a context far away from magnetic alloys, namely that of quantum transport across nanocontacts. Indeed, because of the low dimensionality of the contact region, electronic correlations grow in strength and may stabilize a local magnetism that influences electron tunneling. The Kondo-like zero-bias anomalies first observed in quantum dots [66] are just the simplest manifestation of it. From the theory side, this phenomenon is particularly hard to study, first of all because strong correlations play a major role, secondly because it is inherently an out-of-equilibrium phenomenon. While the zero-bias conductance can be accessed by an equilibrium calculation, and there exist plenty of techniques that are capable to access Kondo physics in detail, the inelastic tunneling spectrum at finite bias is practically unaccessible with reliable techniques unless in extreme cases. Furthermore, the technique that are effective at equilibrium can deal only with simple models, like the single impurity Anderson or Kondo models, and become soon untractable with realistic cases, e.g. tunneling across a transition metal atom, where many orbitals partecipate to magnetism and affect conductance. In this general context, it would be desirable to have at

disposal a technique as simple and flexible as the Gutzwiller variational one but capable to access out-of-equilibrium phenomena. Therefore we decided to study the possibility of extending this method away from equilibrium. The idea that we followed started from a result by Hershfield [67], according to whom the out-of-equilibrium steady state can be regarded as the equilibrium one with an Hamiltonian that includes an effective bias operator. Should this operator be known, one could indeed use the Gutzwiller approach to study steady state properties. Since it is unknown, we had to make several assumptions in the spirit of a local Landau Fermi liquid description [68] to get to some expression for this operator that we think should be valid if the bias is not too large. We then calculated the inelastic tunneling spectrum for the tunneling across a single-orbital Anderson impurity, which is qualitatively in accord with the observed behavior in quantum dots. We proceeded further and applied the method to the less trivial example of a double dot. Although the method is still at the level of a proposal and need to be better justified and further improved, we think this is a promising route to pursue.

1.4 Outline

The thesis is organized as follows:

In **chapter 2** we discuss the Gutzwiller method in detail. After a brief general introduction we will focus on all the new features that we have developed, and that considerably simplify all the pratical calculations for a wide class of problems. In section 2.1 we will underline all the advantages of using the so called mixed-basis rapresentation and present some technical detail about the Gutzwiller-constraint's parametrization; section 2.3 is devoted to the problem of generating variational wavefunctions with a given symmetry; and in the last section we will discuss a well accepted method that allows to extract quasiparticle properties of the system with the Gutzwiller method.

In **chapter 3** we derive, by means of an extended Gutzwiller wavefunction and within the Gutzwiller approximation, the phase diagram of the Kondo lattice model. We find that generically, namely in the absence of nesting, the

model displays an f-electron Mott localization accompanied by a discontinuous change of the conduction electron Fermi surface as well as by magnetism. When the non interacting Fermi surface is close to nesting, the Mott localization disentangles from the onset of magnetism. First the paramagnetic heavy fermion metal turns continuously into an itinerant magnet - the Fermi surface evolves smoothly across the transition - and afterwards Mott localization intervenes with a discontinuous rearrangement of the Fermi surface. We find that the f-electron localization remains even if magnetism is prevented, and is still accompanied by a sharp transfer of spectral weight at the Fermi energy within the Brillouin zone. We further show that the Mott localization can be also induced by an external magnetic field, in which case it occurs concomitantly with a metamagnetic transition.

In **chapter 4** we study by multi-orbital extension of the Gutzwiller wavefunction with enforced spin-rotational symmetry the role of doping in the bilayer Hubbard model, within a regime in which the half-filled Mott insulator at large interaction is non-magnetic; a local version of a valence bond crystal. Using a variational wavefunction which includes Cooper pairing correlations, we find a region of singlet superconductivity that arises close to the half-filled Mott insulator.

In **chapter 5** we develop an approximate method based on the Gutzwiller technique to study non-equilibrium steady state transport across a correlated impurity (mimicking e.g. a quantum dot) coupled to biased leads. The method is based on the Hershfield result that steady state properties can be regarded as equilibrium ones with a proper Boltzmann weight. We test this method to the simple single-orbital Anderson impurity model, finding the correct behaviour of the conductivity as a function of the bias. We finally apply the proposed procedure to a more complicated two-dots model and we discuss our results.

Chapter 2

The Gutzwiller variational method

Since its original formulation in the early 60th's, the Gutzwiller variational approach[6, 7, 8] remains one of the simplest yet effective tools to deal with correlated electron systems. The brilliant idea invented by Martin Gutzwiller was to properly modify the weight of local electronic configurations according with the on-site interaction starting from some uncorrelated reference values. In his original formulation, this is accomplished by means of the variational wavefunction:

$$|\Psi_G\rangle = \mathcal{P}|\Psi_0\rangle = \prod_{\mathbf{R}} \mathcal{P}_{\mathbf{R}} \, |\Psi_0\rangle, \tag{2.1}$$

where $|\Psi_0\rangle$ is an uncorrelated variational wavefunction, conveniently chosen such that Wick's theorem holds, and $\mathcal{P}_{\mathbf{R}}$ a projection operator acting on the local configurations at site $\mathbf{R}$. Both $|\Psi_0\rangle$ and $\mathcal{P}_{\mathbf{R}}$ have to be determined by minimizing the average energy. In what follows we shall assume a generic multiband Hamiltonian, in which case the most general expression for the local operator $\mathcal{P}_{\mathbf{R}}$ is:

$$\mathcal{P}_{\mathbf{R}} = \sum_{\Gamma_1,\Gamma_2} \lambda(\mathbf{R})_{\Gamma_1\Gamma_2} \, |\Gamma_1, \mathbf{R}\rangle\langle\Gamma_2, \mathbf{R}|, \tag{2.2}$$

where each state $|\Gamma_i, \mathbf{R}\rangle$ denotes any electronic configuration belonging to the local Hilbert space of a given multi-band model, whereas the matrix $\lambda(\mathbf{R})$ contains all the variational parameters needed to define the operator $\mathcal{P}_{\mathbf{R}}$. In general, average values of operators on the wavefunction (2.1) must be com-

puted numerically, unless the lattice has infinite coordination number, in which case they can be evaluated analytically [34, 69, 35]. For that purpose, let us assume that the following constraints are satisfied by $\mathcal{P}_{\mathbf{R}}$[34, 69, 35]:

$$\langle\Psi_0|\,\mathcal{P}_{\mathbf{R}}^{\dagger}\,\mathcal{P}_{\mathbf{R}}\,|\Psi_0\rangle = 1, \tag{2.3}$$

$$\langle\Psi_0|\,\mathcal{P}_{\mathbf{R}}^{\dagger}\,\mathcal{P}_{\mathbf{R}}\,\mathcal{C}_{\mathbf{R}}\,|\Psi_0\rangle = \langle\Psi_0|\,\mathcal{C}_{\mathbf{R}}\,|\Psi_0\rangle, \tag{2.4}$$

where $\mathcal{C}_{\mathbf{R}}$ is the local single-particle density-matrix operator with elements $c_{\mathbf{R},\alpha}^{\dagger}c_{\mathbf{R},\beta}$, $c_{\mathbf{R},\alpha}^{\dagger}c_{\mathbf{R},\beta}^{\dagger}$ and $c_{\mathbf{R},\alpha}c_{\mathbf{R},\beta}$; $c_{\mathbf{R},\alpha}^{\dagger}(c_{\mathbf{R},\alpha})$ creating (annihilating) an electron in state α, where α label both spin and orbitals, at site $\mathbf{R}$. In order to enlight the meaning of these constraints, let us consider e.g. a particular case of (2.4), i.e.

$$\langle\Psi_0|\,\mathcal{P}_{\mathbf{R}}^{\dagger}\,\mathcal{P}_{\mathbf{R}}\,c_{\mathbf{R},\alpha}^{\dagger}c_{\mathbf{R},\beta}\,|\Psi_0\rangle = \langle\Psi_0|\,c_{\mathbf{R},\alpha}^{\dagger}c_{\mathbf{R},\beta}\,|\Psi_0\rangle. \tag{2.5}$$

Since Wick's theorem can be used to evaluate average values on $|\Psi_0\rangle$, (2.5) becomes through (2.3)

$$\begin{aligned}\langle\Psi_0|\,\mathcal{P}_{\mathbf{R}}^{\dagger}\,\mathcal{P}_{\mathbf{R}}\,c_{\mathbf{R},\alpha}^{\dagger}c_{\mathbf{R},\beta}\,|\Psi_0\rangle &= \langle\Psi_0|\,\mathcal{P}_{\mathbf{R}}^{\dagger}\,\mathcal{P}_{\mathbf{R}}\,|\Psi_0\rangle\,\langle\Psi_0|\,c_{\mathbf{R},\alpha}^{\dagger}c_{\mathbf{R},\beta}\,|\Psi_0\rangle \\ &\quad +\langle\Psi_0|\,\mathcal{P}_{\mathbf{R}}^{\dagger}\,\mathcal{P}_{\mathbf{R}}\,c_{\mathbf{R},\alpha}^{\dagger}c_{\mathbf{R},\beta}\,|\Psi_0\rangle_{connected} \\ &= \langle\Psi_0|\,c_{\mathbf{R},\alpha}^{\dagger}c_{\mathbf{R},\beta}\,|\Psi_0\rangle \\ &\quad +\langle\Psi_0|\,\mathcal{P}_{\mathbf{R}}^{\dagger}\,\mathcal{P}_{\mathbf{R}}\,c_{\mathbf{R},\alpha}^{\dagger}c_{\mathbf{R},\beta}\,|\Psi_0\rangle_{connected},\end{aligned}$$

where the subscript *connected* means all possible contractions between $c_{\mathbf{R},\alpha}^{\dagger}c_{\mathbf{R},\beta}$ and a pair of single fermion operators from $\mathcal{P}_{\mathbf{R}}^{\dagger}\,\mathcal{P}_{\mathbf{R}}$. Because of the constraint, the right hand side of (2.4), it follows that the sum of all connected terms must vanish. In turns, this implies that selecting any pair of single particle operators from $\mathcal{P}_{\mathbf{R}}^{\dagger}\,\mathcal{P}_{\mathbf{R}}$ and averaging over $|\Psi_0\rangle$ what is left, the net result is zero. Next, suppose we have to calculate the average of a local operator $\mathcal{O}_{\mathbf{R}}$ at site $\mathbf{R}$. It

follows that

$$\begin{aligned}
\langle\Psi_0|\,\mathcal{P}^\dagger\,\mathcal{O}_{\mathbf{R}}\,\mathcal{P}\,|\Psi_0\rangle &= \langle\Psi_0|\prod_{\mathbf{R}'\neq\mathbf{R}}\left(\mathcal{P}^\dagger_{\mathbf{R}'}\,\mathcal{P}_{\mathbf{R}'}\right)\,\mathcal{P}^\dagger_{\mathbf{R}}\,\mathcal{O}_{\mathbf{R}}\,\mathcal{P}_{\mathbf{R}}\,|\Psi_0\rangle \\
&= \prod_{\mathbf{R}'\neq\mathbf{R}}\langle\Psi_0|\,\mathcal{P}^\dagger_{\mathbf{R}'}\,\mathcal{P}_{\mathbf{R}'}\,|\Psi_0\rangle\,\langle\Psi_0|\,\mathcal{P}^\dagger_{\mathbf{R}}\,\mathcal{O}_{\mathbf{R}}\,\mathcal{P}_{\mathbf{R}}\,|\Psi_0\rangle \\
&\quad +\langle\Psi_0|\prod_{\mathbf{R}'\neq\mathbf{R}}\left(\mathcal{P}^\dagger_{\mathbf{R}'}\,\mathcal{P}_{\mathbf{R}'}\right)\,\mathcal{P}^\dagger_{\mathbf{R}}\,\mathcal{O}_{\mathbf{R}}\,\mathcal{P}_{\mathbf{R}}\,|\Psi_0\rangle_{connected} \\
&= \langle\Psi_0|\,\mathcal{P}^\dagger_{\mathbf{R}}\,\mathcal{O}_{\mathbf{R}}\,\mathcal{P}_{\mathbf{R}}\,|\Psi_0\rangle \\
&\quad +\langle\Psi_0|\prod_{\mathbf{R}'\neq\mathbf{R}}\left(\mathcal{P}^\dagger_{\mathbf{R}'}\,\mathcal{P}_{\mathbf{R}'}\right)\,\mathcal{P}^\dagger_{\mathbf{R}}\,\mathcal{O}_{\mathbf{R}}\,\mathcal{P}_{\mathbf{R}}\,|\Psi_0\rangle_{connected},
\end{aligned}$$

where this time *connected* means all terms where operators at different sites are averaged together. Because of (2.4), an operator $\mathcal{P}^\dagger_{\mathbf{R}'}\,\mathcal{P}_{\mathbf{R}'}$ can be connected to other sites only by more than two single-particle operators, the terms with two vanishing exactly as explained above. While these contributions are non-zero in any finite-coordination lattice, they vanish in the limit of infinite coordination, in which case what remains is simply

$$\boxed{\langle\Psi_0|\,\mathcal{P}^\dagger\,\mathcal{O}_{\mathbf{R}}\,\mathcal{P}\,|\Psi_0\rangle = \langle\Psi_0|\,\mathcal{P}^\dagger_{\mathbf{R}}\,\mathcal{O}_{\mathbf{R}}\,\mathcal{P}_{\mathbf{R}}\,|\Psi_0\rangle}, \tag{2.6}$$

which can be readily calculated by means of Wick's theorem. Seemingly, the average of the inter-site density matrix in an infinite-coordination lattice reduces to calculate

$$\begin{aligned}
&\langle\Psi_0|\,\mathcal{P}^\dagger\,c^\dagger_{\mathbf{R},\alpha}c_{\mathbf{R}',\beta}\,\mathcal{P}\;\;|\Psi_0\rangle = \langle\Psi_0|\,\mathcal{P}^\dagger_{\mathbf{R}}\,c^\dagger_{\mathbf{R},\alpha}\,\mathcal{P}_{\mathbf{R}}\,\mathcal{P}^\dagger_{\mathbf{R}'}\,c_{\mathbf{R}',\beta}\,\mathcal{P}_{\mathbf{R}'}\,|\Psi_0\rangle \qquad (2.7)\\
&=\sum_{\gamma\delta}\langle\Psi_0|\,\left(R(\mathbf{R})_{\alpha\gamma}\,c^\dagger_{\mathbf{R},\gamma}+Q(\mathbf{R})_{\alpha\gamma}\,c_{\mathbf{R},\gamma}\right)\,\left(R(\mathbf{R}')^*_{\beta\delta}\,c_{\mathbf{R}',\delta}+Q(\mathbf{R}')^*_{\beta\delta}\,c^\dagger_{\mathbf{R}',\delta}\right)\,|\Psi_0\rangle.
\end{aligned}$$

In other words, the inter-site single-particle density matrix averaged on $|\Psi\rangle$ becomes in an infinite coordination lattice equivalent to averaging over $|\Psi_0\rangle$ a renormalized density matrix with effective fermionic operators, replacing the physical ones according to

$$\boxed{c^\dagger_{\mathbf{R},\alpha}\rightarrow\sum_\beta R(\mathbf{R})_{\alpha\beta}\,c^\dagger_{\mathbf{R},\beta}+Q(\mathbf{R})_{\alpha\beta}\,c_{\mathbf{R},\beta}}, \tag{2.8}$$

where the renormalization matrices R and Q can be determined by inverting the following set of equations [35]:

$$\begin{aligned}\langle\Psi_0|\,\mathcal{P}^\dagger_{\mathbf{R}}c^\dagger_{\mathbf{R},\alpha}\mathcal{P}_{\mathbf{R}}c_{\mathbf{R},\beta}\,|\Psi_0\rangle &= \sum_\gamma R(\mathbf{R})_{\alpha\gamma}\langle\Psi_0|\,c^\dagger_{\mathbf{R},\gamma}c_{\mathbf{R},\beta}\,|\Psi_0\rangle \\ &\quad+\sum_\gamma Q(\mathbf{R})_{\alpha\gamma}\langle\Psi_0|\,c_{\mathbf{R},\gamma}c_{\mathbf{R},\beta}\,|\Psi_0\rangle, \qquad (2.9)\\ \langle\Psi_0|\,\mathcal{P}^\dagger_{\mathbf{R}}c^\dagger_{\mathbf{R},\alpha}\mathcal{P}_{\mathbf{R}}c^\dagger_{\mathbf{R},\beta}\,|\Psi_0\rangle &= \sum_\gamma R(\mathbf{R})_{\alpha\gamma}\langle\Psi_0|\,c^\dagger_{\mathbf{R},\gamma}c^\dagger_{\mathbf{R},\beta}\,|\Psi_0\rangle \\ &\quad+\sum_\gamma Q(\mathbf{R})_{\alpha\gamma}\langle\Psi_0|\,c_{\mathbf{R},\gamma}c^\dagger_{\mathbf{R},\beta}\,|\Psi_0\rangle. \qquad (2.10)\end{aligned}$$

As explained, the above expressions are strictly valid only in the limit of infinite-coordination lattices, although it is quite common to use them as approximated formulas even for finite-dimensional systems. This is usually referred to as the Gutzwiller approximation, and it is known to be equivalent to the saddle-point solution of the slave-boson technique[70, 36], see also section 2.2. However, despite the considerable simplification introduced by the infinite-coordination limit, the variational problem remains still a difficult task to deal with, due to the exponential growth of the local Hilbert space and consequently of the variational matrix when considering multi-orbital models.

A further simplification can be achieved with a proper choice of the basis set spanning the local Hilbert space. This can be done, for instance, by using from the start the natural basis, i.e. the single-particle basis that diagonalizes the variational density matrix $\langle\,\mathcal{C}_{\mathbf{R}}\,\rangle_0$ [35].

2.1 The mixed-basis representation

An alternative more flexible approach that we propose [71] consists in defining the local operator $\mathcal{P}_{\mathbf{R}}$ in a mixed-basis representation, namely expressing $|\Gamma_1,\mathbf{R}\rangle = |\{\Gamma_\alpha\},\mathbf{R}\rangle$ in Eq. (2.2) in the original basis defined by the model Hamiltonian and assuming that $\langle\Gamma_2,\mathbf{R}| = \langle\{n_\alpha\},\mathbf{R}|$ are Fock states in the natural basis. With this choice one has to take into account variational density matrices with only diagonal non-zero elements; a great simplification since the unitary transformation that relates the natural-basis operators $d_{\mathbf{R},\alpha}$ to the original ones $c_{\mathbf{R},\alpha}$ needs not to be known explicitly. We assume that the average

value of the local single-particle density-matrix operator $\mathcal{C}_{\mathbf{R}}$ on the uncorrelated wavefunction Ψ_0 is diagonal in terms of the operators $d^\dagger_{\mathbf{R}\alpha}$ and $d_{\mathbf{R}\alpha}$, related by a unitary transformation to the original ones, $c^\dagger_{\mathbf{R}\alpha}$ and $c_{\mathbf{R}\alpha}$. In other words, for any α and β,

$$\begin{aligned} \langle\Psi_0|\, d^\dagger_{\mathbf{R}\alpha} d_{\mathbf{R}\beta}\,|\Psi_0\rangle &= \delta_{\alpha\beta}\, n^0_{\mathbf{R}\alpha} \\ \langle\Psi_0|\, d^\dagger_{\mathbf{R}\alpha} d^\dagger_{\mathbf{R}\beta}\,|\Psi_0\rangle &= 0 \end{aligned} \tag{2.11}$$

where $0 \leq n^0_{\mathbf{R}\alpha} \leq 1$ are the eigenvalues of $\mathcal{C}_{\mathbf{R}}$. We specify $\mathcal{P}_{\mathbf{R}}$ to be of the form as in Eq. (2.2), namely

$$\mathcal{P}_{\mathbf{R}} = \sum_{\{\Gamma_\alpha\}\{n_\alpha\}} \lambda_{\{\Gamma_\alpha\}\{n_\alpha\}}(\mathbf{R})\, |\{\Gamma_\alpha\}, \mathbf{R}\rangle\langle\{n_\alpha\}, \mathbf{R}|, \tag{2.12}$$

where, by assumption, $|\{\Gamma_\alpha\}, \mathbf{R}\rangle$ are Fock states in the original $c_{\mathbf{R}\alpha}$ basis , while $|\{n_\alpha\}, \mathbf{R}\rangle$ are Fock states in the natural basis, namely in terms of $d_{\mathbf{R}\alpha}$ operators. In other words, and dropping for simplicity the site-label $\mathbf{R}$, a generic state $|n\rangle$ is identified by the occupation numbers $n_\alpha = 0, 1$ and $\alpha = 1, .., M$, M being the total number of single particle states, and has the explicit expression

$$|n\rangle = \left(d^\dagger_1\right)^{n_1} ... \left(d^\dagger_M\right)^{n_M} |0\rangle\,.$$

We introduce the uncorrelated occupation-probability matrix P^0 with elements

$$P^0_{\{n_\alpha\}\{m_\alpha\}} \equiv \langle\Psi_0|\, |\{m_\alpha\}\rangle\langle\{n_\alpha\}|\, |\Psi_0\rangle = \delta_{\{n_\alpha\}\{m_\alpha\}}\, P^0_{\{n_\alpha\}}, \tag{2.13}$$

where

$$P^0_{\{n_\alpha\}} = \prod_{\alpha=1}^{M} \left(n^0_\alpha\right)^{n_\alpha} \left(1 - n^0_\alpha\right)^{1-n_\alpha}. \tag{2.14}$$

We remind that n^0_α are the elements of the diagonal density matrix (to be variationally determined) and $n_\alpha = 0, 1$ denotes the occupation number of the natural state α.

We also introduce the matrix representation of the operators d_α and $d^\dagger_\alpha$, namely

$$\begin{aligned} d_\alpha &\to \left(d_\alpha\right)_{\{n_\beta\}\{m_\beta\}} = \langle\{n_\beta\}|d_\alpha|\{m_\beta\}\rangle, \\ d^\dagger_\alpha &\to \left(d^\dagger_\alpha\right)_{\{n_\beta\}\{m_\beta\}} = \langle\{n_\beta\}|d^\dagger_\alpha|\{m_\beta\}\rangle = \left(\langle\{m_\beta\}|d_\alpha|\{n_\beta\}\rangle\right)^*, \end{aligned}$$

and assume that the variational parameters $\lambda_{\{\Gamma_\beta\}\{n_\beta\}}$ in Eq. (2.12) are the elements of a matrix λ. With the above definitions, the two conditions Eqs. (2.3) and (2.4) that we impose, and which allow for an analytical treatment in infinite-coordination lattices, become [35]

$$\begin{aligned}
\langle\Psi_0|\,\mathcal{P}^\dagger\mathcal{P}\;\,|\Psi_0\rangle &= \mathrm{Tr}\left(P^0\,\lambda^\dagger\,\lambda\;\right)=1, && (2.15)\\
\langle\Psi_0|\,\mathcal{P}^\dagger\mathcal{P}\;\,d^\dagger_\alpha d_\beta\,|\Psi_0\rangle &= \mathrm{Tr}\left(P^0\,\lambda^\dagger\,\lambda\;\,d^\dagger_\alpha d_\beta\right)\\
&= \langle\Psi_0|\,d^\dagger_\alpha d_\beta\,|\Psi_0\rangle=\delta_{\alpha\beta}\,n^0_\alpha && (2.16)\\
\langle\Psi_0|\,\mathcal{P}^\dagger\mathcal{P}\;\,d^\dagger_\alpha d^\dagger_\beta\,|\Psi_0\rangle &= \mathrm{Tr}\left(P^0\,\lambda^\dagger\,\lambda\;\,d^\dagger_\alpha d^\dagger_\beta\right)\\
&= \langle\Psi_0|\,d^\dagger_\alpha d^\dagger_\beta\,|\Psi_0\rangle=0. && (2.17)
\end{aligned}$$

If Eqs. (2.15), (2.16) and (2.17) are satisfied, then the average value of any local operator $\mathcal{O}$ in infinite-coordination lattices is [34, 35]

$$\begin{aligned}
\langle\Psi|\,\mathcal{O}\,|\Psi\rangle &= \langle\Psi_0|\,\mathcal{P}^\dagger\,\mathcal{O}\,\mathcal{P}\,|\Psi_0\rangle\\
&= \mathrm{Tr}\left(P^0\,\lambda^\dagger\,O\,\lambda\right)\,, && (2.18)
\end{aligned}$$

where O is a matrix with elements

$$O_{\{\Gamma_\beta\}\{\Gamma'_\beta\}}=\langle\{\Gamma_\beta\}|\mathcal{O}|\{\Gamma'_\beta\}\rangle.$$

In the mixed original-natural basis representation, the proper definition of the R and Q coefficients in Eqs. (2.9) and (2.10) changes into

$$\begin{aligned}
\langle\,\mathcal{P}^\dagger c^\dagger_\alpha\mathcal{P}d_\beta\,\rangle_0 &= \sum_\gamma R_{\alpha\gamma}\,\langle\,d^\dagger_\gamma d_\beta\,\rangle_0+\sum_\gamma Q_{\alpha\gamma}\,\langle\,d_\gamma d_\beta\,\rangle_0, && (2.19)\\
\langle\,\mathcal{P}^\dagger c^\dagger_\alpha\mathcal{P}d^\dagger_\beta\,\rangle_0 &= \sum_\gamma R_{\alpha\gamma}\,\langle\,d^\dagger_\gamma d^\dagger_\beta\,\rangle_0+\sum_\gamma Q_{\alpha\gamma}\,\langle\,d_\gamma d^\dagger_\beta\,\rangle_0. && (2.20)
\end{aligned}$$

In other words, $c^\dagger_{\mathbf{R},\gamma}$, introducing back the site label, effectively trasforms into

$$\boxed{c^\dagger_{\mathbf{R},\alpha}\rightarrow\sum_\beta R(\mathbf{R})_{\alpha\beta}\,d^\dagger_{\mathbf{R},\beta}+Q(\mathbf{R})_{\alpha\beta}\,d_{\mathbf{R},\beta}}\,. \qquad (2.21)$$

2.2 Explicit formulas and connection with slave-boson mean field theory

To further simplify the calculation, we introduce a new matrix in the mixed basis representation

$$\phi = \lambda \sqrt{P^0}, \tag{2.22}$$

with elements

$$\phi_{\{\Gamma_\alpha\}\{n_\alpha\}} = \lambda_{\{\Gamma_\alpha\}\{n_\alpha\}} \sqrt{P^0_{\{n_\alpha\}}}. \tag{2.23}$$

As we shall see, $\phi_{\{\Gamma_\alpha\}\{n_\alpha\}}$ corresponds to the slave-boson saddle-point value within the multiband extension of the Kotliar-Ruckenstein mean-field scheme recently introduced by Lechermann and coworkers [36], which they named rotationally invariant slave-boson formalism. By means of the definition (2.22) the first condition (2.15) becomes

$$\mathrm{Tr}\left(\phi^\dagger \, \phi\right) = 1,$$

which coincides with the saddle-point value of Eq. (28) in Ref. [36].

Condition Eq. (2.16) becomes

$$\begin{aligned}
&\mathrm{Tr}\left(\sqrt{P^0}\,\phi^\dagger\,\phi\,\sqrt{\frac{1}{P^0}}\;d^\dagger_\alpha d_\beta\right) = \langle\Psi_0|\, d^\dagger_\alpha d_\beta \,|\Psi_0\rangle \\
&= \sqrt{\frac{P^0_{\{n_\alpha\}}}{P^0_{\{m_\alpha\}}}}\;\phi^\dagger_{\{n_\alpha\}\{\Gamma_\alpha\}}\phi_{\{\Gamma_\alpha\}\{m_\alpha\}}\,\langle\{m_\alpha\}|d^\dagger_\alpha d_\beta|\{n_\alpha\}\rangle \\
&= \delta_{\alpha\beta}\, n^0_\alpha,
\end{aligned} \tag{2.24}$$

where we adopted the convention to sum over repeated matrix indices.

We note that the two Fock states $|\{n_\alpha\}\rangle$ and $|\{m_\alpha\}\rangle$ in Eq. (2.24) differ only because $|\{n_\alpha\}\rangle$ has the orbital β occupied but orbital α empty, while it is viceversa for $|\{m_\alpha\}\rangle$, so that

$$\sqrt{\frac{P^0_{\{n_\alpha\}}}{P^0_{\{m_\alpha\}}}} = \sqrt{\frac{n^0_\beta\left(1-n^0_\alpha\right)}{\left(1-n^0_\beta\right)n^0_\alpha}},$$

hence Eq. (2.24) is actually equal to

$$\sqrt{\frac{n^0_\beta\left(1-n^0_\alpha\right)}{\left(1-n^0_\beta\right)n^0_\alpha}}\;\phi^\dagger_{\{n_\alpha\}\{\Gamma_\alpha\}}\phi_{\{\Gamma_\alpha\}\{m_\alpha\}}\,\langle\{m_\alpha\}|d^\dagger_\alpha d_\beta|\{n_\alpha\}\rangle = \delta_{\alpha\beta}\, n^0_\alpha.$$

Because of $\delta_{\alpha\beta}$ on the r.h.s, this equation is equivalent to

$$\begin{aligned} \mathrm{Tr}\left(\phi^\dagger\,\phi\,d_\alpha^\dagger d_\beta\right) &= \delta_{\alpha\beta}\,n_\alpha^0 \\ &= \langle\Psi_0|\,d_\alpha^\dagger d_\beta\,|\Psi_0\rangle. \end{aligned} \tag{2.25}$$

that is the saddle-point value of Eq. (29) in Ref. [36] provided $n_\beta^0 \neq 0$ and $n_\alpha^0 \neq 1$. Similarly, it can be easily proved that condition Eq. (2.17) becomes

$$\mathrm{Tr}\left(\phi^\dagger\,\phi\,d_\alpha^\dagger d_\beta^\dagger\right) = 0 = \langle\Psi_0|\,d_\alpha^\dagger d_\beta^\dagger\,|\Psi_0\rangle. \tag{2.26}$$

Therefore, if the average value of the single-particle density matrix on the uncorrelated wavefunction $|\Psi_0\rangle$ has eigenvalues nor 0 nor 1, the conditions Eqs. (2.15), (2.16) and (2.17) are equivalent to impose

$$\mathrm{Tr}\left(\phi^\dagger\,\phi\right) = 1, \tag{2.27}$$

$$\mathrm{Tr}\left(\phi^\dagger\,\phi\,d_\alpha^\dagger d_\beta\right) = \langle\Psi_0|\,d_\alpha^\dagger d_\beta\,|\Psi_0\rangle = \delta_{\alpha\beta}\,n_\alpha^0, \tag{2.28}$$

$$\mathrm{Tr}\left(\phi^\dagger\,\phi\,d_\alpha^\dagger d_\beta^\dagger\right) = \langle\Psi_0|\,d_\alpha^\dagger d_\beta^\dagger\,|\Psi_0\rangle = 0, \tag{2.29}$$

In terms of ϕ, the average of the local operator $\mathcal{O}$, Eq. (2.18), becomes

$$\langle\Psi|\,\mathcal{O}\,|\Psi\rangle = \mathrm{Tr}\left(\phi^\dagger\,O\,\phi\right), \tag{2.30}$$

Finally we need to evaluate $R_{\alpha\beta}$ and $Q_{\alpha\beta}$ of Eqs. (2.19) and (2.20). We find that

$$\begin{aligned} R_{\alpha\beta} &= \frac{1}{n_\beta^0}\,\mathrm{Tr}\left(\sqrt{P^0}\,\phi^\dagger\,c_\alpha^\dagger\,\phi\,\sqrt{\frac{1}{P^0}}\;d_\beta\right) \\ &= \frac{1}{n_\beta^0}\sqrt{\frac{P^0_{\{n_\alpha\}}}{P^0_{\{m_\alpha\}}}}\;\phi^\dagger_{n\{\Gamma_\alpha\}}\,\langle\{\Gamma_\alpha\}|c_\alpha^\dagger|\{\Gamma'_\alpha\}\rangle\,\phi_{\{\Gamma'_\alpha\}\{m_\alpha\}}\,\langle\{m_\alpha\}|d_\beta|\{n_\alpha\}\rangle \\ &= \frac{1}{\sqrt{n_\beta^0\left(1-n_\beta^0\right)}}\;\phi^\dagger_{\{n_\alpha\}\{\Gamma_\alpha\}}\,\langle\{\Gamma_\alpha\}|c_\alpha^\dagger|\{\Gamma'_\alpha\}\rangle\,\phi_{\{\Gamma'_\alpha\}\{m_\alpha\}}\,\langle\{m_\alpha\}|d_\beta|\{n_\alpha\}\rangle \\ &= \frac{1}{\sqrt{n_\beta^0(1-n_\beta^0)}}\mathrm{Tr}(\phi^\dagger\,c_\alpha^\dagger\,\phi\,d_\beta)\,, \end{aligned} \tag{2.31}$$

and

$$\begin{aligned} Q_{\alpha\beta} &= \frac{1}{1-n^0_\beta}\,\mathrm{Tr}\left(\sqrt{P^0}\,\phi^\dagger\, c^\dagger_\alpha\,\phi\,\sqrt{\frac{1}{P^0}}\,d^\dagger_\beta\right) \qquad (2.32)\\ &= \frac{1}{1-n^0_\beta}\sqrt{\frac{P^0_{\{n_\alpha\}}}{P^0_{\{m_\alpha\}}}}\,\phi^\dagger_{\{n_\alpha\}\{\Gamma_\alpha\}}\,\langle\{\Gamma_\alpha\}|c^\dagger_\alpha|\{\Gamma'_\alpha\}\rangle\,\phi^\dagger_{\{\Gamma_\alpha\}\{m_\alpha\}}\,\langle\{m_\alpha\}|d^\dagger_\beta|\{n_\alpha\}\rangle\\ &= \frac{1}{\sqrt{n^0_\beta\left(1-n^0_\beta\right)}}\,\phi^\dagger_{\{n_\alpha\}\{\Gamma_\alpha\}}\,\langle\{\Gamma_\alpha\}|c^\dagger_\alpha|\{\Gamma'_\alpha\}\rangle\,\phi^\dagger_{\{\Gamma_\alpha\}\{m_\alpha\}}\,\langle\{m_\alpha\}|d^\dagger_\beta|\{n_\alpha\}\rangle\\ &= \frac{1}{\sqrt{n^0_\beta(1-n^0_\beta)}}\mathrm{Tr}(\phi^\dagger\, c^\dagger_\alpha\,\phi\, d^\dagger_\beta)\,. \end{aligned}$$

We note that actually

$$\langle\{\Gamma_\beta\}|c^\dagger_\alpha|\{\Gamma'_\beta\}\rangle = \langle\{m_\beta\}|d^\dagger_\alpha|\{n_\beta\}\rangle \quad \forall\alpha \qquad (2.33)$$

because both the left and the right side of Eq. (2.33) are the matrix elements of a α creation operator in it's own Fock basis, hence they can be calculated and stored once for all. This is the reason why the unitary transformation that relates the natural-basis operators $d_{\mathbf{R},\alpha}$ to the original ones $c_{\mathbf{R},\alpha}$ needs not to be known explicitly.

2.2.1 Parametrization strategy

In order to parametrize the variational matrix ϕ one can introduce a local Hamiltonian h that acts on all possible local electronic configurations, and define

$$\phi^\dagger\phi = \frac{\mathrm{e}^{-\beta h}}{\Omega}, \qquad (2.34)$$

where

$$\Omega = \mathrm{Tr}\left(\mathrm{e}^{-\beta h}\right),$$

is the local partition function and $1/\beta$ a fictitious temperature. With this definition, the conditions Eqs. (2.28) and (2.28) become

$$\frac{1}{\Omega}\,\mathrm{Tr}\left(\mathrm{e}^{-\beta h}\,d^\dagger_\alpha d_\beta\right) = \langle\Psi_0|d^\dagger_\alpha d_\beta|\Psi_0\rangle = \delta_{\alpha\beta}\,n^0_\alpha, \qquad (2.35)$$

$$\frac{1}{\Omega}\,\mathrm{Tr}\left(\mathrm{e}^{-\beta h}\,d^\dagger_\alpha d^\dagger_\beta\right) = \langle\Psi_0|d^\dagger_\alpha d^\dagger_\beta|\Psi_0\rangle = 0. \qquad (2.36)$$

Therefore, the zero-temperature average value of the single-particle density matrix on $|\Psi_0\rangle$ must coincide with the its thermal average with the local Hamiltonian h. Our parametrization strategy is to impose that h is such that

$$\frac{1}{\Omega}\,\mathrm{Tr}\left(\mathrm{e}^{-\beta h}\, d^\dagger_\alpha d_\beta\right) = 0 \quad \forall \alpha \neq \beta, \tag{2.37}$$

$$\frac{1}{\Omega}\,\mathrm{Tr}\left(\mathrm{e}^{-\beta h}\, d^\dagger_\alpha d^\dagger_\beta\right) = 0 \quad \forall \alpha, \beta\,, \tag{2.38}$$

so that

$$\frac{1}{\Omega}\,\mathrm{Tr}\left(\mathrm{e}^{-\beta h}\, d^\dagger_\alpha d_\alpha\right) = n^0_\alpha[h] \tag{2.39}$$

depends parametrically on h. After, we impose the following conditions

$$\langle\Psi_0|d^\dagger_\alpha d_\beta|\Psi_0\rangle = \delta_{\alpha\beta}\, n^0_\alpha[h], \tag{2.40}$$

$$\langle\Psi_0|d^\dagger_\alpha d^\dagger_\beta|\Psi_0\rangle = 0, \tag{2.41}$$

on the uncorrelated wavefunction $|\Psi_0\rangle$. In terms of h

$$\phi = U\ \ \frac{\mathrm{e}^{-\beta h/2}}{\sqrt{\Omega}}, \tag{2.42}$$

with U a unitary matrix. The expressions of the renormalization factors are then obtained through

$$\begin{aligned}&\frac{1}{\Omega}\,\mathrm{Tr}\left(\mathrm{e}^{-\frac{\beta}{2}h}\, U^\dagger\, c^\dagger_\alpha\, U\ \ \mathrm{e}^{-\frac{\beta}{2}h}\, d_\beta\right)\\ &= R_{\alpha\beta}\,\sqrt{n^0_\beta\left(1-n^0_\beta\right)},\end{aligned} \tag{2.43}$$

$$\begin{aligned}&\frac{1}{\Omega}\,\mathrm{Tr}\left(\mathrm{e}^{-\frac{\beta}{2}h}\, U^\dagger\, c^\dagger_\alpha\, U\ \ \mathrm{e}^{-\frac{\beta}{2}h}\, d^\dagger_\beta\right)\\ &= Q_{\alpha\beta}\,\sqrt{n^0_\beta\left(1-n^0_\beta\right)},\end{aligned} \tag{2.44}$$

We found that it is more convenient to use as variational parameters those of the local Hamiltonian $h_{\mathbf{R}}$ and of the unitary matrix $U_{\mathbf{R}}$, introducing back the site label. In the case of a paramagnetic wavefunction that does not break translationally symmetry, $h_{\mathbf{R}}$ and $U_{\mathbf{R}}$ are independent of $\mathbf{R}$. On the contrary, for instance in an antiferromagnetic wavefunction on a bipartite lattice, going from one sublattice to the other the role of spin $\uparrow$ ($\downarrow$) is interchanged with that of spin $\downarrow$ ($\uparrow$).

2.3 Implementation of symmetries

The variational matrix ϕ can be parametrized in such a way that constraints (2.27)-(2.29) are satisfied from the onset. It may happen however that the variational space thus generated is unnecessarily large. For instance, if one looks for a variational wavefunction which preserves particle number, all the elements of the matrix λ connecting subspaces of the local Hilbert space with different particle number should be zero. It would be desirable then to specialize the general procedure sketched above in such a way that given symmetries can be built in the variational wavefunction from the onset. In general terms, given a symmetry group G under which the variational wavefunction is assumed to be invariant, this would amount to define a $\mathcal{P}_{\mathbf{R}}$ which satisfies

$$[\mathcal{P}_{\mathbf{R}}, G] = 0\,. \tag{2.45}$$

However, in the mixed representation there may be some symmetry operations that can not be defined without an explicit knowledge of the natural basis in terms of the original one, which would make the whole method much less convenient. If one decides not to implement these symmetries, but only those, symmetry group G, whose generators are invariant under the most general unitary transformation U connecting original and natural basis, i.e.

$$[U, G] = 0\,, \tag{2.46}$$

compatibly with the variational ansatz, the above described variational method can be still used with the following modification.

Let us assume this case and define a unitary operator V that transforms the Fock states in the original basis $|\{\Gamma_\alpha\}, \mathbf{R}\rangle$ into states that decompose the local Hilbert space in irreducible representations of the group G,$|\{\bar{\Gamma}_\alpha\}, \mathbf{R}\rangle$, i.e.

$$V|\{\Gamma_\alpha\}, \mathbf{R}\rangle = |\{\bar{\Gamma}_\alpha\}, \mathbf{R}\rangle \quad \forall\Gamma. \tag{2.47}$$

We define $\bar{G}$ the representation of G in this basis. Because of our choice of G, V does the same job even in the natural basis, although this is unknown. Since the trace is invariant under unitary transformations, all formulas (2.2), (2.27)-(2.29) and (2.32)-(2.33) remain the same even if the variational matrix

ϕ and the matrix representation of the single fermion operators are defined in the states of the irreducible representations

$$\bar{\phi} = V^\dagger \phi V \tag{2.48}$$

$$\begin{aligned} \bar{c}_\alpha &= V^\dagger c_\alpha V, \\ \bar{d}_\alpha &= V^\dagger d_\alpha V \end{aligned} \tag{2.49}$$

with the additional symmetry constraint

$$[\bar{\phi}, \bar{G}] = 0, \tag{2.50}$$

which follows from (2.45). We note that the single fermion operator matrix representation in these states is readily obtained once V is known, and is trivially the same for both original and natural operators. Therefore it is sufficient to create and store it at the beginning of any calculation.

As an example let us look for a variational wavefunction which doesn't break spin-$SU(2)$ symmetry.

2.3.1 Example: implementation of $SU(2)$ symmetry

According to the general scheme just sketched, we can apply the following standard procedure:

- the local Hilbert space $H_{\mathbf{R}}$ is decomposed in S^2 eigenspaces:

$$H_{\mathbf{R}} = \bigoplus_l H_l; \tag{2.51}$$

- each subpace H_l is decomposed in the S_3-component eigenspaces

$$H_l = \bigoplus_{m=-l}^{l} H_l^m; \quad \dim(H_l^m) = g_l \ \ \forall m; \tag{2.52}$$

- the required basis $|\bar{\Gamma}, \mathbf{R}\rangle$ (and the unitary matrix V) is then obtained by applying $2l+1$ times the creation operator S_+ onto any orthogonal basis of each subspace H_l^{-l}.

The parametrization of the matrix $\bar{\phi}$ is then carried on in each subspace of the local Hilbert space. To satisfy Eq. (2.50) we look for matrices $\bar{\phi}$ that have the following form in each subspace H_l:

$$\bar{\phi} = \begin{pmatrix} p_{11}\mathbb{1}_l & \cdots & p_{1g_l}\mathbb{1}_l \\ \vdots & \ddots & \vdots \\ p_{g_l1}\mathbb{1}_l & \cdots & p_{g_lg_l}\mathbb{1}_l \end{pmatrix} \tag{2.53}$$

which, according to Schur's lemma, is the most general ϕ' with the required symmetry ($\mathbb{1}_l$ being identity matrices of size $2l+1$ and p_{ij} variational parameters).

2.4 Variational energy and Gutzwiller quasi-particles

Let us consider a general tight-binding Hamiltonian

$$\begin{aligned} \mathcal{H} &= -\sum_{\mathbf{R}\mathbf{R}'}\sum_{\alpha\beta} t^{\alpha\beta}_{\mathbf{R}\mathbf{R}'}\, c^\dagger_{\mathbf{R},\alpha} c_{\mathbf{R},\beta} \\ &+ \sum_{\mathbf{R}}\sum_{\{\Gamma_\alpha\}\{\Gamma'_\alpha\}} U(\mathbf{R})\,|\{\Gamma_\alpha\},\mathbf{R}\rangle\langle\{\Gamma'_\alpha\},\mathbf{R}| \end{aligned} \tag{2.54}$$

where the Hermitean matrix $U(\mathbf{R})$ is the representation of the local interaction in the original representation. The average value of this Hamiltonian on the Gutzwiller wavefunction is, in the Gutzwiller approximation,

$$\begin{aligned} \mathcal{E}_{var} &= -\sum_{\mathbf{R}\mathbf{R}'}\sum_{\alpha\beta\gamma\delta} t^{\alpha\beta}_{\mathbf{R}\mathbf{R}'} \Big[R(\mathbf{R})_{\alpha\gamma}\, R^*(\mathbf{R}')_{\beta\delta}\, \langle\, d^\dagger_{\mathbf{R},\gamma} d_{\mathbf{R}',\delta}\,\rangle_0 \\ &\quad + R(\mathbf{R})_{\alpha\gamma}\, Q^*(\mathbf{R}')_{\beta\delta}\, \langle\, d^\dagger_{\mathbf{R},\gamma} d^\dagger_{\mathbf{R}',\delta}\,\rangle_0 \\ &\quad + Q(\mathbf{R})_{\alpha\gamma}\, R^*(\mathbf{R}')_{\beta\delta}\, \langle\, d_{\mathbf{R},\gamma} d_{\mathbf{R}',\delta}\,\rangle_0 \\ &\quad + Q(\mathbf{R})_{\alpha\gamma}\, Q^*(\mathbf{R}')_{\beta\delta}\, \langle\, d_{\mathbf{R},\gamma} d^\dagger_{\mathbf{R}',\delta}\,\rangle_0 \Big] \\ &\quad + \mathrm{Tr}\left(\phi(\mathbf{R})^\dagger\, U(\mathbf{R})\, \phi(\mathbf{R})\right) \\ &= \mathcal{E}^0 + \mathrm{Tr}\left(\phi(\mathbf{R})^\dagger\, U(\mathbf{R})\, \phi(\mathbf{R})\right). \end{aligned} \tag{2.55}$$

The variational energy (2.55) has to be minimized respect to all the possible variational parameter ϕ which satisfy Eqs. (2.37)-(2.38) and all the possible

uncorrelated wavefunction $|\Psi_0\rangle$ which satisfy Eqs. (2.40)-(2.41). It can be shown that $|\Psi_0\rangle$ is nothing but the ground state of the Hamiltonian

$$\begin{aligned}\mathcal{H}^* &= -\sum_{\mathbf{R}\mathbf{R}'}\sum_{\alpha\beta\gamma\delta} t^{\alpha\beta}_{\mathbf{R}\mathbf{R}'}\Big[R(\mathbf{R})_{\alpha\gamma}\,R^*(\mathbf{R}')_{\beta\delta}\,d^\dagger_{\mathbf{R},\gamma}d_{\mathbf{R}',\delta} \\ &\quad +R(\mathbf{R})_{\alpha\gamma}\,Q^*(\mathbf{R}')_{\beta\delta}\,d^\dagger_{\mathbf{R},\gamma}d^\dagger_{\mathbf{R}',\delta} \\ &\quad +Q(\mathbf{R})_{\alpha\gamma}\,R^*(\mathbf{R}')_{\beta\delta}\,d_{\mathbf{R},\gamma}d_{\mathbf{R}',\delta} \\ &\quad +Q(\mathbf{R})_{\alpha\gamma}\,Q^*(\mathbf{R}')_{\beta\delta}\,d_{\mathbf{R},\gamma}d^\dagger_{\mathbf{R}',\delta}\Big] \\ &\quad +\sum_{\mathbf{R}}\sum_{\alpha\beta}\mu(\mathbf{R})_{\alpha\beta}\,\left(d^\dagger_{\mathbf{R},\alpha}d_{\mathbf{R}',\beta}-\delta_{\alpha\beta}\,n^0_{\mathbf{R},\alpha}\right) \\ &\quad +\sum_{\mathbf{R}}\sum_{\alpha\beta}\left(\nu(\mathbf{R})_{\alpha\beta}\,d^\dagger_{\mathbf{R},\alpha}d^\dagger_{\mathbf{R}',\beta}\,+\,h.c.\right). \end{aligned} \tag{2.56}$$

The parameters $\mu(\mathbf{R})_{\alpha\beta}$ and $\nu(\mathbf{R})_{\alpha\beta}$ are Lagrange multipliers. They can for instance be found by calculating at fixed $\mu(\mathbf{R})$ and $\nu(\mathbf{R})$ the ground state energy of (2.56), and find its maximum with respect to $\mu(\mathbf{R})$ and $\nu(\mathbf{R})$. Once these parameters are determined, then $\mathcal{E}^0$ in (2.55) is obtained as

$$\mathcal{E}^0 \equiv \langle\Psi_0|\,\mathcal{H}^*\,|\Psi_0\rangle. \tag{2.57}$$

The variational Hamiltonian (2.56) has rigorously no physical meaning but for the ground state properties. However, it is common [40] to interpret it as the Hamiltonian of the quasi-particles. Within such an assumption, the Gutzwiller approximation technique can be regarded as a tool to extract quasi-particle properties. More precisely, suppose we diagonalize the Hamiltonian (2.56) with the optimized values of the Lagrange multipliers,

$$\mathcal{H}^* = \sum_n \epsilon^*_k\,\psi^\dagger_k\,\psi_k, \tag{2.58}$$

so that $|\psi_0\rangle$ is the corresponding Fermi sea, hence

$$\mathcal{E}^0 = \sum_k \epsilon^*_k\,n^*_k, \tag{2.59}$$

where $n^*_k = \langle\Psi_0|\,\psi^\dagger_k\,\psi_k\,|\Psi_0\rangle$. If we further suppose that the eigenoperators ψ_k correspond to delocalized single-particle wavefunctions, then, to leading order

in the inverse volume, the variational wavefunction

$$|\zeta_k\rangle = \mathcal{P}\,\psi_k^\dagger\,|\Psi_0\rangle, \tag{2.60}$$

with k empty in $|\Psi_0\rangle$ will have an average energy

$$\mathcal{E}_k = \mathcal{E}^0 + \epsilon_k^*, \tag{2.61}$$

as if this excitation corresponds to a coherent single-particle one, a *quasi-particle*. If one believes in this identification, then he may follow the following procedure to evaluate single-particle spectral functions at low frequency:

$$\begin{aligned}\mathcal{A}_{\mathbf{R}\alpha,\mathbf{R}'\alpha'}(\omega) &\simeq \frac{1}{\pi}\,\langle\phi_0|\mathcal{P}^\dagger\,c_{\mathbf{R},\alpha}\,\delta\left(\omega-\mathcal{H}+\mathcal{E}_{var}\right)\,c^\dagger_{\mathbf{R}',\alpha'}\,\mathcal{P}\;|\phi_0\rangle \qquad (2.62)\\ &\simeq \frac{1}{\pi}\,\sum_{kk'}\langle\phi_0|\mathcal{P}^\dagger\,c_{\mathbf{R},\alpha}|\zeta_k\rangle\langle\zeta_k|\,\delta\left(\omega-\mathcal{H}+\mathcal{E}_{var}\right)\,|\zeta_{k'}\rangle\langle\zeta_{k'}|c^\dagger_{\mathbf{R}',\alpha'}\mathcal{P}\;|\phi_0\rangle.\end{aligned}$$

Using Eqs. (2.60) and (2.21) it follows that

$$\begin{aligned}\langle\zeta_{k'}|c^\dagger_{\mathbf{R}',\alpha'}\,\mathcal{P}\;|\phi_0\rangle &= \langle\phi_0|\psi_{k'}\,\mathcal{P}^\dagger c^\dagger_{\mathbf{R}',\alpha'}\mathcal{P}\;|\phi_0\rangle\\ &= \sum_{\beta'} R(\mathbf{R}')_{\alpha'\beta'}\,\langle\phi_0|\psi_{k'}\,d^\dagger_{\mathbf{R}',\beta'}|\phi_0\rangle\\ &+ \sum_{\beta'} Q(\mathbf{R}')_{\alpha'\beta'}\,\langle\phi_0|\psi_{k'}\,d_{\mathbf{R}',\beta'}|\phi_0\rangle, \qquad (2.63)\end{aligned}$$

which can be easily calculated. Furthermore, since, by definition,

$$\begin{aligned}\langle\zeta_k|\,\delta\left(\omega-\mathcal{H}+\mathcal{E}_{var}\right)\,|\zeta_{k'}\rangle &= \langle\phi_0|\,\psi_k\delta\left(\omega-\mathcal{H}^*+\mathcal{E}^0\right)\psi^\dagger_{k'}\,|\phi_0\rangle\\ &= \delta_{kk'}\,\delta\left(\omega-\epsilon_k^*\right)\,\left(1-n_k^*\right), \qquad (2.64)\end{aligned}$$

the spectral function (2.62) can be finally computed.

Chapter 3

Fermi-surface evolution across the magnetic phase transition in the Kondo lattice model

3.1 Introduction

The physics of heavy-fermion compounds remains a fascinating and challenging issue within strongly correlated materials. Recently, considerable experimental and theoretical interest has focused on the physical behavior across the magnetic quantum phase transition that is traditionally expected to occur when the Ruderman-Kittel-Kasuya-Yosida (RKKY) interaction overwhelms Kondo screening. [72] This transition is induced experimentally by external parameters like chemical composition, pressure or magnetic field, see for instance Refs. [10] and [51] as well as references therein, and is commonly accompanied by topological changes of the Fermi surface [46, 47, 48, 49, 50] and anomalous behavior of various transport and thermodynamic quantities. [10, 51] The theoretical debate on this subject has so far mainly followed two different directions. [51] One ascribes the changes of the Fermi surface to an f-electron Mott localization, [55] which is assumed to occur concomitantly with magnetism. In this scenario, the appearance of transport and thermodynamics anomalies is assumed to arise by the local magnetic susceptibility of the f-orbitals that grows singularly as Kondo temperature diminishes [56, 57, 58, 59]. The alter-

native proposal assumes that magnetism is predominantly an instability of an itinerant phase [52, 53], hence that the Fermi surface changes arise simply by the spin polarization of dispersing bands [52, 53] and the anomalous behavior by a singular magnetic scattering at the q-vector of the magnetic order that is going to establish [54], which differs substantially from the local in space singularity expected in the Mott f-localization above mentioned.

This issue has been very recently addressed theoretically in the periodic Anderson model by De Leo, Civelli and Kotliar [73, 74] using a cluster extension of dynamical mean field theory (CDMFT). Upon decreasing the hybridization between f-orbitals and conduction electrons, a weak first order phase transition from a heavy-fermion paramagnet to an itinerant antiferromagnet has been found. Remarkably, when these authors force CDMFT not to break spin $SU(2)$ symmetry and follow the metastable paramagnetic solution, they find an orbital-selective Mott localization - a pseudogap opens in the f-electron spectral function at the chemical potential, although low energy spectral weight remains within the Mott-Hubbard gap [75, 76] - for a hybridization between f and conduction electrons almost coincident with the value at which, allowing for magnetism, the antiferromagnetic transition occurs. This result suggests that the magnetic phase transition masks an incipient Mott localization of the f-electrons, which could become visible above the Neèl temperature or by suppressing antiferromagnetism. A complementary attempt has been almost contemporaneously performed by Watanabe and Ogata [77, 78]. These authors analyse by a variational Monte-Carlo (VMC) technique a Gutzwiller wavefunction for a Kondo lattice model in a two-dimensional square lattice. The variational phase diagram as function of the Kondo exchange depends non-trivially on the electron density. Very close to the compensated regime (one conduction electron per impurity-spin), upon decreasing the Kondo exchange there is first a second-order paramagnetic-to-antiferromagnetic phase transition, followed by a first-order transition between two magnetic phases with different Fermi surfaces. Moving away from the compensated regime, the second order phase transition disappears and they find a single first order line separating a paramagnetic phase from an antiferromagnetic one with different Fermi surfaces. These VMC results suggest that the magnetic transition and the topological change of the Fermi surface are not necessarily coincident,

which has been also observed in recent experiments. [60, 61] Since a variational calculation can only access ground state properties and not subtle dynamical features like an orbital-selective Mott transition, and keeping into account the differences between the periodic Anderson model and the Kondo lattice model, the VMC [77] and CDMFT [73] results might not be incompatible one to the other, and instead describe the same physical scenario although from two different perspectives. Should this be the case, it would undoubtly represent a step forward in the comprehension of heavy-fermion physics. To settle this question, one should for instance try to get closer to the compensated regime by CDMFT and check whether the f-localization and the on-set of magnetism disentangle from each other as predicted by VMC. Alternatively, one could carry on with variational calculations trying to uncover features that indirectly signal the f-localization. This is the aim of the present work. We note, by the way, that finite average values of the hybridization between f orbitals and conduction electrons, in the periodic Anderson model, or of the Kondo exchange, in the Kondo lattice model, must not be interpreted as absence of f-localization in a proper variational calculation, since the hybridization or the Kondo exchange are part of the Hamiltonian. Therefore other quantities must be identified that are accessible by a variational calculations.

In particular, in the work presented in this chapter we adopt a variational technique based on the multi-band extension [71, 35] of the so-called Gutzwiller approximation to evaluate analytically average values on Gutzwiller variational wavefunctions. [6, 7] This method is not exact like VMC, unless in the case of infinite-coordination lattices. However, we have found that a variational wavefunction richer than that of Ref. [77] seems to compensate for the approximation adopted to calculate average values, thus leading to the same phase-diagram as the one obtained by VMC in the case of a two-dimensional square lattice [77]. Encouraged by this result, we have extended the analysis of Ref. [77]. Specifically, we have derived the phase diagram forcing the wavefunction to remain paramagnetic. Similarly to the CDMFT calculation of Ref. [73], we have found that a first order transition that we think might correspond to an orbital selective Mott transition, which is masked by magnetism when we allow for it. Finally, we have analyzed the role of a uniform magnetic field in the paramagnetic phase and found a matamagnetic instabil-

ity near the above phase transition, suggestive of the metamagnetism observed experimentally. [62]

3.2 The Model and the variational wavefunction

We consider a Kondo lattice model (KLM) described by the Hamiltonian

$$\begin{aligned}\mathcal{H} &= -t \sum_{<\mathbf{R}\mathbf{R}'>} \sum_{\sigma} \left(c^{\dagger}_{\mathbf{R}\sigma} c_{\mathbf{R}'\sigma} + H.c. \right) \\ &\quad + J \sum_{\mathbf{R}} \mathbf{S}_{f\mathbf{R}} \cdot \mathbf{S}_{c\mathbf{R}} \equiv \mathcal{H}_0 + \mathcal{H}_J, \end{aligned} \tag{3.1}$$

where $c^{\dagger}_{\mathbf{R}\sigma}$ creates a conduction electron at site $\mathbf{R}$ with spin σ that can hop with amplitude $-t$ to nearest neighbor sites, $\mathbf{S}_{f\mathbf{R}}$ is the spin-1/2 operator of the f-orbital and $\mathbf{S}_{c\mathbf{R}}$ the conduction electron spin-density at site $\mathbf{R}$. In what follows, we assume a bipartite lattice. To study this Hamiltonian we introduce the following variational Gutzwiller wavefunction

$$|\Psi\rangle = \prod_{\mathbf{R}} \mathcal{P}_{\mathbf{R}} \, |\Psi_0\rangle, \tag{3.2}$$

where $|\Psi_0\rangle$ is the ground state of a non-interacting two-band variational Hamiltonian describing hybridized c and f orbitals, while $\mathcal{P}_{\mathbf{R}}$ is a local operator that modifies the relative weights of the local electronic configurations with respect to the uncorrelated wavefunction. In particular, we will assume for $\mathcal{P}_{\mathbf{R}}$ the general expression

$$\mathcal{P}_{\mathbf{R}} = \sum_{\Gamma,n} \lambda_{\Gamma n}(\mathbf{R}) \, |\Gamma, \mathbf{R}\rangle\langle n, \mathbf{R}|, \tag{3.3}$$

where $|\Gamma, \mathbf{R}\rangle$ and $|n, \mathbf{R}\rangle$ span all electronic configurations of the c and f orbitals at site $\mathbf{R}$, with the constraint that the states $|\Gamma, \mathbf{R}\rangle$, but not $|n, \mathbf{R}\rangle$, have just a single f-electron.

The variational wavefunction (3.2) has been widely used to study the periodic Anderson model as well as its strong coupling counterpart, the Kondo lattice model, within the Gutzwiller approximation. [12, 11, 79, 80, 13, 14]. However, in all the earlier works the operator $\mathcal{P}_{\mathbf{R}}$ has been chosen to act

only on the f-orbitals states. For instance, in the KLM that we consider, this choice would reduce to take $\mathcal{P}_{\mathbf{R}}$ as the projector onto singly occupied f-orbitals, namely

$$\mathcal{P}_{\mathbf{R}} = \sum_{\Gamma} |\Gamma, \mathbf{R}\rangle\langle\Gamma, \mathbf{R}| = \left(n_{f\mathbf{R}\uparrow} - n_{f\mathbf{R}\downarrow}\right)^2, \tag{3.4}$$

where $n_{f\mathbf{R}\sigma} = f^{\dagger}_{\mathbf{R}\sigma} f_{\mathbf{R}\sigma}$. This assumption implies that the spin correlations induced by the exchange J in (3.1) are only provided by the uncorrelated wavefunction $|\Psi_0\rangle$. The more general form of $\mathcal{P}_{\mathbf{R}}$, Eq. (3.3), that we assume in what follows, permits to include additional correlations besides those included in the wavefunction $|\Psi_0\rangle$, in particular the tendency of the conduction electrons to couple into a singlet with the localized spins.

The variational procedure amounts to optimize both the parameters $\lambda_{\Gamma n}(\mathbf{R})$ as well as those that identify $|\Psi_0\rangle$ by minimizing the average value of the Hamiltonian (3.1). In general this task can be accomplished only numerically, for instance by means of VMC as actually done by Watanabe and Ogata [77, 78] with the simple choice of $\mathcal{P}_{\mathbf{R}}$ of Eq. (3.4). However, in infinite coordination lattices many simplification intervene that allow to evaluate average values analytically. [37, 38, 34] In this work we follow an extension [35] of the multi-band method developed by Bünemann, Weber and Gebhard [34, 81] that allows to handle with non-hermitean operators $\mathcal{P}_{\mathbf{R}}$, which is generally the case since the bra $\langle n, \mathbf{R}|$ in (3.3) can have any number of f-electrons while the ket $|\Gamma, \mathbf{R}\rangle$ is forced to have only one.

We start assuming that $\mathcal{P}_{\mathbf{R}}$ is not the most general as possible but is subject to the following two conditions

$$\langle\Psi_0|\, \mathcal{P}^{\dagger}_{\mathbf{R}}\, \mathcal{P}_{\mathbf{R}}\, |\Psi_0\rangle = 1, \tag{3.5}$$

$$\langle\Psi_0|\, \mathcal{P}^{\dagger}_{\mathbf{R}}\, \mathcal{P}_{\mathbf{R}}\, \mathcal{C}_{\mathbf{R}\sigma}\, |\Psi_0\rangle = \langle\Psi_0|\, \mathcal{C}_{\mathbf{R}\sigma}\, |\Psi_0\rangle, \tag{3.6}$$

where

$$\mathcal{C}_{\mathbf{R}\sigma} = \begin{pmatrix} c^{\dagger}_{\mathbf{R}\sigma} c_{\mathbf{R}\sigma} & c^{\dagger}_{\mathbf{R}\sigma} f_{\mathbf{R}\sigma} \\ f^{\dagger}_{\mathbf{R}\sigma} c_{\mathbf{R}\sigma} & f^{\dagger}_{\mathbf{R}\sigma} f_{\mathbf{R}\sigma} \end{pmatrix}, \tag{3.7}$$

is the local single-particle density matrix operator. If Eqs. (3.5) and (3.6) are satisfied, then, as discussed in chapter 2, in an infinite-coordination lattice the

average value of (3.1) that has to be minimized is simply [34, 81, 35]

$$\begin{aligned} E &= \frac{\langle\Psi|\,\mathcal{H}\,|\Psi\rangle}{\langle\Psi|\Psi\rangle} \\ &= -t\sum_{<\mathbf{R}\mathbf{R}'>\sigma}\langle\Psi_0|\left[\left(R_{cc\sigma}(\mathbf{R})\,c^\dagger_{\mathbf{R}\sigma}+R_{cf\sigma}(\mathbf{R})\,f^\dagger_{\mathbf{R}\sigma}\right)\right. \\ &\quad \left.\left(R^*_{cc\sigma}(\mathbf{R}')\,c_{\mathbf{R}'\sigma}+R^*_{cf\sigma}(\mathbf{R}')\,f_{\mathbf{R}'\sigma}\right)+H.c.\right]|\Psi_0\rangle \\ &\quad +J\sum_{\mathbf{R}}\langle\Psi_0|\,\mathcal{P}^\dagger_{\mathbf{R}}\,\mathbf{S}_{f\mathbf{R}}\cdot\mathbf{S}_{c\mathbf{R}}\,\mathcal{P}_{\mathbf{R}}\,|\Psi_0\rangle. \end{aligned} \tag{3.8}$$

The hopping renormalization coefficients R are obtained through the following equations, compare with Eq. (2.9) with $Q=0$, since in this case we do not allow for superconductivity,

$$\begin{aligned} \langle\Psi_0|\,\mathcal{P}^\dagger_{\mathbf{R}}\,c^\dagger_{\mathbf{R}\sigma}\,\mathcal{P}_{\mathbf{R}}\,c_{\mathbf{R}\sigma}\,|\Psi_0\rangle &= R_{cc\sigma}(\mathbf{R})\,\langle\Psi_0|c^\dagger_{\mathbf{R}\sigma}c_{\mathbf{R}\sigma}|\Psi_o\rangle \\ &+ R_{cf\sigma}(\mathbf{R})\,\langle\Psi_0|f^\dagger_{\mathbf{R}\sigma}c_{\mathbf{R}\sigma}|\Psi_o\rangle \qquad (3.9) \\ \langle\Psi_0|\,\mathcal{P}^\dagger_{\mathbf{R}}\,c^\dagger_{\mathbf{R}\sigma}\,\mathcal{P}_{\mathbf{R}}\,f_{\mathbf{R}\sigma}\,|\Psi_0\rangle &= R_{cc\sigma}(\mathbf{R})\,\langle\Psi_0|c^\dagger_{\mathbf{R}\sigma}f_{\mathbf{R}\sigma}|\Psi_o\rangle \\ &+ R_{cf\sigma}(\mathbf{R})\,\langle\Psi_0|f^\dagger_{\mathbf{R}\sigma}f_{\mathbf{R}\sigma}|\Psi_o\rangle. \qquad (3.10) \end{aligned}$$

Therefore the variational calculation reduces, in infinite coordination lattices and provided Eqs. (3.5) and (3.6) are satisfied, to calculate expectation values on the Slater determinant uncorrelated wavefunction, which is analytically feasible since Wick's theorem applies.

Before moving to the presentation of our variational results, we want to mention some important consequences of choosing $\mathcal{P}_{\mathbf{R}}$ that acts both on the f and on the c orbitals. A drawback of the conventional Gutzwiller wavefunction with $\mathcal{P}_{\mathbf{R}}$ of Eq. (3.4), which was pointed out already by Fazekas and Müller-Hartmann in Ref. [14], is that, for small J, the paramagnetic solution gains a singlet-condensation energy that has a Kondo-like expression $\propto \exp(-1/J\rho)$, with ρ the conduction electron density of states at the chemical potential. On the contrary, any magnetic solution gains a local exchange energy of order $J^2\rho$ - the average value of $J\sum_{\mathbf{R}}\,\mathbf{S}_{f\mathbf{R}}\cdot\mathbf{S}_{c\mathbf{R}}$ - independently of the spatial arrangement of the magnetic ordering. This result would remain true even for a single impurity Kondo model and is obviously incorrect. Our wavefunction partially

cures this deficiency because $\mathcal{P}_{\mathbf{R}}$ is able to induce additional spin-correlations among c and f electrons, although only locally.

We further note from (3.8) that the action of the Gutzwiller operator $\mathcal{P}_{\mathbf{R}}$ effectively generates an intersite hopping between the f-electrons, absent in the original Hamiltonian (3.1), which correlates different sites hence can play an important role in determining the topology of the Fermi surface as well as in stabilizing magnetic structures. Even though our method for computing average values is not exact in finite-coordination lattices, the more involved form of $\mathcal{P}_{\mathbf{R}}$ of Eq. (3.3) with respect to (3.4) partly compensates for this weakness – the variational Hamiltonian contains inter-site f-f and f-c hopping – leading to results that are very similar to those obtained by exact VMC, as we are going to show.

3.3 Variational phase diagram

We have solved the variational problem numerically using, for numerical convenience, a flat conduction-electron density-of-states with half-bandwidth D, our unit of energy. We do not expect that a more realistic density of states could qualitatively change the phase diagram that we find. Let us discuss our variational results.

In Fig. 3.1 we show the variational phase diagram as function of the Kondo exchange J, in units of D, versus the conduction electron density $0 \leq n_c < 1$. Close to the compensated regime $n_c = 1$, one conduction electron per spin, we do find, similarly to Watanabe and Ogata [77, 78], two successive transitions as J/D is reduced from the heavy-fermion paramagnetic phase. First, Nèel antiferromagnetism appears by a second order phase transition, see Fig. 3.2. Within the antiferromagnetic phase, a first-order phase transition further occurs at smaller J/D, see the jump of the order parameter in Fig. 3.2, accompanied by a rearrangement of the Fermi surface. This is shown in Fig. 3.3, where we draw the quasiparticle (emission) spectral function at the chemical potential, defined by

$$A(\mathbf{k}) = -\int d\epsilon A(\mathbf{k},\epsilon)\,\frac{\partial f(\epsilon)}{\partial \epsilon}, \tag{3.11}$$

where $f(\epsilon)$ is the Fermi distribution function at low temperature. $A(\mathbf{k},\epsilon)$ is

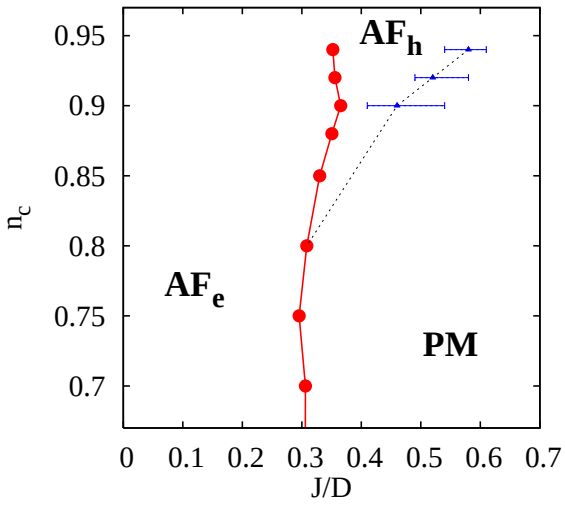

Figure 3.1: (Color online) Variational phase diagram as function of the conduction electron density n_c and of the Kondo exchange in units of half the bandwidth, J/D. The solid line with the circles represents a first order line, while the dotted line is a second order transition. The error bars along the second order phase transition line reflect the variational uncertainty of a precise location of the continuous transition. The same problem does not arise along the discontinuous first order line. PM stands for paramagnetic heavy-fermion metal, while AF stands for an itinerant antiferromagnet, the subscripts "e" and "h" are borrowed from Ref. [77] and refer to the electron-like, "e", or hole-like, "h", character of the Fermi surface, see Fig. 3.3.

calculated using the method described in chapter 2 with a nearest-neighbor hopping on a two dimensional square lattice, though with variational parameters optimized using a flat density of states at the same values of n_c and J/D.

The $\mathbf{k}$-points where $A(\mathbf{k}, \epsilon)$ is large identify the effective Fermi surface. We note that, in the paramagnetic phase, the Fermi surface is hole-like just as if the f spins do partecipate the Luttinger sum rules - two bands with $1 + n_c \leq 2$ electrons per site; one band empty and the other occupied by $1 < 1 + n_c < 2$ electrons. The same feature is also found beyond the second order phase transition. However, for J/D below the first order phase transition, the Fermi

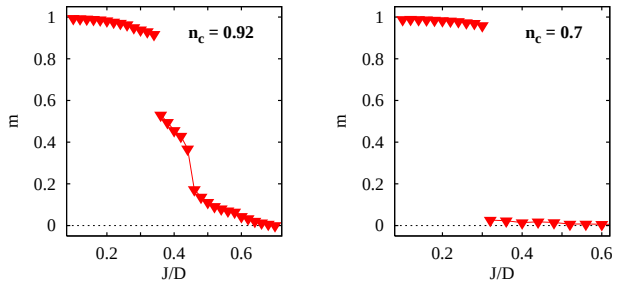

Figure 3.2: (Color online) The magnetic order parameter as function of J/D for $n_c = 0.92$ (left panel) and $n_c = 0.7$ (right panel). Notice that for $n_c = 0.92$ the order parameter grows continuously below a critical $J/D \simeq 0.6$ – second order phase transition – until at $J/D \simeq 0.36$ it jumps abruptly – first order transition. For $n_c = 0.7$ only a first order transition with a jump from zero to a finite value of the order parameter is observed.

surface changes topology and become electron-like, as if the f-electrons disappear from the Fermi surface. Comparing the phase diagram Fig. 3.1 with the one obtained by VMC [77], we find that the two agree well, even quantitatively. [82] In order to identify the origin of the Fermi surface rearrangement, it is convenient to write the general expression of the variational Hamiltonian $\mathcal{H}_*$, see Eq. (2.56), of which $|\Psi_0\rangle$ is the ground state. In momentum space and within the magnetic Brillouin zone

$$\mathcal{H}_* = \sum_{\mathbf{k}\sigma} \psi^\dagger_{\mathbf{k}\sigma} \begin{pmatrix} t_{cc}\epsilon_{\mathbf{k}} & V_u + t_{cf}\epsilon_{\mathbf{k}} & \sigma m & \sigma V_s + \sigma t'_{cf}\epsilon_{\mathbf{k}} \\ V_u + t_{cf}\epsilon_{\mathbf{k}} & \epsilon_f + t_{ff}\epsilon_{\mathbf{k}} & \sigma V_s - \sigma t'_{cf}\epsilon_{\mathbf{k}} & \sigma M \\ \sigma m & \sigma V_s - \sigma t'_{cf}\epsilon_{\mathbf{k}} & -t_{cc}\epsilon_{\mathbf{k}} & V_u - t_{cf}\epsilon_{\mathbf{k}} \\ \sigma V_s + \sigma t'_{cf}\epsilon_{\mathbf{k}} & \sigma M & V_u - t_{cf}\epsilon_{\mathbf{k}} & \epsilon_f - t_{ff}\epsilon_{\mathbf{k}} \end{pmatrix} \psi_{\mathbf{k}\sigma}, \tag{3.12}$$

where $\epsilon_{\mathbf{k}}$ is the energy dispersion of the conduction electrons,

$$\psi^\dagger_{\mathbf{k}\sigma} = \left(c^\dagger_{\mathbf{k}\sigma}, f^\dagger_{\mathbf{k}\sigma}, c^\dagger_{\mathbf{k}+\mathbf{Q}\sigma}, f^\dagger_{\mathbf{k}+\mathbf{Q}\sigma} \right),$$

a Fermi spinor, its hermitean conjugate being $\psi_{\mathbf{k}\sigma}$, $\mathbf{Q}$ the Nèel magnetic vector, and all the Hamiltonian parameters are variational but $\epsilon_{\mathbf{k}}$.

In Fig. 3.4 we plot the variational bands in the antiferromagnetic phase below and above the first order phase transition along the trajectory repre-

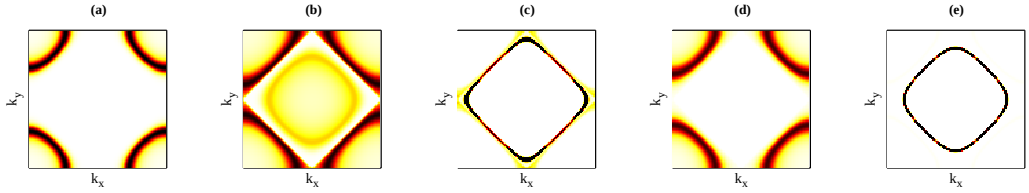

Figure 3.3: (Color online) The conduction electron spectral function at the chemical potential for a two-dimensional square lattice. Panels (a)-(b)-(c) show the evolution of the spectral function $A(\mathbf{k})$ at the chemical potential for $n_c = 0.92$ in the paramagnetic phase, panel (a) with $J/D = 0.8$, right after the second-order transition, panel (b) with $J/D = 0.4$, and finally below the first-order transition, panel (c) with $J/D = 0.16$. Panels (d)-(e) show the same evolution with $n_c = 0.7$ where there is only the first-order transition.

sented in Fig. 3.5. In agreement with the interpretation given by Watanabe and Ogata in Ref. [77], the bands in the antiferromagnetic phase at low J/D can be thought as antiferromagnetically split c and f bands very weakly hybridized, panels (a) and (b) in Fig. 3.6, while those at larger J/D as strongly hybridized c and f bands weakly antiferromagnetically split, panels (c) and (d) in Fig. 3.6. The main control parameter of the transition is the relative strength of the f-orbital energy, ϵ_f in (3.12), with respect to the antiferromagnetic splittings, mostly σM in (3.12).

Above a critical doping away from the compensated regime, we only find a single first-order phase transition transition, see Fig. 3.2, directly from a paramagnet at large J/D, with a band structure similar to panel (c) in Fig. 3.6 unfolded in the whole Brillouin zone, to an antiferromagnet with a band structure similar to panel (b) in Fig. 3.6. In other words, this phase transition is accompanied by a drastic reconstruction of the Fermi surface.

3.4 Fermi-surface reconstruction vs. magnetism

The variational phase diagram, Fig. 3.1, shows that the onset of magnetism is not necessarily accompanied by a Fermi surface reconstruction. Viceversa, one could speculate that the latter might not require magnetism, which would

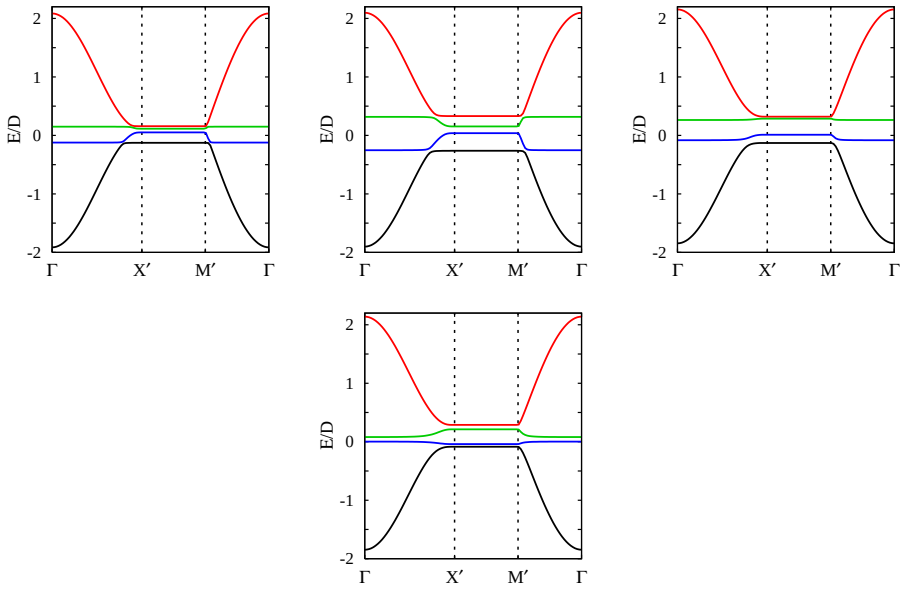

Figure 3.4: (Color online) Evolution of the band structure of the optimized variational Hamiltonian Eq. (3.12) for $n_c = 0.92$ as a function of J/D and across the first order transition. From top left to bottom right panel: $J/D = 0.1$, $J/D = 0.2$, $J/D = 0.34$ (below the first-order transition) and $J/D = 0.36$ (above the first-order transition).

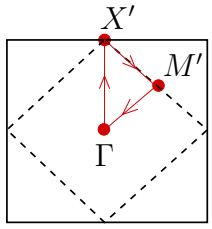

Figure 3.5: The magnetic Brillouin zone

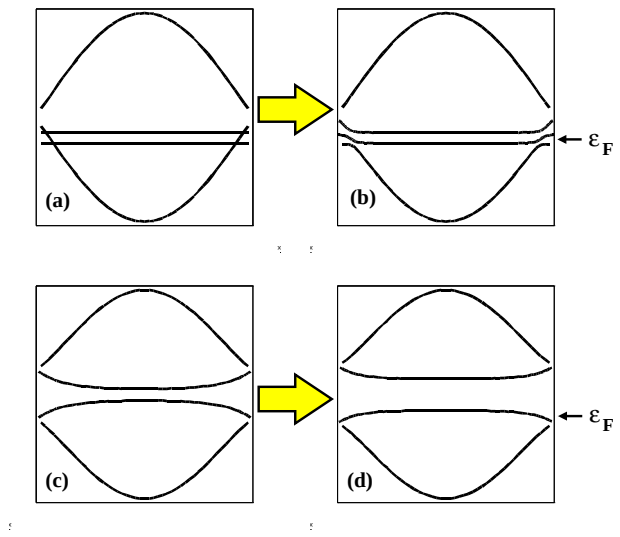

Figure 3.6: (Color online) One-dimensional representation of the different variational band structures in the two magnetic phases close to $n_c = 1$, drawn in the magnetic Brillouin zone. Small J/D phase: panel (a) represents non-hybridized c and f bands split by antiferromagnetism; panel (b) what happens once a small hybridization is switched on. Large J/D phase: panel (c) represents non-magnetic hybridized c and f bands in the folded Brillouin zone; panel (d) what happens once a small antiferromagnetic order parameter is switched on.

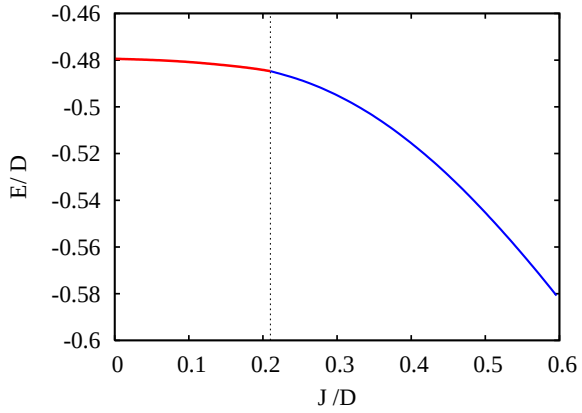

Figure 3.7: (Color online) Variational energy as function of J/D at $n_c = 0.8$ in the paramagnetic sector. A kink is visible at $J/D \simeq 2.1$. We note the finite curvature of the energy at low J/D, which, as we checked, is compatible with second order perturbation theory.

be the case if the Fermi-surface change were caused by the f-electron localization [55]. This aspect makes worth investigating the properties of the variational wavefunction (3.2) preventing antiferromagnetism, which amounts to assume $\lambda_{\Gamma n}(\mathbf{R})$ in Eq. (3.3) independent of $\mathbf{R}$ and $|\Psi_0\rangle$ a paramagnetic Slater determinant.

At first sight, one would not expect to find anything special varying J/D in the paramagnetic sector. In fact, we previously mentioned that the change of the Fermi surface within the magnetic phase reflects essentially the change of the band structure, which, in turn, depends variationally only on the value of the f-orbital energy with respect to the magnetic splitting, respectively ϵ_f and $2M$ in Eq. (3.12). Therefore, without magnetism, i.e. $M = 0$, the topology of the band structure must remain invariant whatever $J/D \neq 0$ is, as we indeed find. Nevertheless, even in this case, we do observe a very weak first order phase transition for values of J/D slightly smaller than those at which the first order transition occurs when we allow for magnetism, as shown by the behavior of the variational energy in Fig. 3.7. Although strictly at zero temperature the Fermi surface must enclose a volume that contains $1 + n_c$ electrons, a very small but finite temperature in Eq. (3.11) is able to emphasize features close

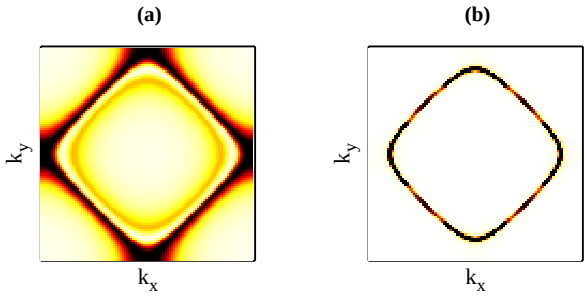

Figure 3.8: (Color online) Low temperature spectral function at the chemical potential for $n_c = 0.8$ and J/D above, panel (a), and below, panel (b), the critical value.

to the chemical potential that, as shown in Fig. 3.8, undergo a sharp change across the transition. For J/D above the critical value, the $T \neq 0$ Fermi surface includes the f-electrons, while, below, it does not, exactly as we find when magnetism is present. Note that, should we set the temperature $T = 0$ in (3.11), only the hole-like sheet of panel (a) Fig. 3.8 would appear, even for J/D below the transition. It is only because $T \neq 0$ that panel (b) shows a different electron-like Fermi surface.

The observed changes at $T \neq 0$ occur now not because the band structure is modified but because the spectral weight of the conduction electrons at the Fermi energy changes discontinuously. Indeed, looking carefully at the spectral function in Fig. 3.8a, one can distinguish two sheets of the Fermi surface, a small one, which corresponds to the non-interacting conduction electron Fermi surface, and a large one that includes also the f electrons. Across the transition, it is the relative weight of these two sheets that change discontinuously. We believe that this must be regarded as a manifestation of the f-localization, or, better, of the orbital-selective localization, as proposed in Refs. [73] and [74], since a tiny spectral weight at the Fermi energy remains on the small Fermi surface for low J/D, see Fig. 3.8a. This result also demonstrates that the rearrangement observed along the first-order line in the phase diagram Fig. 3.1 is caused by the f-electron orbital-selective localization rather than by magnetism.

Inspection of the behavior of the average Kondo exchange and hopping,

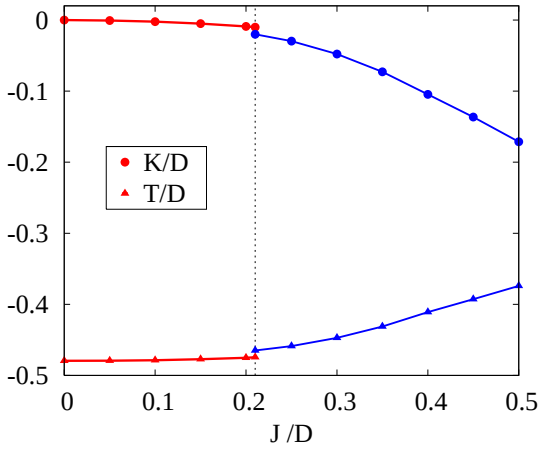

Figure 3.9: (Color online) Behavior of the average Kondo exchange and hopping.

Fig. 3.9, shows that the "localized" phase has a better conduction-electron hopping energy, while the "delocalized" one a better Kondo exchange. This suggests that the abrupt change of the Fermi surface is primarily consequence of the competition between the conduction electron band-energy and the Kondo exchange, and not of the commonly invoked competion between Kondo and RKKY interactions.

In light of these results, also the transition lines in the phase diagram, Fig. 3.1, assume a different meaning. The first-order line that separates the paramagnet from the antiferromagnet is primarily due to the f-localization, magnetism being just its by-product. On the contrary, the second-order line close to the compensated regime is more likely to be interpreted as a Stoner's instability of the paramagnetic Fermi-liquid, driven by the nesting property of the Fermi surface at $n_c = 1$. Across this second-order phase transition, the Fermi surface changes, smoothly, following the spin splitting of the bands.

3.5 Metamagnetism

Another indirect signal of the f-localization can be found by studying the behavior of the paramagnet in the presence of a uniform magnetic field. Indeed,

if the f-orbitals are close to a Mott localization, they are also very prompt to order magnetically. Let alone, they would prefer some magnetic order along with the structure of the RKKY exchange, in our bipartite lattice model not far from half-filling the natural candidate being a Néel ordering. However, in the presence of a magnetic field, they could equally prefer to order ferromagnetically. In other words, it is plausible to foresee that the f-localization could be driven by a weak magnetic field, the weaker the closer the f-localization is, thus accompanied by a sharp increase of magnetization, so-called metamagnetism, as well as by a discontinuous change of the Fermi surface.

This expectation is confirmed by our variational calculation. In Fig. 3.10 we show the evolution of the uniform magnetization as function of the applied magnetic field in the paramagnetic phase at $J/D = 0.45$ and $n_c = 0.88$. Indeed, as function of the magnetic field, we do find a first order phase transition that is accompanied by a abrupt increase of the magnetization as well as by a discontinuous change of the conduction electron Fermi surface, specifically of the majority spin one. In fact, since the critical field is smaller than the Kondo exchange J, once the f electrons localize and their spins align with the external field, the effective Zeman field felt by the conduction electrons is opposite to the applied one. Consequently, the Fermi surface of the majority spin becomes smaller than the minority spin one, contrary to the case for external fields below the metamagnetic transition, which is what we find, although hardly visible in Fig. 3.10.

3.6 Conclusions

We have calculated within the Gutzwiller approximation the phase diagram of the Kondo lattice model as function of the conduction electron density and of the Kondo exchange J. The novel feature of our approach with respect to earlier ones is that the Gutzwiller projector acts on all the electronic configurations of each f orbital plus the conduction state to which it is hybridized. This allows to include additional local correlations between f and conduction electrons, specifically those that favour singlet pairing among them. Summarizing our variational results, we have found that:

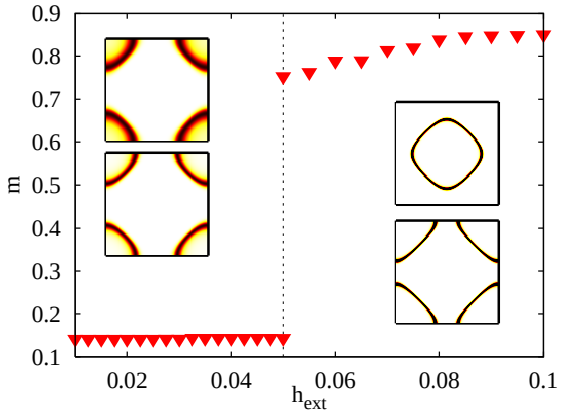

Figure 3.10: (Color online) Evolution of the uniform magnetization as function of an external magnetic field applied in the paramagnetic phase ($J/D = 0.45$ at $n_c = 0.88$). Insets show the spectral functions for the majority (top panel) and minority (bottom panel) spins across the metamagnetic transition.

- there exists an orbital selective Mott localization of the f electrons accompanied by a discontinuous change of the Fermi surface;
- away from any nesting instability, this first-order transition in accompanied by magnetism;
- on the contrary, when the conduction electron Fermi surface is perfectly or almost perfectly nested, magnetism occurs before the f-localization, via a second order transition with a continuous change of the Fermi surface;
- the f-electron Mott localization can be also induced by a uniform magnetic field, in which case it is revealed by a metamagnetic transition at which the magnetization jumps and the Fermi surface changes discontinuously.

These findings bridge between the cluster dynamical mean field theory results of Refs. [73]-[74] and the variational Monte Carlo ones of Refs. [77]-[78], and suggest that generically, i.e. without nesting, magnetism is a by-product of the f-electron Mott localization rather than the outcome of the competition

between Kondo screening and RKKY interaction. We must mention that the weak first-order character of the Mott transition that we find might be a spurious outcome of the variational procedure, so that we can not exclude that in reality such a transition is continuous.

The question we can not address, since ours is a variational approach for the ground state, concerns the anomalous thermodynamic behavior observed around the magnetic transition. In other words, we can not establish whether such a behavior is associated with the incipient magnetism [54] or is just a consequence of the f-electron localization, [56, 57] or better of the orbital selective Mott localization. [58, 59, 83, 74]

Chapter 4

Superconductivity in a liquefied valence-bond crystal: the doped bilayer Hubbard model

4.1 Introduction

The concept of resonating-valence-bond (RVB) superconductivity introduced by Anderson [26, 84] in the early days after the discovery of high-temperature superconductors has during the years branched out into a whole series of interesting subsidiary questions. While a lot of efforts have need systematically devoted to uncover the RVB scenario in models of cuprates [24, 85, 86, 30, 87, 32, 88, 33, 89, 90], there have been also attempts to extend the idea well beyond cuprates. For instance, the simple follow up of the RVB hypothesis is that doping a spin-liquid, i.e. a phase of magnetic moments that does not break any symmetry, inevitably leads to superconductivity. Supports to this idea came from the observation that a metallic phase with dominant superconducting fluctuations appears upon doping the gaped-spin-liquid Mott-insulating state of a half-filled two-leg Hubbard ladder [91, 92] but also of the spontaneously dimerized insulating phase of the half-filled Hubbard chain with nearest and next-nearest neighbor hopping [93], both model cases believed to be relevant to actual superconducting quasi-one-dimensional materials [94, 95, 96]. In reality, the Mott phases of the ladder and of the spontaneoulsy dimerized chain

should not be regarded as spin-liquids in the strict sense, but rather as valence-bond (VB) crystals, the dimerized chain even breaking translational symmetry. Their *superconducting* behavior therefore suggests that the RVB hypothesis may actually include a larger class of VB insulators, either real spin-liquids or short range RVBs. This same idea has been also advocated to explain superconductivity in organic alkali-doped fullerenes [97, 65], whose insulating phases can be regarded as local versions of VB crystals, where singlet pairing takes place within each molecule by the Jahn-Teller effect.

In order to verify with a simple method this hypothesis, a model of two Hubbard planes coupled by an inter-plane hybridization was studied at half-filling by a multi-band extension of the Gutzwiller approximation in Ref. [35]. This model, just like its one-dimensional counterpart, the aforementioned ladder, has a Mott insulating phase at half-filling and for a sufficiently large inter-plane hopping that is a non-magnetic VB crystal, a collection of inter-plane singlets. It was found that, upon melting the VB crystal by decreasing the Hubbard repulsion, a superconducting phase emerges just next to the Mott insulator. Following up this work, we have decided to study the same model away from half-filling, namely to study the melting of the VB crystal induced by doping. As we expected and wished, superconductivity emerges once more for very low doping, at higher doping a normal metal being stable, in remarkable similarity with the phase diagram of cuprates and with existing DMFT results [64].

4.2 The Model

The model consists of two Hubbard planes coupled through a single-particle hopping $t_\perp$, each one being defined on a lattice with nearest neighbor hopping

t. The Hamiltonian reads:

$$\begin{aligned}
\mathcal{H} &= -\sum_{\mathbf{R}\mathbf{R}'}\sum_{i=1}^{2}\sum_{\sigma} t_{\mathbf{R}\mathbf{R}'}\, c^{\dagger}_{\mathbf{R},i\sigma}c_{\mathbf{R}',i\sigma} + H.c. + \frac{U}{2}\sum_{\mathbf{R}}\sum_{i=1}^{2}(n_{\mathbf{R},i}-1)^2 \\
&\quad -t_{\perp}\sum_{\mathbf{R}}\sum_{\sigma}\left(c^{\dagger}_{\mathbf{R},1\sigma}c_{\mathbf{R},2\sigma} + H.c.\right) \\
&= \sum_{\mathbf{k}\sigma}\sum_{i=1}^{2}\epsilon(\mathbf{k})\, c^{\dagger}_{\mathbf{k},i\sigma}c_{\mathbf{k},i\sigma} + \frac{U}{2}\sum_{\mathbf{R}}\sum_{i=1}^{2}(n_{\mathbf{R},i}-1)^2 \\
&\quad -t_{\perp}\sum_{\mathbf{k}\sigma}\left(c^{\dagger}_{\mathbf{k},1\sigma}c_{\mathbf{k},2\sigma} + H.c.\right) \\
&\equiv \mathcal{H}_{hop} + \mathcal{H}_U + \mathcal{H}_{\perp}, \qquad (4.1)
\end{aligned}$$

where $t_{\perp} > 0$, $c^{\dagger}_{\mathbf{R},i\sigma}$ and $c_{\mathbf{R},i\sigma}$ create and annihilate, respectively, an electron at site $\mathbf{R}$ in plane $i = 1, 2$ with spin σ, $n_{\mathbf{R},i} = \sum_{\sigma} c^{\dagger}_{\mathbf{R},i\sigma}c_{\mathbf{R},i\sigma}$ is the local occupation on layer i, and U is the Hubbard repulsion on each lattice site. In order to study the doped system it is more convenient to work in the grand-canonical ensemble adding a chemical potential term $-\mu\sum_{\mathbf{R},i} n_{\mathbf{R},i}$ to the model Hamiltonian (4.1). The particle number is then controlled by tuning μ. In Eq. (4.1) $c^{\dagger}_{\mathbf{k},i\sigma}$ creates an electron in layer i and spin σ with momentum $\mathbf{k}$, and $\epsilon(\mathbf{k}) \in [-D, D]$ is the intra-layer dispersion in momentum space, where D is half the bandwidth that will be our unit of energy. The non-interacting part of the Hamiltonian is better rewritten introducing the bonding (e) and antibonding (o) combinations

$$\begin{aligned}
c^{\dagger}_{\mathbf{k},e\sigma} &= \frac{1}{\sqrt{2}}\left(c^{\dagger}_{\mathbf{k},1\sigma} + c^{\dagger}_{\mathbf{k},2\sigma}\right), \\
c^{\dagger}_{\mathbf{k},o\sigma} &= \frac{1}{\sqrt{2}}\left(c^{\dagger}_{\mathbf{k},1\sigma} - c^{\dagger}_{\mathbf{k},2\sigma}\right),
\end{aligned}$$

through which

$$\mathcal{H}_{hop} + \mathcal{H}_{\perp} = \sum_{\mathbf{k}\sigma}\sum_{a=e,o}\epsilon_a(\mathbf{k})\, c^{\dagger}_{\mathbf{k},a\sigma}c_{\mathbf{k},a\sigma}, \qquad (4.2)$$

where $\epsilon_e(\mathbf{k}) = \epsilon(\mathbf{k}) - t_{\perp} \in [-D - t_{\perp}, D - t_{\perp}]$ and $\epsilon_o(\mathbf{k}) = \epsilon(\mathbf{k}) + t_{\perp} \in [-D + t_{\perp}, D + t_{\perp}]$ are, respectively, the bonding and antibonding band dispersions, see Fig. 4.2.

If $U = 0$ and the density is one electron per site, half-filling, the model describes a metal until the two bands overlap, i.e. $t_{\perp} \leq D$, and a band insulator otherwise.

For $U \gg D + t_\perp$, the model becomes equivalent to two Heisenberg planes coupled to each other by an inter-plane antiferromagnetic exchange $J_\perp = 4t_\perp^2/U$. If each plane is a square lattice with only nearest neighbor hopping t, hence $D = 4t$, each Heisenberg model is characterized by a nearest neighbor antiferromagnetic exchange $J = 4t^2/U$. This model has been studied in detail by quantum Monte Carlo [98, 99] and it is known to have a quantum critical point that separates a a Neèl antiferromagnet, for $J_\perp \leq 2.5520\, J$, from a gaped spin-liquid phase, for larger $J_\perp$. The latter can be interpreted as a kind of VB crystal, each bond being an inter-layer singlet, adiabatically connected to the band insulator at $U = 0$. In terms of the hopping parameters of the original Hubbard bilayer, the critical point should correspond to $(t_\perp/t)_c = \sqrt{2.5220} \simeq 1.5881$. This value is in good agreement with direct QMC simulations of the Hubbard bilayer [100, 101], which find $(t_\perp/t)_c \simeq 1.5$ to 2. According to these results, when $1.6 \leq (t_\perp/t) \leq 4$ one could start at $U = 0$ with a metallic phase, and, upon increasing U, find a direct transition into the VB Mott insulator. However, the story must become more complicated if the $U = 0$ Fermi surface at half-filling has nesting at the edge of the Brillouin zone, as it happens for a square lattice with only nearest neighbor hopping. In this case, the $U = 0$ and $t_\perp < 4t = D$ metal has a Stoner instability towards Neèl antiferromagnetism for arbitrary small U, so that it is *a priori* not obvious that one could find any direct metal to VB Mott insulator transition. In reality, both cluster DMFT [102] and QMC simulations find evidence that such a transition does exist. Nevertheless, one may always bypass this problem assuming that the intra-layer hopping is such as not to lead to any nesting, the latter being more an accident than the rule in realistic systems. In this case, which we will implicitly assume hereafter, it is safe to believe that a direct transition at half-filling from a metal to a VB Mott insulator does exist.

Within this scenario, the melting of the VB crystal into a metallic phase can therefore occur either by doping away from half-filling but also upon decreasing U below the Mott transition, still keeping half-filled density. In the latter case, a recent study [35] has shown that, within the Gutzwiller approximation, the VB crystal first turns into a superconducting phase that eventually gives way to a normal metal upon further decreasing U. This finding supports the RVB superconductivity scenario [26] and shows that the one-dimensional

behavior persists in higher dimensions. It also agrees with the indication of an enhanced pairing susceptibility obtained in earlier studies by QMC [103, 104]. However the lowest temperatures attainable so far by QMC are still above the eventual superconducting critical temperature, so that the existence of a true superconducting phase at half-filling is numerically still an open issue. DMFT calculations, that could in principle be carried out at zero temperature, was performed [105, 102] but did not search explicitly for any superconducting phase.

Away from half-filling, QMC indications of enhanced pairing fluctuations are more convincing [104, 101], although the existence of a superconducting phase at low temperature is still uncertain [104]. This makes it worth addressing this issue by the Gutzwiller approximation, which is not as rigorous as QMC but at least can provide results at zero temperature.

4.3 The method

In order to study the doped system it is more convenient to work in the grand-canonical ensemble hence adding a chemical potential term $-\mu \sum_{\mathbf{R},i} n_{\mathbf{R},i}$ to the model Hamiltonian (4.1). The particle number is then controlled by tuning the value of μ.

Following Ref. [35], we decided to search for a variational solution that allows for singlet superconductivity, hence doesn't break spin-$SU(2)$ symmetry. Since any unitary transformation, which diagonalizes a generic single-particle density matrix that includes an anomalous term in the spin-singlet Cooper channel, leaves the spin-$SU(2)$ generators invariant, this case is perfectly suitable for applying the method described in chapter 2.

In Ref. [35] it has been shown that, at half-filling and for values of $t_\perp$ such that the Mott insulator at large U is non-magnetic – a collection of inter-layer singlets, as mentioned a local version of a valence bond (VB) crystal – the transition to a conducting phase below a critical U_c occurs via a superconducting region that intrudes between the Mott insulator and the normal metal. On general grounds [26, 64] one may expect that the melting of the VB solid by doping rather than by decreasing U should also result in the appearance of a superconducting dome that disappears above a critical doping, a scenario

that we aim to investigate with the Gutzwiller variational technique. To this purpose, we consider the variational wavefunction

$$|\Psi\rangle = \prod_{\mathbf{R}} \mathcal{P}_{\mathbf{R}} \, |\Psi_0\rangle, \tag{4.3}$$

where the operator $\mathcal{P}_{\mathbf{R}}$ acts on the two sites at $\mathbf{R}$ belonging to the two planes. This choice allows to us enforce better the tendency of the two sites forming a spin-singlet. The uncorrelated wavefunction is assumed to be a generic BCS wavefunction with real inter-plane singlet pairing, i.e.

$$\langle \Psi_0 | \, c^\dagger_{\mathbf{R},1\uparrow} c^\dagger_{\mathbf{R},2\downarrow} \, |\Psi_0\rangle = \langle \Psi_0 | \, c^\dagger_{\mathbf{R},2\uparrow} c^\dagger_{\mathbf{R},1\downarrow} \, |\Psi_0\rangle \neq 0.$$

According to the results of chapter 2, the variational energy to be minimized is obtained as the sum of two terms, one being the contribution of the local, same $\mathbf{R}$ but both layers, terms:

$$E_{loc} = \mathrm{Tr} \left[\phi^\dagger \left(\mathcal{H}_U + \mathcal{H}_\perp - \mu \sum_{\mathbf{R}i} n_{\mathbf{R},i} \right) \phi' \right] \tag{4.4}$$

where all operators are meant to be matrices in the local representation invariant under $SU(2)$ symmetry, and the hopping contribution E_{hop}. This can be shown to coincide with the ground-state energy of a variational single-particle Hamiltonian[35]:

$$\mathcal{H}^*_{hop} = \sum_{\mathbf{k}} \psi^\dagger_{\mathbf{k}} \, \hat{T}_{\mathbf{k}} \, \psi_{\mathbf{k}}, \tag{4.5}$$

where $\psi^\dagger_{\mathbf{k}} = (d^\dagger_{\mathbf{k}1\uparrow}, d^\dagger_{\mathbf{k}2\uparrow}, d_{-\mathbf{k}1\downarrow}, d_{-\mathbf{k}2\downarrow})$ is the Nambu spinor in momentum space and $\hat{T}_{\mathbf{k}}$ a 4×4 matrix in the natural basis which depends explicitly on momentum and on some Lagrange multipliers included to enforce that the average of the single particle density matrix on the ground state – to be identified with $|\Psi_0\rangle$ in (2.1) – is diagonal in the natural basis, with matrix elements satisfying

$$\langle \Psi_0 | d^\dagger_{\mathbf{R}i\sigma} d_{\mathbf{R}i\sigma} | \Psi_0 \rangle = \mathrm{Tr} \left(\phi^\dagger \phi \, d^\dagger_{i\sigma} d_{i\sigma} \right) \equiv n^0_i,$$

The matrix $\hat{T}_{\mathbf{k}}$ has the general expression:

$$\hat{T}_{\mathbf{k}} = \begin{pmatrix} \epsilon(\mathbf{k})\hat{Z} + \hat{\eta} & \epsilon(\mathbf{k})\hat{\Delta} + \hat{\delta} \\ \epsilon(\mathbf{k})\hat{\Delta}^\dagger + \hat{\delta}^\dagger & -\epsilon(\mathbf{k})\hat{Z}^t - \hat{\eta}^t \end{pmatrix}, \tag{4.6}$$

where the 2×2 matrices $\hat{\eta}$ and $\hat{\delta}$ are the aforementioned Lagrange multiplier, while $\hat{Z}$ and $\hat{\Delta}$ have elements (labelled by $j, l = 1, 2$, the layer indices)

$$\hat{Z}_{j,l} = \sum_{i=1}^{2} \left(R_{i,j} R^*_{i,l} - Q_{i,l} Q^*_{i,j} \right) \tag{4.7}$$

$$\hat{\Delta}_{j,l} = \sum_{i=1}^{2} \left(R_{i,j} Q^*_{i,l} + Q^*_{i,j} R_{i,l} \right) \tag{4.8}$$

and $\epsilon(\mathbf{k})$ is the intra-layer band dispersion.

4.4 Variational results

We solved numerically the variational problem assuming for simplicity a flat density of states with half-bandwidth D (we do not expect the results to change qualitatively by adopting a more realistic density of states). In order to compare with the half-filling results reported in Ref. [35], we fixed the value of the intra-dimer hopping $t_\perp/D = 0.5$ and solved the variational problem for different values of U/D and μ/D. Note that this value in the case of a square lattice with nearest neighbor hopping t corresponds to $t_\perp = 2t$, above the critical value for the stability at large U of the VB Mott insulator [99].

At half-filling, $\mu/D = 0$ and we recover all results of Ref. [35]. Specifically, we find a first order metal to VB insulator transition. In the metallic phase just before the transition, singlet superconductivity emerges. In Fig. 4.1 we show as function of U/D the behavior of the inter-layer, $\Delta_\perp$ and intra-layer, $\Delta_{||}$, superconducting order parameters, defined as

$$\Delta_\perp = \langle \Psi_G | \, c^\dagger_{\mathbf{R},1\uparrow} c^\dagger_{\mathbf{R},2\downarrow} + c^\dagger_{\mathbf{R},2\uparrow} c^\dagger_{\mathbf{R},1\downarrow} \, | \Psi_G \rangle, \tag{4.9}$$

$$\Delta_{||} = \langle \Psi_G | \, c^\dagger_{\mathbf{R},i\uparrow} c^\dagger_{\mathbf{R}',i\downarrow} + c^\dagger_{\mathbf{R}',i\uparrow} c^\dagger_{\mathbf{R},i\downarrow} \, | \Psi_G \rangle, \tag{4.10}$$

where $\mathbf{R}$ and $\mathbf{R}'$ are nearest neighbor sites on layer $i = 1, 2$. We find that, near the first order transition that we think identifies the actual Mott transition, both order parameters are finite and have opposite sign, the so-called $d_{z^2-r^2}$ symmetry known to be dominant in the two-chain model [92], and which QMC simulations [103, 104] indicate as the leading pairing instability. The variational energy that we obtain appears to be slightly lower than that found in Ref. [35],

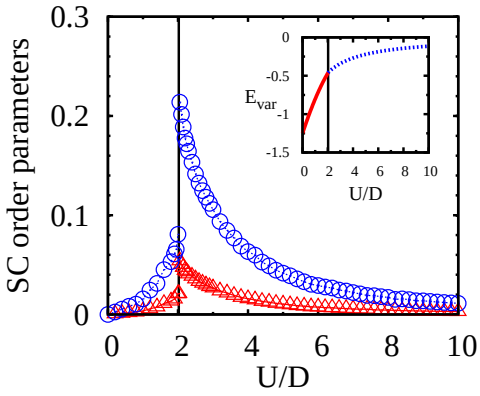

Figure 4.1: (Color online) Inter-plane (blue circles) and, with reversed sign, intra-plane (red triangles) superconducting order parameters at half-filling as function of U/D. The vertical line indicates the first order transition that we think identifies the on-set of Mott insulating behavior. Inset shows the variational energy in units of D

as one could have expected due to the larger number of variational parameters. Nonetheless, the critical U_c at the Mott transition is only slightly reduced to $U_c/D \simeq 2.02$ for $t_\perp/D = 0.5$. We note that the phase at $U > U_c$, that we believe is Mott insulating, still shows a finite superconducting order parameter that dies out upon increasing U. As discussed in [35], we think this might be a spurious result of our variational approach that lacks intersite charge correlations crucial in stabilizing a genuine Mott insulating phase [106].

We study finite hole doping by varying $\mu/D < 0$ at different values of U/D.

4.4.1 The non-interacting system

Before discussing the variational results, we briefly sketch the behavior of the doped non-interacting system, $U/D = 0$. The inter-layer coupling gives rise to bonding and antibonding bands, see Eq. (4.2). With the chosen value of $t_\perp = 0.5D$, these bands overlap at half-filling and the system displays a metallic behavior. When the chemical potential is lowered, holes are injected into the system inducing a depletion of both bands until, at a given value of the chemical potential, the upper (antibonding) band empties. For the chosen $t_\perp$

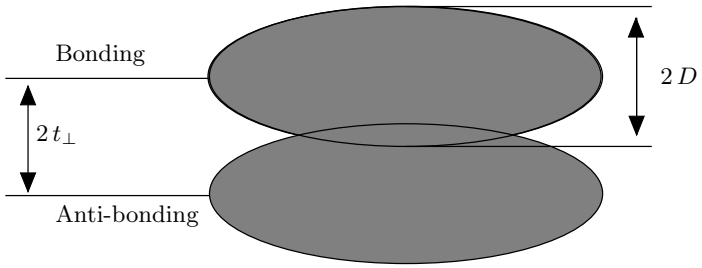

Figure 4.2: The non-interacting density of states of the lattice of dimers. The bonding and anti-bonding state of each dimer give rise to two bands that overlap, leading to a metallic phase in the absence of interaction.

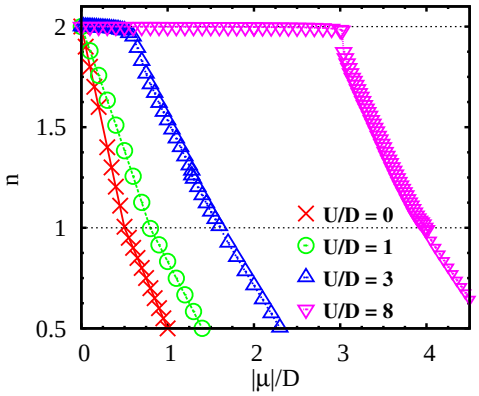

Figure 4.3: (Color online) Average density n summed over both layer as a function of the chemical potential $\mu < 0$ for selected values of interaction U/D.

and for a flat density of states the complete depletion of the antibonding band happens at $\mu = 0.5D$, corresponding to quarter filling $n = 1$. As a consequence, both the intra-layer (E_{hop}) and inter-layer ($E_\perp$) hopping contributions display a discontinuity in their first derivatives at quarter filling, signaling that the antibonding band is no longer contributing. The total energy however remains smooth for any value of μ (or equivalently n), as it should.

When $U/D \neq 0$, the behavior that we find depends crucially if U is smaller or greater than U_c, namely if the half-filled state is a metal or an insulator.

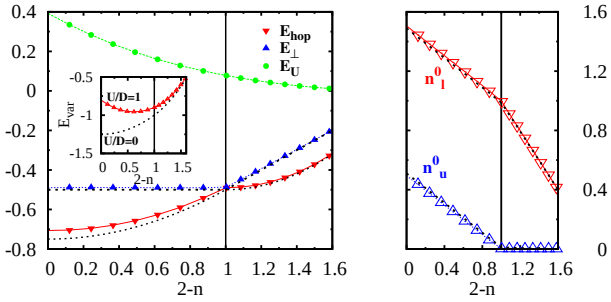

Figure 4.4: (Color online) Left panel: The different contributions to the variational energy as a function of doping for $U/D = 1$ and per lattice site $\mathbf{R}$, i.e. summed over both layer. As a reference, the behavior of non-interacting inter- and intra-layer hopping contributions is plotted (dotted lines). In the inset the total energy $E_{var}(n) = E_{var} + \mu n$ is shown: despite the cusp observed in the hopping contributions, the evolution of $E_{var}(n)$ is smooth. Right panel: Occupation of the variational lower and upper bands as function of n. Dotted lines represent average occupation of even and odd orbitals.

4.4.2 Doping the metal at $U < U_c$

As long as $U < U_c$, any change of μ induces a continuous change in the total particle number; a finite compressibility signal of a metallic behavior, as shown in Fig. 4.3. Alike the uncorrelated case, a cusp appears in the evolution of n at quarter-filling, that we explain seemingly as the depletion of the antibonding band. Indeed, when $U < U_c$, the metallic solution evolves just like the non-interacting case. The main effect of interaction is to slightly reduce inter- and intra-layer hopping contributions with respect to their uncorrelated counterparts, as shown in Fig. 4.4 where we plot the different contributions E_{hop}, $E_\perp$ and E_U to the variational energy. The intra-layer hopping contribution E_{hop} diminishes in absolute value with increasing doping because of the depletion of the bands, as it occurs in the non-interacting system; at quarter-filling it displays a cusp and correspondingly the inter-layer hopping $E_\perp$ starts to rapidly decrease, the effects of U being more and more negligible as the low-density regime is approached. In the right panel of Fig. 4.4 we show the occupancies n_l^0 and n_u^0 of the variational lower and upper bands, respectively, which are obtained by diagonalizing the associated variational Hamiltonian, Eq. (4.5),

and actually coincide with the eigenvalues of the single-particle density matrix. As in the uncorrelated system, the occupancy of the upper band vanishes at quarter filling. We stress the fact that in the present approach these states are variationally determined and may not correspond to the even and odd combinations of the original operators. However, as long as $U < U_c$, we find that the average values of bonding and antibonding band occupancies, n_e and n_o, almost coincide with, respectively, n_l^0 and n_u^0.

Concerning superconductivity, we find that the inter-layer order parameter, Eq. (4.9), is extremely small, practically zero within our numerical precision, see Fig. 4.5. The intra-layer order parameter strictly follows the inter-layer one, hence is also zero.

4.4.3 Doping the VB Mott insulator at $U > U_c$

When $U > U_c$, i.e. when the half-filled system is insulating, the particle number remains stuck to its half-filled value $n = 2$ until $|\mu| \leq |\mu^*| \approx (U - U_c)/2$. This simply follows from the existence of the Mott gap at half-filling. Upon doping, i.e. when $|\mu| > |\mu^*|$, a metallic behavior is clearly found. However, within our numerical precision we can not establish whether the evolution from the insulator to the metal occurs smoothly (yet with a diverging compressibility) or through a weak first-order transition. Till the largest value of U we considered, we could not find any appreciable discontinuity in the evolution of n at large doping, unlike for $U < U_c$ where a cusp is observed at quarter filling. In addition, contrary to the case $U < U_c$, here we find a clear superconducting signal between half and quarter filling, see e.g. the behavior of $\Delta_\perp$, Eq. 4.9, shown in Fig. 4.5. We note that $\Delta_\perp$ has a non-monotonous behavior, first increases quite rapidly with U and for larger values decreases. Like at half-filling, a finite $\Delta_\perp$ produces through Eq. (2.8) also a finite intra-layer $\Delta_{||}$, Eq. 4.10, not shown here, which happens to have opposite sign.

Let us now consider in detail the energetic balance for $U > U_c$ and its differences with respect to $U < U_c$. At very large U (not shown), as holes are injected into the system, both intra- and inter-layer hopping contributions first increase in absolute value, then saturate around approximatively quarter-filling, and eventually decrease as the low-density regime is attained, as ex-

pected when approaching the bottom of the variational bands. In other words, the behavior at large U between half- and quarter-filling is quite different from the non-interacting case, while becomes quite similar below. This points to a very different influence of a strong interaction close to half-filling and far away from it and, indirectly, emphasizes the role of the superconductivity that we find for $2 > n > 1$. For $U \gtrsim U_c$, i.e. closer to the half-filled metal-insulator transition, the picture is slightly different, as shown in Fig. 4.6 for $U/D = 3$. To begin with, at small dopings the system gains in intra-layer hopping energy while the inter-layer one seems to be slightly reduced. Remarkably, even if the total energy is, within our numerical accuracy, a smooth function of n, both hopping contributions display a discontinuity at $\mu/D \simeq 1.28$, which corresponds to a local density of $n \approx 1.27$. Here the occupation of the upper variational band goes to zero (cfr. right panel of Fig. 4.6), even though nothing similar occurs in the occupation of the physical antibonding band. At this filling fraction, the inter-layer hopping energy gain has an upward jump, contrary to the intra-layer one, even though further doping leads to a reduction of both. A drop in the amplitude of the superconducting order parameter $\Delta_\perp$ is also found at this point. Further doping diminishes $\Delta_\perp$, which vanishes approximatively at quarter filling. A similar feature is observed in another quantity. Indeed, just like n_l^0 and n_u^0 may not correspond to the occupation of the bonding and antibonding bands, $n^0 = n_l^0 + n_u^0$, which is the average density of the BCS-like variational wavefunction, may differ from the physical one. In the inset of Fig. 4.5 we show their difference for $U/D = 3$. We observe that they actually deviate when superconductivity is found and their difference jumps down abruptly for $n < 1.27$.

4.5 Conclusions

In this work we have studied by means of an extension of the Gutzwiller approximation the effect of doping a bilayer Hubbard model. We have considered a value of the inter-layer hopping $t_\perp$ such that, at half-filling, the model should undergo a direct transition at $U = U_c$ from a metal to a non-magnetic Mott insulator, a valence bond crystal consisting of inter-layer dimers. This choice offers the opportunity to study how a valence bond crystal liquefies either by

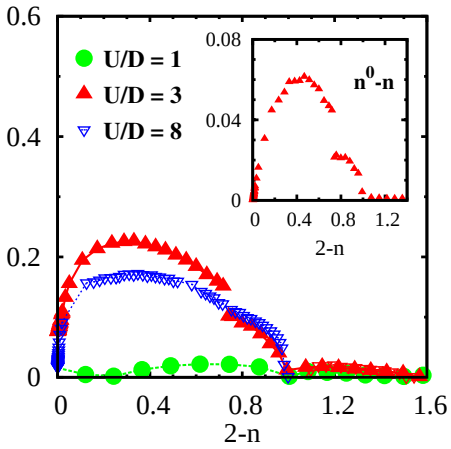

Figure 4.5: (Color online) Superconducting inter-layer order parameter $\Delta_\perp$ for different U/Ds. In the inset we plot the difference between the local densities of the BCS variational wavefunction $|\Psi_0\rangle$ and of the actual one $|\Psi_G\rangle$, at $U/D = 3$.

reducing the Coulomb repulsion keeping the density fixed at one electron per site, or by adding mobile holes. The melting upon decreasing U was already shown [35] to lead to a superconducting phase intruding between the valence bond insulator at large $U > U_c$ and the normal metal at weak $U \ll U_c$. Here we show that superconductivity arises also upon melting the valence bond crystal by doping. In other words, the superconducting dome that exists at half-filling close to U_c extends into a whole region at finite doping. The maximum superconducting signal is found at 20% doping, and beyond that it smoothly diminishes, disappearing roughly at quarter filling within our choice of parameters. These results are appealing as they show that the well established behavior of a two-leg Hubbard ladder [35, 107, 108, 92] seems to survive in higher dimensions, actually in the infinite-dimension limit where our Gutzwiller approximation becomes exact. It is obvious that, in spite of all improvements of the Gutzwiller variational approach, to which we contribute a bit with this work, this method remains variational hence not exact. Therefore it is still under question if superconductivity indeed arises by metallizing the valence bond Mott insulating phase of a Hubbard bilayer, which we believe is an important issue of broader interest than the simple bilayer model we have investigated [64]. There are actually quantum Monte Carlo simulations [100, 103, 104, 101] that

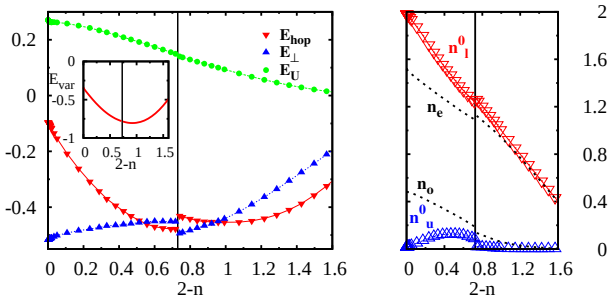

Figure 4.6: (Color online) Left panel: Contributions to the variational energy as function of doping for $U/D = 3$. In the inset the total energy $E_{var}(n) = E_{var} + \mu n$ is shown: despite the discontinuities observed in the hopping contributions, the evolution of $E(n)$ is, to our numerical accuracy, smooth. Right panel: Occupancies of lower, n_l^0 and upper, n_u^0, variational bands as function of n. Dotted lines represent average occupation of even, n_e, and odd, n_o, orbitals. Note that the insulating phase at half-filling is identified by the lower band fully occupied and the upper one empty. The latter empties again for doping $2 - n > 0.73$.

partially support our results as they show a pronounced enhancement of superconducting fluctuations close to the half-filled Mott insulator. However a true superconducting phase is still unaccessible to the lowest temperatures that can be reached by quantum Monte Carlo. On the other hand, dynamical mean field calculations, that can access zero temperature phases, did not so far looked for superconductivity [105, 102]. Therefore we think it would be worth pursuing further this issue.

Chapter 5

Transport in quantum dots within the Gutzwiller approach

Nanocontacts of quantum dots, single molecules or atoms, and nanowires are ideal candidates to realize electronic devices where a source-drain current across the contact can be magnetically controlled. Indeed, because of the low dimensionality of the contact region, electronic correlations grow in strength and may stabilize a local magnetism that influences electron tunneling. The Kondo-like zero-bias anomalies first observed in quantum dots [66] are just the simplest manifestation of such a local magnetism, but one can foresee even more spectacular phenomena, like giant magnetoconductance [109]. From the theory side, this is a complicated problem first of all because electronic correlation is the main actor and is difficult to treat, and secondly because the inelastic tunneling spectrum requires full out-of-equilibrium calculations. Many complementary techniques have been used to characterize the nanocontact at equilibrium. For instance ab initio LDA calculations can provide the electronic structure and predict whether magnetism could indeed be stabilized [109, 110, 111], at least at the mean field level. Inclusion of quantum fluctuations requires many-body techniques, like numerical renormalization group [112, 113], which are often applied to oversimplified models, like the single-orbital Anderson impurity model, although there are recent attempts to join together the two approaches [114, 115, 116]. Unfortunately, out of equilibrium properties are much more difficult to study. Apart from many-body Keldish perturbation

theory [117], many sophisticated numerical techniques have been developed in recent years to cope simultaneously with out-of-equilibrium and strong correlations, [118, 119, 120, 121, 122, 123]. However, given the complexity of the electronic structure that may arise at a nanocontact e.g. of a molecule or a bridging transition metal atom, it would be desirable to have at disposal approximate techniques enough simple and flexible to deal with realistic situations otherwise prohibitive with more accurate numerical approaches, as those previously mentioned. In this paper we shall propose one of such methods that is based on an out-of-equilibrium extension of the conventional Gutzwiller approximation [6, 7] for correlated electron systems.

5.1 The problem

We consider two biased macroscopic leads described by non-interacting electrons coupled to a bridging region described by discrete electronic multiplets

$$\mathcal{H} = \mathcal{H}_0 + V + \mathcal{H}_{int}, \tag{5.1}$$

where V describes the tunnelling between the leads and the nanocontact and $\mathcal{H}_{int}$ describes the local interaction of the nanocontact.

One assumes that initially the leads are not coupled through the bridging region, each lead being subject to a different electrochemical potential. Such a situation can be described by a density matrix

$$\rho_0 = e^{-\beta\mathcal{H}_0^*(\Phi)}/\mathrm{Tr}(e^{-\beta\mathcal{H}_0^*(\Phi)}) \tag{5.2}$$

where

$$\mathcal{H}_0^*(\Phi) = \mathcal{H}_0 + \Phi Y_0, \tag{5.3}$$

with $\mathcal{H}_0$ the non-interacting Hamiltonian of the independent left (L) and right (R) leads plus the nanocontact, and

$$Y_0 = (N_L - N_R)/2 \tag{5.4}$$

that describes the potential drop and commutes with $\mathcal{H}_0$ – the initial state is stationary though out-of-equilibrium, equilibrium meant to be the two leads at the same chemical potential.

Suddenly the coupling to the bridging region is switched on - namely the Hamiltonian changes from $\mathcal{H}_0 + \mathcal{H}_{int}$ into $\mathcal{H} = \mathcal{H}_0 + \mathcal{H}_{int} + V$ - and a current starts to flow. If

$$U(t) = e^{-i\mathcal{H}t} \tag{5.5}$$

is the time evolution operator with the full interaction, the initial density matrix ρ_0 evolves maintaining the functional form of a Boltzmann exponential

$$\rho(t) = e^{-\beta\mathcal{H}^*(t,\Phi)}/\mathrm{Tr}(e^{-\beta\mathcal{H}^*(t,\Phi)}) \tag{5.6}$$

where

$$\mathcal{H}^*(t,\Phi) = \mathcal{H}(t) + \Phi Y(t) \tag{5.7}$$

and

$$\begin{aligned} \mathcal{H}(t) &= U(t)(\mathcal{H}_0 + \mathcal{H}_{int})U(t)^\dagger, \\ Y(t) &= U(t)Y_0U(t)^\dagger \end{aligned} \tag{5.8}$$

For time t sufficiently large, namely after a transient time T, the system reaches a steady state with constant current. If we are interested only in steady state properties, a good starting point is offered by Hershfield's results [67]. Hershfield showed that the stationary state value of certain observables coincide with their equilibrium value obtained through an effective density matrix

$$\rho = e^{-\beta\mathcal{H}^*(\Phi)}/\mathrm{Tr}(e^{-\beta\mathcal{H}^*(\Phi)}), \tag{5.9}$$

with

$$\mathcal{H}^*(\Phi) = \mathcal{H} + \Phi Y, \tag{5.10}$$

being Y the time evolution, in the Schrödinger picture, of Y_0 and still satisfying[1]

$$[\mathcal{H}, Y] = 0. \tag{5.11}$$

Should Y be known, steady state properties could be obtained, in principle, by any equilibrium technique.

[1]The physical meaning of (5.11) is that the steady state can be reached only when all terms of Y_0 that do not commute with the Hamiltonian $\mathcal{H}$ have been filtered out.

5.2 The resonant-model out of equilibrium

Let us consider the simple case of a non-interacting single-level bridging region

$$\mathcal{H} = \mathcal{H}_0 + \hat{V}, \tag{5.12}$$

with

$$\begin{aligned} \mathcal{H}_0 &= \sum_{\alpha=-1,1} \sum_{k\sigma} \epsilon_k \, c^\dagger_{\alpha k\sigma} c_{\alpha k\sigma} + \sum_\sigma \epsilon_d \, d^\dagger_\sigma d_\sigma, \\ \hat{V} &= \sum_{\alpha=-1,1} \sum_{k\sigma} \frac{V_k}{\sqrt{\Omega}} \, d^\dagger_\sigma c_{\alpha k\sigma} + H.c.\,, \end{aligned} \tag{5.13}$$

where $c^\dagger_{\alpha k\sigma}$ creates a conduction electron on the left ($\alpha = -1$) or right ($\alpha = 1$) lead with quantum number k and spin σ while $d^\dagger_\sigma$ creates an electron into the dot with spin σ, and Ω is the quantization volume of the system. Notice that, quite generally only a single channel of conduction electrons is coupled to the impurity, so that the model can always be mapped onto two one-dimensional leads hybridized at the contiguous edges with an impurity. Therefore it is perfectly legitimate to regard the quantum number k as one-dimensional momentum and Ω as the linear size of the system.

The non-equilibrium Hamiltonian

$$\mathcal{H}^*(\Phi) = \mathcal{H} + \Phi Y \tag{5.14}$$

can be calculated explicitly in this simple case. It can be proven [67] that, in the thermodynamic limit and in the absence of bound states,

$$\begin{aligned} \mathcal{H} &= \sum_{\alpha=-1,1} \sum_{k\sigma} \epsilon_k \, \psi^\dagger_{\alpha k\sigma} \, \psi_{\alpha k\sigma}, \\ Y &= \sum_{\alpha=-1,1} \sum_{k\sigma} \frac{\alpha}{2} \, \psi^\dagger_{\alpha k\sigma} \, \psi_{\alpha k\sigma}\,; \end{aligned} \tag{5.15}$$

where $\psi^\dagger_{\alpha k\sigma}$ are the fermionic creation operators that generate the left ($\alpha = -1$) and right ($\alpha = 1$) incident scattering waves

$$\begin{aligned} \psi^\dagger_{\alpha k\sigma} &= \left(1 + \frac{1}{\epsilon_k - \mathcal{H} + i\,0^+} \, \hat{V}\right) c^\dagger_{\alpha k\sigma} \\ &= c^\dagger_{\alpha k\sigma} + \frac{V_k}{\sqrt{\Omega}} \, g_d(\epsilon_k) \, d^\dagger_\sigma \\ &\quad + \sum_{\alpha' k'\sigma'} \frac{V_k V_{k'}}{\Omega} \, \frac{g_d(\epsilon_k)}{\epsilon_k - \epsilon_{k'} + i\,0^+} \, c^\dagger_{\alpha' k'\sigma'}\,; \end{aligned} \tag{5.16}$$

being $g_d(\epsilon)$ the retarded Green's function of the impurity at equilibrium, which is, in the infinite bandwidth limit,

$$g_d(\epsilon) = \frac{1}{\epsilon - \epsilon_d + i\Gamma}\,. \tag{5.17}$$

We underline that Eq. (5.16) is meaningful only in the termodinamic limit, i.e. when $\Omega \to \infty$. For a finite system the time evolution of an incident state

$$|\psi^{in}_{\alpha k\sigma}\rangle = c^\dagger_{\alpha k\sigma}|0\rangle \tag{5.18}$$

oscillates, namely it doesn't converge to a well defined scattering state

$$|\psi_{\alpha k\sigma}\rangle = \psi^\dagger_{\alpha k\sigma}|0\rangle \tag{5.19}$$

Sobstituting Eq. (5.16) in Eq. (5.15) we find that

$$\begin{aligned} Y \;=\; & \sum_{\alpha k\sigma} \frac{\alpha}{2}\, c^\dagger_{\alpha k\sigma} c_{\alpha k\sigma} \\ & + \sum_{\alpha k\sigma} \frac{\alpha}{2} \sum_{\alpha' k'} \frac{V_k V_{k'}}{\Omega}\, \frac{g(\epsilon_{k'})}{\epsilon_k - \epsilon_{k'} + i0^+}\, c^\dagger_{\alpha' k'\sigma} c_{\alpha k\sigma} + H.c. \\ & + \sum_{\alpha k\sigma} \frac{\alpha}{2}\, \frac{V_k}{\sqrt{\Omega}}\, g(\epsilon_k)\, d^\dagger_\sigma c_{\alpha k\sigma} + H.c. \end{aligned} \tag{5.20}$$

The scattering states (5.16) are, in the thermodynamic limit, a complete basis

$$\sum_{\alpha k\sigma} \psi^\dagger_{\alpha k\sigma}\, \psi_{\alpha k\sigma} = \sum_{\alpha k\sigma} c^\dagger_{\alpha k\sigma} c_{\alpha k\sigma} + \sum_\sigma d^\dagger_\sigma d_\sigma\,. \tag{5.21}$$

Eq. (5.21) allows us to formally expand the c and d operators in terms of scattering states

$$\begin{aligned} c^\dagger_{\bar\alpha \bar k\bar\sigma} \;&=\; \psi^\dagger_{\bar\alpha \bar k\bar\sigma} + \sum_{\alpha k} \frac{V_{\bar k} V_k}{\Omega}\, \frac{g^*(\epsilon_k)}{\epsilon_k - \epsilon_{\bar k} - i0^+}\, \psi^\dagger_{\alpha k\bar\sigma} \\ d^\dagger_{\bar\sigma} \;&=\; \sum_{\alpha k} \frac{V_k}{\sqrt{\Omega}}\, g^*(\epsilon_k)\, \psi^\dagger_{\alpha k\bar\sigma}\,, \end{aligned} \tag{5.22}$$

and to calculate the average of any operator using the result

$$\langle\Psi(\Phi)|\, \psi^\dagger_{\alpha k} \psi_{\alpha' k'}\, |\Psi(\Phi)\rangle = \delta_{\alpha\alpha'}\delta_{kk'}\, f\left(\epsilon_k + \phi\frac{\alpha}{2}\right) \tag{5.23}$$

- being $|\Psi(\Phi)\rangle$ the ground state of $\mathcal{H}^*(\Phi)$ and $f(\epsilon)$ the Fermi function. The correct value of the average is finally obtained taking the limit for $\Omega \to \infty$ of the result. It can be proven that the obtained value is the same that one could obtain within the Keldish technique.

In order to state variationally the problem for finding the solution of the Hershfield Hamiltonian $\mathcal{H}^*(\Phi)$ in the presence of interaction we should be able to evaluate the energy

$$\delta\mathcal{E}_\Phi(\Psi) = \langle\Psi|\,\mathcal{H}^*(\Phi)\,|\Psi\rangle - \mathcal{E}_0\,, \tag{5.24}$$

being $\mathcal{E}_0$ the minimum energy of the Hershfield Hamiltonian $\mathcal{H}_0^*(\Phi)$ in absence of tunnelling

$$\mathcal{H}_0^*(\Phi) = \sum_{\alpha=-1,1}\sum_{k\sigma}\left(\epsilon_k + \Phi\frac{\alpha}{2}\right)c^\dagger_{\alpha k\sigma}c_{\alpha k\sigma} + \sum_\sigma \epsilon_d\, d^\dagger_\sigma d_\sigma, \tag{5.25}$$

and we should minimize $\delta\mathcal{E}_\Phi(\Psi)$, which is of order $1/\Omega$ with respect to $\mathcal{E}_0$, with respect to $|\Psi\rangle$.

Unfortunately, as it is explicitly proven in appendix A.2.1, $\delta\mathcal{E}_\Phi(\Psi)$ is ill defined in the above formulation that implicitly assume the thermodynamic limit; it contains diverging terms which partly cancel each other to give a result of order one. The appearence of infinities can be easily traced back observing that the first term of Eq. (5.20) is

$$\sum_{\alpha k\sigma}\frac{\alpha}{2}\,c^\dagger_{\alpha k\sigma}c_{\alpha k\sigma} \equiv \frac{\delta\hat{\mathcal{Q}}}{2}\,, \tag{5.26}$$

where $\hat{\mathcal{Q}}$ is the operator that represents the charge difference between the two leads. The contribution of $\delta\hat{\mathcal{Q}}$ to the variational energy $\delta\mathcal{E}_\Phi(\Psi)$ is, defining $|\Psi_0\rangle$ the ground state of $\mathcal{H}_0^*(\Phi)$,

$$\delta\mathcal{Q}_\Phi(\Psi) = \langle\Psi|\,\hat{\mathcal{Q}}\,|\Psi\rangle - \langle\Psi_0|\,\hat{\mathcal{Q}}\,|\Psi_0\rangle\,, \tag{5.27}$$

which is the charge passed from one lead to the other during the "infinite" transient time necessary to reach the steady state. This is obviously infinite, hence, to produce at the end something of order one, which is the contribution of the impurity, other singular terms should partly cancel it. This cancellation of singularities is hard to accomplish in the above formulation. In order to

circumvent such a difficulty, we propose here an alternative but well defined procedure.

We consider once again the Hamiltonian (5.12) at finite size Ω and at zero bias, and introduce s- and p-wave states, omitting the spin label, through

$$\begin{aligned} s_k &= \frac{1}{\sqrt{2}}\left(c_{+1k} + c_{-1k}\right), \\ p_k &= \frac{1}{\sqrt{2}}\left(c_{+1k} - c_{-1k}\right). \end{aligned}$$

We assume that the quantum numbers k label discrete one-dimensional momenta, and the single-particle energy is a simple function of them: $\epsilon_k = \epsilon(k)$. The addition of the impurity has two effects: (1) the number of allowed momenta k in the s-channel increases by one – the impurity is absorbed in the conduction sea; (2) the energy in the s-channel as function of momenta changes into

$$\epsilon_k = \epsilon(k) \to \epsilon_k^* = \epsilon\left(k - \frac{\delta(\epsilon_k^*)}{\Omega}\right),$$

where $\delta(\epsilon)$ are so-called phase-shifts. The diagonalized Hamiltonian then reads

$$\begin{aligned} \mathcal{H}_0 + \hat{V} &= \sum_{\text{allowed}k's} \epsilon\left(k - \frac{\delta(\epsilon_k^*)}{\Omega}\right) \bar{s}_k^\dagger \bar{s}_k + \epsilon(k)\, p_k^\dagger p_k \\ &\simeq \Omega \int \frac{dk}{\pi}\, \epsilon\left(k - \frac{\delta(\epsilon_k^*)}{\Omega}\right) \bar{s}_k^\dagger \bar{s}_k + \epsilon(k)\, p_k^\dagger p_k, \end{aligned} \tag{5.28}$$

the last expression being the continuous limit, where the difference between the allowed set of k's in the two channels disappears, and $\bar{s}^\dagger$ being the eigen-operators of the s-channel plus impurity Hamiltonian. One can indeed show that the continuous limit reproduces all known results in scattering theory. For instance, the change in electron number is found to be

$$\begin{aligned} \delta N &= \Omega \int \frac{dk}{\pi} \left[f\left(\epsilon\left(k - \frac{\delta(\epsilon_k^*)}{\Omega}\right)\right) - f(\epsilon(k)) \right] \simeq \Omega \int \frac{dk}{\pi} \frac{\partial f(\epsilon_k)}{\partial \epsilon_k} \frac{\partial \epsilon_k}{\partial k} \frac{\delta(\epsilon_k)}{\Omega} \\ &= \int \frac{d\epsilon}{\pi} \frac{\partial f(\epsilon)}{\partial \epsilon}\, \delta(\epsilon) = \frac{\delta(0)}{\pi}, \end{aligned}$$

which is the well known Friedel's sum rule. Formally, one can now introduce

back right and left incident waves by

$$\psi_{+1k} = \frac{1}{\sqrt{2}}\left(\bar{s}_k + p_k\right),$$
$$\psi_{-1k} = \frac{1}{\sqrt{2}}\left(\bar{s}_k - p_k\right),$$

which is however strictly valid only in the continuous limit. Assuming blindly Hershfield's results to hold, one would conclude that the bias evolves in the steady state into the operator

$$\Phi\, Y \simeq \frac{\Phi}{2}\sum_k \psi^\dagger_{+1k}\psi_{+1k} - \psi^\dagger_{-1k}\psi_{-1k} = \frac{\Phi}{2}\sum_k \bar{s}^\dagger_k p_k + p^\dagger_k \bar{s}_k. \tag{5.29}$$

One can diagonalize $\mathcal{H}_0 + \hat{V} + \Phi\, Y$ and calculate the total energy $\mathcal{E}_\Phi$ to find, up to order $O(1)$ in the volume,

$$\begin{aligned}\mathcal{E}_\Phi &= \Omega \int \frac{dk}{\pi} \sum_{\alpha=\pm 1} \left(\epsilon(k) + \alpha\frac{\Phi}{2}\right) f\left(\epsilon(k) + \alpha\frac{\Phi}{2}\right) \\ &\quad - \int \frac{d\epsilon}{2\pi}\delta(\epsilon)\left[f\left(\epsilon + \frac{\Phi}{2}\right) + f\left(\epsilon - \frac{\Phi}{2}\right)\right] + O\left(\frac{1}{\Omega}\right) \\ &\quad \equiv \mathcal{E}^0_\Phi - \int \frac{d\epsilon}{2\pi}\delta(\epsilon)\left[f\left(\epsilon + \frac{\Phi}{2}\right) + f\left(\epsilon - \frac{\Phi}{2}\right)\right].\end{aligned} \tag{5.30}$$

In the absence of bias, this expression reduces to the well known result at equilibrium. We will assume in what follows that Eq. (5.30) is the "energy" of the Hershfield Hamiltonian. At equilibrium is well known that

$$\delta(\epsilon) = -\mathrm{Im}\ \ln\left(\frac{\epsilon + i0^+ - \epsilon_d - \Delta(\epsilon + i0^+)}{\epsilon + i0^+ - \epsilon_d}\right), \tag{5.31}$$

where

$$\Delta(z) = \frac{1}{\Omega}\sum_{k\alpha}\frac{V_k^2}{z - \epsilon_k} \tag{5.32}$$

is the hybridization function. An alternative way of writing (5.30) is

$$\mathcal{E}_\Phi - \mathcal{E}^0_\Phi = -T\sum_n \sum_\alpha \ln\left(\frac{i\epsilon_n + \alpha\frac{\Phi}{2} - \epsilon_d - \Delta(i\epsilon_n)}{i\epsilon_n + \alpha\frac{\Phi}{2} - \epsilon_d}\right), \tag{5.33}$$

where ϵ_n are Matsubara frequencies. This expression has been derived in an alternative way in the appendix A.

We observe that the value of $\delta\mathcal{E}_\Phi$ defined in Eq. (5.33) is exactly the $1/\Omega$ contribution to the average of $\mathcal{H}$ calculated on the ground state of the Hershfield Hamiltonian (5.15) defined through the scattering states, as it is proved explicitly in Appendix A. From this point of view $\delta\mathcal{E}_\Phi$ can be interpreted as the energy of the system gained, in the presence of the bias, during the transient time necessary to reach the steady state after the introduction of the dot, that is not zero because the action to switch on the tunnelling term is "external". In other words, $\delta\mathcal{E}_\Phi$ is finite because the system is not isolated.

We conclude this section calculating explicitly $\delta\mathcal{E}_\Phi$ for the non-interacting model Eq. (5.12). Let us assume that the density of states is flat

$$\begin{aligned} \Delta(z) &= \int \frac{d\epsilon}{\pi} \frac{\Gamma(\epsilon)}{z-\epsilon} \\ \Gamma(\epsilon) &= \Gamma \chi_{[-1,1]}(\epsilon)\,, \end{aligned} \tag{5.34}$$

where $\chi_{[-1,1]}(\epsilon)$ is 1 if $\epsilon \in [-1,1]$ and is 0 otherwise, and that $\Gamma \ll W = 1$. It can be easily verified that

$$\Gamma^2 \frac{\partial}{\partial\Gamma}\left(\frac{\delta\mathcal{E}_\Phi(\Gamma)}{\Gamma}\right) = \epsilon \arctan\left(\frac{\Gamma}{\epsilon}\right)\Bigg]_{-1}^{-\frac{\Phi}{2}} \tag{5.35}$$

We observe that when $\Phi = 0$ the right member of Eq. (5.35) is $-\Gamma$, so that the solution of Eq. (5.35) is

$$\delta\mathcal{E}_0 = -\frac{2}{\pi}\,\Gamma \log\left(\frac{e}{\Gamma}\right)\,, \tag{5.36}$$

while, when

$$W \gg \Phi \gg \Gamma\,, \tag{5.37}$$

the right member of Eq. (5.35) vanishes, so that

$$\delta\mathcal{E}_\Phi = \frac{2}{\pi}\,\Gamma \log\left(\frac{\Phi}{2}\right)\,. \tag{5.38}$$

5.3 The concept of quasi-particles out of equilibrium

We consider now the general interacting system described by the Hamiltonian

$$\mathcal{H} = \mathcal{H}_0 + V + \mathcal{H}_{int}, \tag{5.39}$$

We know that if we prepare the two leads at a different chemical potentials and we let it evolve within the interacting Hamiltonian

$$U(t) = e^{-i\mathcal{H}t}, \tag{5.40}$$

for times t longer than some transient time T the final non-equilibrium state is described by the Hershfield Hamiltonian

$$\mathcal{H}^*(\Phi) = \mathcal{H} + \Phi Y, \tag{5.41}$$

formally defined in Eq. (5.8)

In general Y is a complicated many body operator that must satisfy Eq. (5.11) and in addition share the same symmetry properties as Y_0, i.e. a spin-singlet operator odd under interchanging the two leads. Therefore, generally the steady-state Hamiltonian $\mathcal{H}^*(\Phi)$ is an interacting one, the interaction presumably remaining local as it was originally. Furthermore, since the nanocontact can not change the bulk properties of the leads, e.g. inducing a spontaneous symmetry breaking, $\mathcal{H}^*(\Phi)$ should still describe a metal. It is therefore tempting to assume that, if in the absence of external bias the system, leads plus nanocontact, is described by a local Fermi liquid theory in the Nozières sense [68], which is generally the case, the same should hold even in the steady state after the bias is applied. It then follows that it should be possible to represent the low energy/temperature/bias properties in terms of weakly interacting *quasi-particles*, which, by continuity with the non-interacting case, should be better regarded as *renormalized* scattering states with an Hamiltonian of the same form as (5.15) with renormalized (bias dependent) energies plus additional weak local-interaction terms [68]. This local Fermi-liquid assumption seems to us quite plausible. However, since the bias is coupled to a non-conserved quantity, the charge difference between the leads, the effective bias felt by the

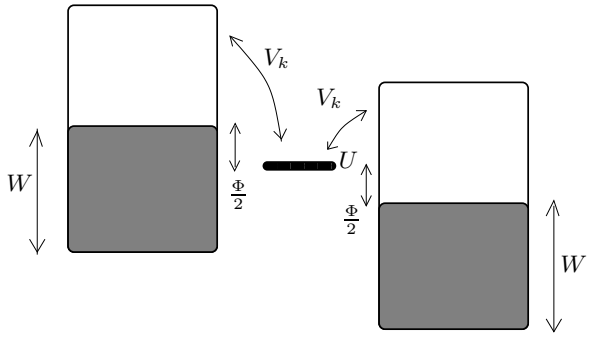

Figure 5.1: The single dot system

quasi-particles will generally differ from the applied one and the quasi-particle current not correspond to the real one. This implies that the current can not be expressed simply in terms of Landau parameters and an explicit calculation is required.

5.4 The Gutzwiller approximation at equilibrium

Let us forget for a moment the bias and consider the same problem at equilibrium. Although the method we shall present is quite general, for sake of simplicity we shall show how it works in the simple case of a bridging region described by a single-orbital Anderson impurity model at half-filling. The equilibrium Hamiltonian is

$$\begin{aligned} \mathcal{H} &= \sum_{\alpha k\sigma} \epsilon_k \, c^\dagger_{\alpha k\sigma} c_{\alpha k\sigma} + \sum_{\alpha k\sigma} \frac{V_k}{\sqrt{\Omega}} \, d^\dagger_\sigma c_{\alpha k\sigma} + H.c. \\ &+ \frac{U}{2}(n_d - 1)^2 \equiv H^0 + \hat{U} \end{aligned} \tag{5.42}$$

The physical properties of the above Anderson impurity model are very well known [43]. For large U the model effectively maps into a Kondo model, the impurity electron behaving as a local moment Kondo screened by the conduction electrons. A simple way to describe qualitatively and to some extent also quantitatively the Kondo screening is by a Gutzwiller-type of variational

wavefunction [14, 13]

$$|\Psi\rangle = \mathcal{P}_d\,|\Psi_0\rangle \tag{5.43}$$

where $\mathcal{P}_d$ is an operator that modifies the relative weights of the impurity electronic configurations with respect to the uncorrelated wavefunction $|\Psi_0\rangle$, and $|\Psi_0\rangle$ is the ground state of a non-interacting variational resonant level Hamiltonian.

The variational procedure amounts to optimize both the local projector $\mathcal{P}_d$ as well as the non-interacting wavefunction $|\Psi_0\rangle$ by minimizing the average value of the Hamiltonian (5.42).

We assume that $\mathcal{P}_d$ is subject to the following two conditions

$$\langle\Psi_0|\,\mathcal{P}_d^\dagger\,\mathcal{P}_d\,|\Psi_0\rangle = 1, \tag{5.44}$$

$$\langle\Psi_0|\,\mathcal{P}_d^\dagger\,\mathcal{P}_d\,n_{d\sigma}\,|\Psi_0\rangle = \langle\Psi_0|\,n_{d\sigma}\,|\Psi_0\rangle, \tag{5.45}$$

where

$$n_{d\sigma} = d_\sigma^\dagger d_\sigma \tag{5.46}$$

is the impurity number operator. Condition (5.44) is the normalization requirement of the variational wavefunction. Condition (5.45) - that ensures that all the Wick contractions between the conduction electron operators and the impurity operators are zero - allows to evaluate average values straightforwardly.

In particular, the average value of the Hamiltonian (5.42), that has to be minimized, is

$$\begin{aligned} E &= \frac{\langle\Psi|\,\mathcal{H}\,|\Psi\rangle}{\langle\Psi|\Psi\rangle} \\ &= \langle\Psi_0|\left[\sum_{\alpha k\sigma}\epsilon_k\,c_{\alpha k\sigma}^\dagger c_{\alpha k\sigma}\right. \\ &\quad \left. + \sum_{\alpha k\sigma}\frac{R\,V_k}{\sqrt{\Omega}}\,d_\sigma^\dagger c_{\alpha k\sigma} + H.c.\right]|\Psi_0\rangle \\ &\quad + \frac{U}{2}\,\langle\Psi_0|\mathcal{P}_d^\dagger(n_d-1)^2\mathcal{P}_d|\Psi_0\rangle \\ &\equiv \langle\Psi_0|\mathcal{H}_R^0|\Psi_0\rangle \\ &\quad + \frac{U}{2}\,\langle\Psi_0|\mathcal{P}_d^\dagger(n_d-1)^2\mathcal{P}_d|\Psi_0\rangle \end{aligned} \tag{5.47}$$

where the hopping renormalization coefficient R is obtained through the following equation:

$$\langle\Psi_0|\,\mathcal{P}_d^\dagger\, d_\sigma^\dagger\,\mathcal{P}_d\, d_\sigma\,|\Psi_0\rangle = R\,\langle\Psi_0|d_\sigma^\dagger d_\sigma|\Psi_0\rangle\,. \tag{5.48}$$

The calculation of the first term in Eq. (5.47) reduces, provided Eqs. (5.44) and (5.45) are satisfied, to calculate the energy gain of $\mathcal{H}_R^0$ due to the renormalized tunnelling term

$$\hat{V}_R \;=\; \sum_{\alpha k\sigma} \frac{R\,V_k}{\sqrt{\Omega}}\, d_\sigma^\dagger c_{\alpha k\sigma} + H.c.\,, \tag{5.49}$$

that is, as shown in appendix (A), a functional of the impurity Green's function $G_R(\omega)$ of $\mathcal{H}_R^0$

$$\langle\Psi_0|\mathcal{H}_R^0|\Psi_0\rangle = \mathcal{F}[G_R(\omega)]\,. \tag{5.50}$$

The variational Hamiltonian whose ground state is the uncorrelated wavefunction $|\Psi_0\rangle$ has rigorously no physical meaning but for the ground state properties. However, it is common [124] to interpret it as the Hamiltonian of the quasi-particles and

$$R^2 = z \tag{5.51}$$

as the quasi-particle weight of a single-particle excitation. Within such an assumption, the Gutzwiller approximation technique can be regarded as a tool to extract quasi-particle properties.

From now on the unit of energy is given by the conduction electron half-bandwidth.

In figure 5.4 we show the value of R^2, as a function of U. At $U = 0$ we find that $z = 1$ as expected and has a finite curvature. When $U \to \infty$ we find that

$$z(U) \sim \frac{1}{\Gamma}\exp\left(-\frac{\pi}{16}\frac{U}{\Gamma}\right)\,; \tag{5.52}$$

that is the behaviour of the Kondo temperature, although the correct universal prefactor of U/Γ should be $\pi/8$

$$T_K \sim \exp\left(-\frac{\pi}{8}\frac{U}{\Gamma}\right)\,. \tag{5.53}$$

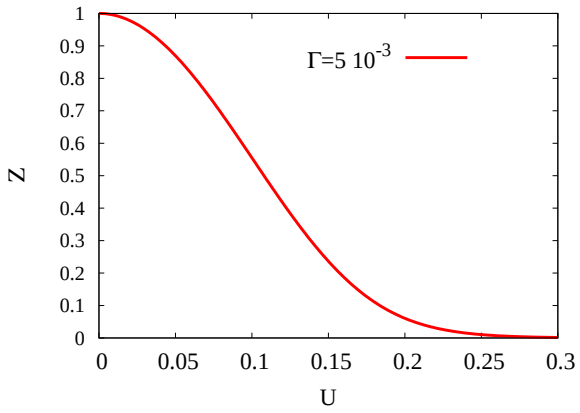

Figure 5.2: (Color online) R^2, as a function of U

We conclude this section observing that at large U the value of z vanishes exponentially remaining finite because

$$\langle \Psi_0 | \mathcal{H}_R^0 | \Psi_0 \rangle = -\frac{2}{\pi} z\Gamma \log\left(\frac{e}{z\Gamma}\right) , \tag{5.54}$$

that vanishes at $z = 0$ with an infinite derivative because of the presence of z in the logarithm.

5.5 The Gutzwiller approximation out of equilibrium

We want to study now the half filled Anderson model

$$\begin{aligned} \mathcal{H} &= \sum_{\alpha k\sigma} \epsilon_k \, c^\dagger_{\alpha k\sigma} c_{\alpha k\sigma} + \sum_{\alpha k\sigma} V_k \, d^\dagger_\sigma c_{\alpha k\sigma} + H.c. \\ &+ \frac{U}{2}(n_d - 1)^2 \end{aligned} \tag{5.55}$$

when it is driven out of equilibrium preparing the leads at two different chemical potentials (Fig. 5.1). Turning on the tunnelling interaction we know that a current starts to flow and the system, after a transient time, reaches the steady state formally defined by Eq. (5.9). At zero temperature the steady state is therefore the ground state of

$$\mathcal{H}(\Phi) = \mathcal{H} + \Phi Y. \tag{5.56}$$

We want to approximate the Hershfield steady state with the usual equilibrium Gutzwiller variational wavefunction

$$|\Psi\rangle = \mathcal{P}_d\,|\Psi_0\rangle \tag{5.57}$$

which satisfies conditions (5.44) and (5.45).

The average on $|\Psi\rangle$ of $\mathcal{H}$ is equal to the average on $|\Psi_0\rangle$ of the renormalized Hamiltonian

$$\begin{aligned}\mathcal{H}_R^0 &= \mathcal{P}_d^\dagger\,\mathcal{H}\,\mathcal{P}_d = \sum_{\alpha k\sigma}\epsilon_k\,c_{\alpha k\sigma}^\dagger c_{\alpha k\sigma}\\ &\quad+\sum_{\alpha k\sigma}\frac{R\,V_k}{\sqrt{\Omega}}\,d_\sigma^\dagger c_{\alpha k\sigma}+H.c.\,.\end{aligned}\tag{5.58}$$

What can we say about $\mathcal{P}_d^\dagger\,Y\,\mathcal{P}_d$? We do not known Y explicitly. However, just like at equilibrium, we expect that $\mathcal{P}_d^\dagger\,(\mathcal{H}+\Phi\,Y)\,\mathcal{P}_d$ should describe weakly interacting quasiparticles in the presence of a bias. Since any bias dependent interaction term (recall that the bias can only generate terms that are odd upon exchanging the leads, hence can not renormalize the Hubbard U but at most induce an interaction term between the impurity and the leads) will affect conductance at higher orders in the bias, we assume that $\mathcal{H}_R^0+\mathcal{P}_d^\dagger\,Y\,\mathcal{P}_d$ corresponds to the non-equilibrium Hamiltonian

$$\begin{aligned}\mathcal{H}_R^{0*}(\Phi) &= \sum_{\alpha k\sigma}\epsilon_k\,\psi_{\alpha k\sigma}^\dagger(R)\,\psi_{\alpha k\sigma}(R)\\ &+ \quad\Phi\sum_{\alpha k\sigma}\frac{\alpha}{2}\,\psi_{\alpha k\sigma}^\dagger(R)\,\psi_{\alpha k\sigma}(R)\\ &\equiv \mathcal{H}_R^0+\Phi Y_R^0\,,\end{aligned}\tag{5.59}$$

where $\psi_{\alpha k\sigma}^\dagger(R)$ are appropriate scattering waves identified by R, and to interpret it as the Hamiltonian of the quasi-particles. In other words, we assume that the Fermi liquid renormalization affects the bias opeartor only through the definition of the quasiparticle scattering waves.

Given the above assumption, our procedure amounts to minimize the following energy functional

$$\begin{aligned}E &= \langle\Psi_0(\Phi)|\,\mathcal{H}_R^0+\Phi Y_R^0\,|\Psi_0(\Phi)\,\rangle\\ &+\frac{U}{2}\,\langle\Psi_0(\Phi)|\,\mathcal{P}_d^\dagger(n_d-1)^2\mathcal{P}_d\,|\Psi_0(\Phi)\rangle\,,\end{aligned}\tag{5.60}$$

where $\Psi_0(\Phi)$ is the ground state of $\mathcal{H}_R^{0*}(\Phi)$, subject to conditions (5.44-5.45). This corresponds to assume that we can approximate the average of Y on the projected state $|\Psi\rangle = \mathcal{P}_d |\Psi_0\rangle$ with the average of Y_R^0 on the uncorrelated state $|\Psi_0\rangle$. In other words, we substitute the equilibrium energy gain due to the tunnelling term (5.49) for the energy gain due to the tunnelling term in the non equilibrium quasi-particle Hamiltonian (5.59).

We stress that our functional, and then the value of R after the optimization, depends on the bias Φ. This is crucial in order to properly take into account the strong correlation effects induced by the Hubbard repulsion.

The expression for the average of the current after the optimization is

$$\begin{aligned} I &= -i \sum_{k\sigma} \frac{V_k}{\sqrt{\Omega}} \left(\langle \Psi_0(\Phi)| \, d_\sigma^\dagger c_{k\sigma,-1} \, |\Psi_0(\Phi)\rangle - c.c. \right) \\ &= \int_{-\frac{\phi}{2}}^{\frac{\phi}{2}} d\epsilon \, \Gamma^* \rho_d^{\Gamma^*}(\epsilon) \end{aligned} \tag{5.61}$$

where $\rho_d^{\Gamma^*}(\epsilon)$ is the spectral function of the dot, that is

$$\rho_d^{\Gamma^*}(\epsilon) = \frac{1}{\pi} \frac{\Gamma^*}{\epsilon^2 + \Gamma^{*2}} \chi_{[-1,1]}(\epsilon) \tag{5.62}$$

with

$$\Gamma^*(\epsilon) = R^2 \, \Gamma(\epsilon) \tag{5.63}$$

having assumed that the density of states is flat and that $\Gamma \ll W = 1$

$$\begin{aligned} \Delta(z) &= \int \frac{d\epsilon}{\pi} \frac{\Gamma(\epsilon)}{z - \epsilon} \\ \Gamma(\epsilon) &= \Gamma \chi_{[-1,1]}(\epsilon) \end{aligned} \tag{5.64}$$

We notice that Eq. (5.61) fails to describe the system accurately when $\Phi \sim U$, because it doesn't take into account the spectral contribution of the Hubbard bands. However, for the simple single-band Anderson model we can reproduce artificially the correct qualitative behaviour of the current in this regime by substituting $R^2 \rho_d^{\Gamma^*}(\epsilon)$ with

$$\rho_d^U(\epsilon) = R^2 \rho_d^{\Gamma^*}(\epsilon) + \frac{1}{2}(1 - R^2) \sum_{\alpha=-1,1} \rho_d^\Gamma \left(\epsilon - U \frac{\alpha}{2} \right) \tag{5.65}$$

in Eq. (5.61).

In Fig. 5.3 we show the results for the conductance G of the Anderson model. The data are obtained with the method described above applied to the system at particle-hole symmetry

$$\epsilon_d = 0\,. \tag{5.66}$$

The obtained value of the conductance at zero bias is universal as expected, and the curvature is given by

$$\left.\frac{d^2G}{d\Phi^2}\right|_{\Phi=0} = -\frac{1}{2\pi(R^2\Gamma)^2} \sim -\frac{1}{(T_K^G)^2} \tag{5.67}$$

- being T_K^G the Kondo temperature with the incorrect prefactor predicted by the Gutzwiller method

$$T_K^G \;\sim\; e^{-\frac{\pi}{16}\frac{U}{\Gamma}}\,. \tag{5.68}$$

Nevertheless for large enough value of U we found (not showed) that the conductance may become negative, which is unrealistic. In order to establish the regime of validity of our method, we note that the Fermi-liquid description that we assume is applicable only for values of the bias much lower then the Kondo temperature T_K. For the single-orbital Anderson impurity model we can calculate analitically the minimum value of the energy functional (5.60) when

$$W \gg \Phi \gg \Gamma\,, \tag{5.69}$$

namely when Eq. (5.38) can be applied, so that

$$\langle\Psi_0(\Phi)|\,\mathcal{H}_R^0 + \Phi Y_R^0\,|\Psi_0(\Phi)\,\rangle = \frac{2}{\pi}\,R^2\,\Gamma\log\left(\frac{\Phi}{2}\right)\,. \tag{5.70}$$

In particular, it can be easily proven that the value of z vanishes at

$$\Phi^* = e^{-\frac{\pi}{16}\frac{U}{\Gamma}} \;\sim T_K^G\,, \tag{5.71}$$

namely out of the expected regime of validity.

We finally notice that the procedure proposed in this section is generalizable, in principle, to any complicated impurity model.

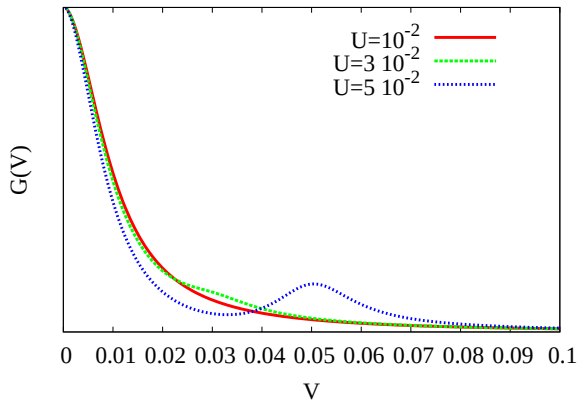

Figure 5.3: (Color online) Conductance as a function of the bias for $\Gamma = 10^{-3}$ and three different values of U.

5.5.1 The method out of particle-hole symmetry

Let us consider the Anderson model out of particle-hole symmetry

$$\begin{aligned} \mathcal{H} &= \sum_{\alpha k\sigma} \epsilon_k \, c^\dagger_{\alpha k\sigma} c_{\alpha k\sigma} + \sum_{\alpha k\sigma} \frac{V_k}{\sqrt{\Omega}} \, d^\dagger_\sigma c_{\alpha k\sigma} + H.c. \\ &+ \epsilon_d \sum_\sigma d^\dagger_\sigma d_\sigma + \frac{U}{2}(n_d - 1)^2 \,, \end{aligned} \tag{5.72}$$

namely with $\epsilon_d \neq 0$. The state $|\psi_0\rangle$ which minimize the energy $\mathcal{H}_R$ and satisfies Eq. (5.45)

$$\langle \Psi_0 | \, d^\dagger_\sigma d_\sigma \, | \Psi_0 \rangle = n \tag{5.73}$$

can be calculated within the Lagrange multipliers method, namely $|\psi_0\rangle$ is the ground state of the Hamiltonian

$$\mathcal{H}^{Lag}_R = \mathcal{H}_R + \mu \sum_\sigma (d^\dagger_\sigma d_\sigma - n) \tag{5.74}$$

with a proper chemical potential μ.

In particular, when $\epsilon_d = 0$ the ground state of $\mathcal{H}_R$ satisfies the constraint (5.45) automatically, namely $\mathcal{H}^{Lag}_R = \mathcal{H}_R$, and the correspondent non-equilibrium Hamiltonian $\mathcal{H}^*_R(\Phi)$ automatically satisfies the constraint (5.45) too, namely

$$\langle \Psi_0 | \, d^\dagger_\sigma d_\sigma \, | \Psi_0 \rangle = \langle \Psi_0(\Phi) | \, d^\dagger_\sigma d_\sigma \, | \Psi_0(\Phi) \rangle = \frac{1}{2} \tag{5.75}$$

Let us consider now the general case $\epsilon_d \neq 0$. In this case

$$\mathcal{H}_R^{Lag} = \sum_{\alpha k\sigma} \epsilon_k \, \psi^\dagger_{\alpha k\sigma}(R) \, \psi_{\alpha k\sigma}(R) \,, \tag{5.76}$$

where $\psi^\dagger_{\alpha k\sigma}(R)$ where $\psi^\dagger_{\alpha k\sigma}(R)$ are the scattering waves constructed with renormized hybridization $R\,V_k$, which depend on the retarded impurity Green's function

$$g_{dR}(\epsilon) = \frac{1}{\epsilon - \mu + iR^2\Gamma} \,. \tag{5.77}$$

We observe that, if μ is taken to be the value that satisfies the constraint (5.45) at equilibrium, the ground state $|\Psi_0(\Phi)\rangle$ of the non-equilibrium Hamiltonian

$$\begin{aligned} \mathcal{H}_R^*(\Phi) &= \sum_{\alpha k\sigma} \epsilon_k \, \psi^\dagger_{\alpha k\sigma}(R) \, \psi_{\alpha k\sigma}(R) \\ &+ \Phi \sum_{\alpha k\sigma} \frac{\alpha}{2} \, \psi^\dagger_{\alpha k\sigma}(R) \, \psi_{\alpha k\sigma}(R) \end{aligned} \tag{5.78}$$

is not such that

$$\langle \Psi_0(\Phi)| \, d^\dagger_\sigma d_\sigma \, |\Psi_0(\Phi)\rangle = n \,, \tag{5.79}$$

namely it doesn't satisfy anymore (5.45). The procedure described for $\epsilon_d = 0$ should then be modified without fulfilling this condition, renouncing to the consequent simplification of the calculations.

5.6 Study of a two-dot model at equilibrium

We consider a system (represented in Fig. 5.4) of two antiferromagnetically-interacting levels coupled among each other by an antiferromagnetic exchange J; each one is hybridized with two bands of conduction electrons with energy dispersion ϵ_k and suffers from an Hubbard interaction U

$$\begin{aligned} \mathcal{H} &= \sum_{\alpha=-1,1} \sum_{\beta k\sigma} \epsilon_k \, c^\dagger_{\alpha\beta k\sigma} c_{\alpha\beta k\sigma} \\ &+ \sum_{\alpha=-1,1} \sum_{\beta k\sigma} \frac{V_k}{\sqrt{\Omega}} \, d^\dagger_{\sigma\beta} c_{\alpha\beta k\sigma} + H.c. \\ &+ J \, \mathcal{S}_1 \mathcal{S}_2 + \sum_\beta \frac{U}{2} (n_\beta - 1)^2 \end{aligned} \tag{5.80}$$

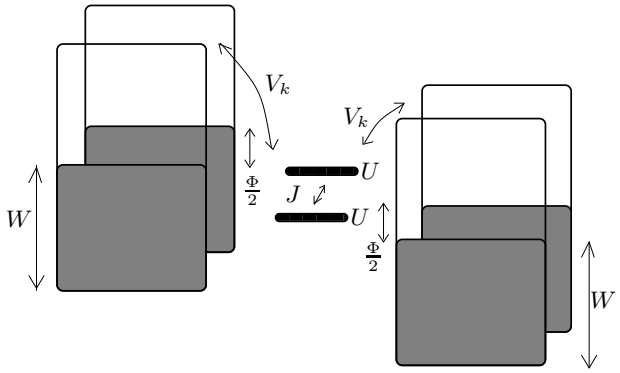

Figure 5.4: The two-dot system

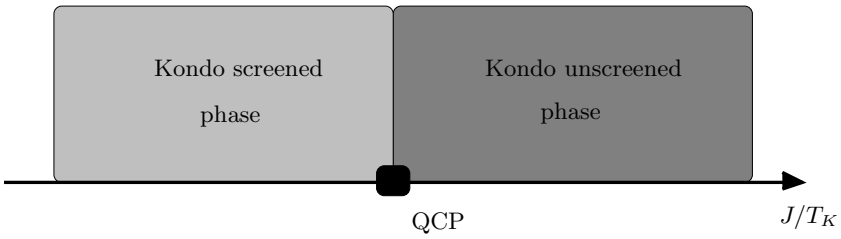

Figure 5.5: The phase diagram of the two-dot system at equilibrium

where S_i represents the spin operator of the dot i.

At equilibrium this model is known [125, 126] to have a second order quantum phase transition upon increasing the antiferromagnetic exchange between the two levels (see Fig. 5.5). The quantum critical point (QCP) separates a Kondo screened phase (for $J < J_c$) from a Kondo unscreened phase (for $J > J_c$), that are both Fermi-liquid-like in Noziéres sense; namely, they correspond asymptotically to well defined limits of free-elecrons scattering off a structure-less impurity potential, infinite in the Kondo screened and zero in the unscreened one.

The theory at the QCP is an unstable fixed point respect to the conformal group, that can be destabilized by the following three relevant symmetry breaking operators

$$h_{AF}(S_1 - S_2)\,; \quad h_{SC}\left(d^\dagger_{1\uparrow}d^\dagger_{2\downarrow} - d^\dagger_{1\downarrow}d^\dagger_{2\uparrow}\right)\,; \quad \sum_\sigma h_\perp d^\dagger_{1\sigma}d_{2\sigma} + h.c.\,. \tag{5.81}$$

so that the susceptibility with respect to the operators (5.81) diverges at the

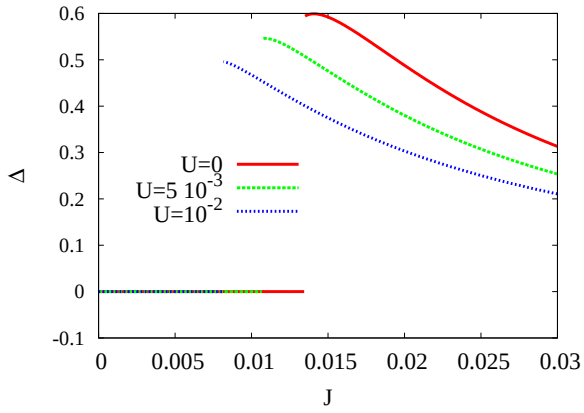

Figure 5.6: (Color online) Δ as a function of J for $\Gamma = 2\,10^{-3}$ and three different values of U.

QCP.

This model has been already studied at equilibrium within the slave-bosons technique [127], and the transition between the Kondo e non-Kondo regime was found to be either first order or second order, depending on the values of the coupling constants. We analyzed the same problem increasing the variational freedom of the Gutzwiller wavefunction, allowing it to have a finite value of Δ [35]

$$\Delta \;=\; \frac{1}{2}\,\langle\, d^{\dagger}_{1\uparrow} d^{\dagger}_{2\downarrow} - d^{\dagger}_{1\downarrow} d^{\dagger}_{2\uparrow} \,\rangle\,, \tag{5.82}$$

although it is impossible for a single impurity to break a bulk symmetry (see appendix B for the the technical details of our calculation). An eventual tendency of our trial state to have $\Delta \neq 0$ should be interpreted as the tendency of the system to have a large susceptibility respect to Δ. The additional variational freedom that we have introduced allows the impurity spectral function to develop a two-peaks structure, that can mimic the actual behavior [128].

In Fig. 5.6 we plot Δ as a function of the antiferromagnetic coupling J and $\Gamma = 2\,10^{-3}$ for some value of the Hubbard U. In this cases we found a weak first order phase transition at a critical value of J that decreases upon increasing U.

In Fig. 5.11 we plot the impurity spectral functions for a value of J greater

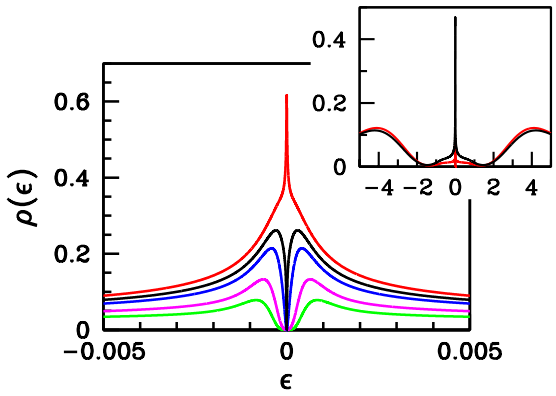

Figure 5.7: (Color online) From Ref. [129]. Main panel: low energy behavior of the impurity DOS of the dimer model at equilibrium, with $U = 8$, $J = 0.00125$ and, from top to bottom, $\Gamma = 0.44, 0.42, 0.4, 0.35, 0.3$ in units of half the conduction bandwidth. Upper inset: the DOS behavior in the whole energy range with the same U and J and with $\Gamma = 0.6$, top curve, and $\Gamma = 0.3$. The Hubbard bands are clearly visible, while the low energy parts are hardly distinguishable.

then the critical value, and in Fig. 5.12 we plot the impurity spectral functions for a value of J is lower then the equilibrium critical value. Our result is qualitatevely consistent with the NRG results showed in Fig. 5.7: in the Kondo screened phase there is a Kondo peak on top of a broad resonance, while in the Kondo unscreened phase the Kondo peak disappears, developing a two-peaks structure.

5.7 Double dot model out of equilibrium

This section is devoted to a tentative study of the half-filled two-dot model described by Eq. (5.80) out of equilibrum (see Fig. 5.4), by means of the method described in section 5.5.

If the problem is studied with a variational Gutzwiller wavefunction which doesn't break any symmetry of the Hamiltonian, the uncorrelated wavefunction $|\Psi_0(\Phi)\rangle$ - the ground state of the non-equilibrium Hamiltonian $H_R^{0*}(\Phi)$ defined in Eq. (5.59) - has the same density matrix of $|\psi_0\rangle$ - the ground state of H_R^0. This is not true anymore if we allow the wavefunction to have a finite value of the parameter Δ. In this case, we should in principle impose that $|\Psi_0(\Phi)\rangle$ is subject to the Gutzwiller constraints

$$\langle\Psi_0(\Phi)|\,\mathcal{P}_d^\dagger\,\mathcal{P}_d\,\mathcal{C}\,|\Psi_0(\Phi)\rangle = \langle\Psi_0(\Phi)|\,\mathcal{C}\,|\Psi_0(\Phi)\rangle\,, \tag{5.83}$$

where $\mathcal{C}$ is the local single-particle density-matrix operator with elements $d_i^\dagger d_j$, $d_i^\dagger d_j^\dagger$ and $d_i d_j$ (i label both spin and orbitals). It comes out that, enforcing (5.83) leads to out of equilibrium results that we do not understand completely when $\Delta \neq 0$. We find that the bias is able to induce the transition that is observed at equilibrium upon increasing J, something that we expected since the bias weakens Kondo effect hence effectively strengthen J. However this transition comes out to be strongly first order because in order to fulfill (5.83) with $\Delta \neq 0$, the latter must be sizable, hence a smooth transition can not occur. We are tempted to believe that this is an artifact of the method, which forces us to explicitly break a symmetry that could not be broken spontaneously. Therefore we have decided to adopt a different approach that leads to a smoother behavior. Essentially, we fixed the constraint (5.83) at equilibrium, which amounts to determine Lagrange multipliers similarly as in (5.74), and we keep the latter fixed even at finite bias. We stress that this problem does not occur if variationally $\Delta = 0$, in which case particle-hole symmetry guarantees that all Lagrange multipliers are zero.

In Fig. 5.8 and Fig. 5.9 we plot the behaviour of Δ as a function of the bias Φ calculated as discussed above and for two different values J at fixed U. In Fig. 5.10 we plot the conductance.

We find that, if J is smaller then the equilibrium critical value, a second order transition can be induced upon increasing the bias; the conductance decreases and has a jump at the QCP, when Δ starts to be finite. If J is greater then the equilibrium critical value, instead, the conductance grows upon increasing the bias and is continuous.

The origin of this difference can be clarified if we look at the impurity

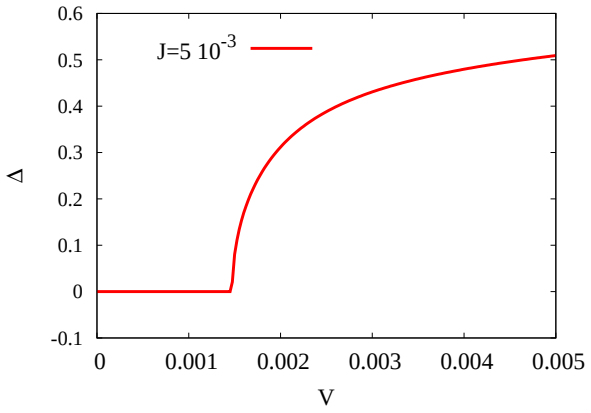

Figure 5.8: (Color online) Δ as a function of the bias V for $\Gamma = 2\,10^{-3}$, $U = 10^{-2}$ and $J = 5\,10^{-3}$ - slightly before the equilibrium critical value of J.

spectral functions at $\Phi = 0$ (Figg. 5.11 and 5.12). If J is greater then the equilibrium critical value when we start applying bias, the spectral function has already a two-peak structure, so that the interval $[-\frac{\Phi}{2}, \frac{\Phi}{2}]$ includes, upon increasing Φ, an increasing additional spectral weight. When J is lower then the equilibrium critical value and Φ is below the bias critical value, instead, the spectral function has a single peak structure, so that the interval $[-\frac{\Phi}{2}, \frac{\Phi}{2}]$ includes, upon increasing Φ, a decreasing (normalized to Φ itself) additional spectral weight.

5.8 Conclusions

We have proposed a novel generalization of the Gutzwiller variational method for studying the steady-state zero-temperature properties of a general quantum-dot driven out of equilibrium through the application of a bias. Our method is based on:

- the Hershfield [67] idea that the out-of-equilibrium steady state can be regarded as the equilibrium one with an Hamiltonian $\mathcal{H}^*(\Phi)$ that includes an effective non-equilibrium term proportional to the bias ΦY.

- the assumption that the effective Hershfield Hamiltonian $\mathcal{H}^*(\Phi)$ describes

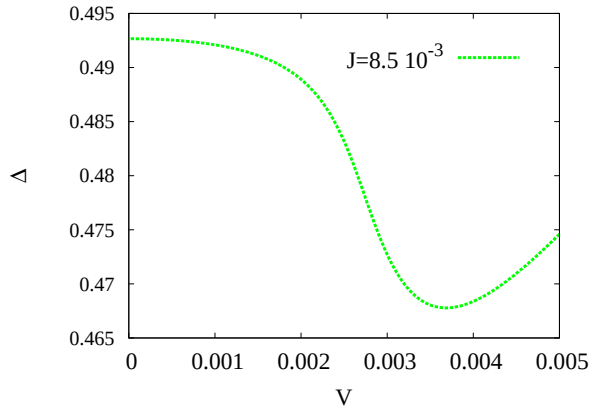

Figure 5.9: (Color online) Δ as a function of the bias V for $\Gamma = 2\,10^{-3}$, $U = 10^{-2}$ and $J = 8.5\,10^{-3}$ - beyond the equilibrium critical value of J.

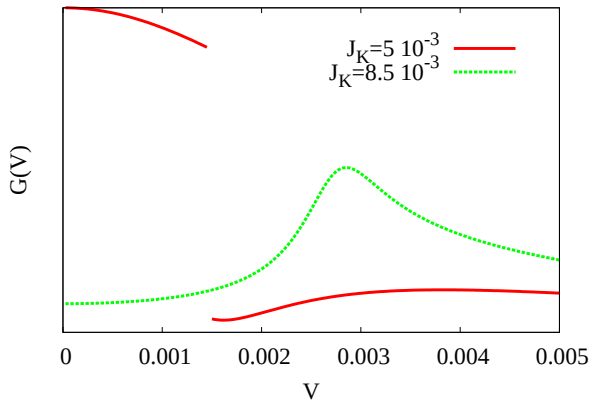

Figure 5.10: (Color online) Conductance as a function of the bias V for $\Gamma = 2\,10^{-3}$, $U = 10^{-2}$ and $J = 5\,10^{-3}$,$J = 8.5\,10^{-3}$.

a local Fermi liquid theory in the Noziéres sense [68].

These ideas lead us to define an expression for the non-equilibrium operator Y that, we think, should be valid if the bias is not too large compared with the Kondo temperature.

In order to test our method, we have applied it to the simple single orbital Anderson impurity model, finding a good qualitative accord with the observed behavior in quantum dots for the expected regime of validity.

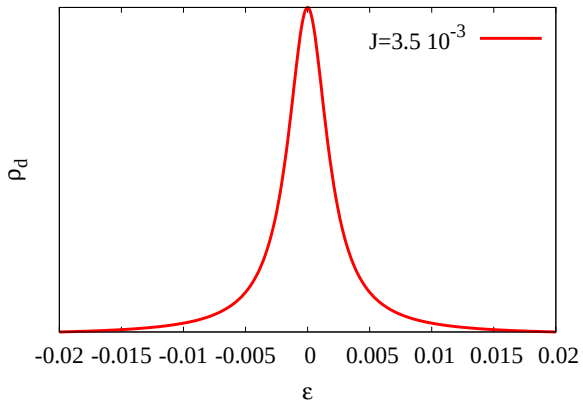

Figure 5.11: (Color online) Impurity Green's function for $\Gamma = 2\,10^{-3}$, $U = 10^{-2}$, $J = 3.5\,10^{-3}$ at equilibrium.

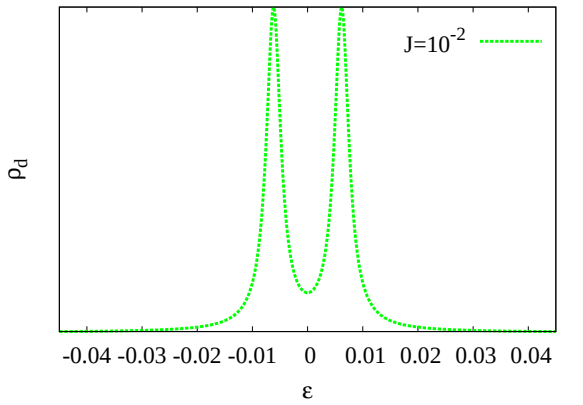

Figure 5.12: (Color online) Impurity Green's function for $\Gamma = 2\,10^{-3}$, $U = 10^{-2}$, $J = 10^{-2}$ at equilibrium.

We have then studied within the Gutzwiller method the phase diagram of the more complicated two-dot model Eq. (5.80) enlarging the variational space to the wavefunction with a finite mean value of a BCS operator in the inter-bath Cooper singlet channel. Within this expedient we have been able to partially recover some of the correct qualitative features of the phase diagram, that would not be accessible to the Gutzwiller method otherwise. Finally, we have performed a preliminary (not rigorous) study of the two-dot model within our

non-equilibrium generalization of the Guzwiller method. Our results suggest that a second order transition can be driven by the bias starting from a Kondo-like regime with a zero-bias anomaly. The simple explanation is that, as the bias progressively decouple the leads from the two dots, the tendency of the latter to couple among each other into a singlet state increases. These effects enforce each other and finally lead to a drop in conductance that variationally appears to be related to a second order phase transition.

The method that we have proposed has the important advantage to be simple and flexible enough to deal with realistic situations. For example, the idea to generalize the LDA + Gutzwiller method to non-equilibrium problems seems us to be a very interesting perspective.

Chapter 6

Conclusions and Perspectives

In this thesis we have faced, by means of the Gutzwiller variational approach, the following three different problems of current interest:

- The Fermi surface evolution in heavy fermions systems.

In this work we have applied the Gutzwiller ansatz to the Kondo lattice model. We have computed its phase diagram as a function of conduction electron density and Kondo exchange, finding that for any value of the density there is an orbital selective Mott transition accompanied by a discontinuous change of the Fermi surface. Away from the compensated regime the first order transition occurs in concomitance with magnetism, while near the compensated regime the f-localization occurs after the appearance of magnetism via a second order transition (with a continuous change of the Fermi surface). We have then studied the behaviour of the system when a uniform magnetic field is applied to a paramagnetic state, finding that a first order phase transition - accompanied by a abrupt increase of magnetization and a discontinuous change of the conduction electron Fermi surface - can be induced upon increasing it (metamagnetism).

Our results suggest that (without nesting) antiferromagnetism is a by-product of the f-electron Mott localization rather than the outcome of the competition between Kondo screening and RKKY interaction.

- The emergence of superconductivity upon doping a simple spin-liquid,

We have considered the model of two Hubbard planes coupled by an inter-plane hybridization. In particular, we have studied, within the Gutzwiller approximation method, the melting induced by hole doping of the valence bond crystal (a collection of inter-plane singlets) that exists at half-filling for large enough inter-plane tunneling. We have found that a superconducting solution emerges as soon as the non-magnetic Mott insulator is doped, which gives up to a normal-metal phase for large enough doping. This behavior is closely related to the RVB superconductivity scenario [26], and quite reminiscent of the actual behavior of cuprates superconductors, although our model has nothing to do with models for cuprates. This suggests that the RVB scenario might be correct and relevant to the physics of high T_c superconductors, as originally claimed by Anderson [26, 27].

- The quantum transport across a correlated microscopic object.

We have proposed a generalization of the Gutzwiller variational method for studing steady-state properties of a general quantum-dot system driven out of equilibrium by a finite bias.

The starting point of our idea has been the results by Hershfield [67], according to whom the steady state value of certain observables can be regarded as the equilibrium value calculated with a Boltzmannian density matrix constructed by a "non-equilibrium" Hamiltonian (the Hershfield Hamiltonian), that includes an effective bias operator. Such operator, although is formally well defined, can't be generally calculated explicitly, and for that reason we had to make several assumptions in the spirit of a local Landau Fermi liquid hypothesis [68] to get to some expression that, we think, should be valid if the bias is not too large.

We have tested our method applying it to the single-orbital Anderson impurity model, finding a good qualitative accord with the observed behavior in quantum dots for the expected regime of validity, i.e. bias much smaller then the Kondo temperature.

Next we have studied a two-dot model, see Eq. (5.80). Each dot is assumed to be coupled to two leads, and the dot are coupled among each other by an antiferromagnetic exchange. At equilibrium, no bias applied to the leads, this model is known [125, 126] to posses a second order quantum phase transition

between a Kondo screened phase and a Kondo unscreened one, as the inter-dot exchange increases. The conventional Gutzwiller approximation using a variational wavefunction that shares the same symmetry of the Hamiltonian, is known to fail [127] in capturing the second order transition. For this reason we have enlarged the variational space allowing the variational wavefunction to posses a finite BCS order parameter, whose susceptibility is known to diverge at the QCP [126] although rigorously it can not spontaneously rise. This expedient provides a better description of the actual phase diagram. Finally, we have studied the model out of equilibrium using our non-equilibrium generalization of the Guzwiller method. Our preliminary results suggest that a second order accompanied by a rapid drop of conductance can be induced by the application of the bias.

We underline that our method is simple and flexible. Therefore we think that it might be exploited in combination with electronic structure calculations to provide more realistic description of nanocontacts.

While addressing all these problems, we have been forced to improve along several directions the Gutzwiller method. In particular, we have found very convenient to use a "mixed-basis" representation for the projector operators $|\Gamma\rangle\langle\widetilde{\Gamma}|$ that defines the Gutzwiller operator. Here $|\Gamma\rangle$ is a local configuration in a known basis, e.g. multiplets with given electron number and total spin, while $|\widetilde{\Gamma}\rangle$ is a configuration in an unknown basis, which we assume to be the "natural" one, namely that one which diagonalizes the single-particle local density matrix of the variational uncorrelated wavefunction. Indeed, one of the issues that arise while applying a Gutzwiller projector to a set of many-body operators is the ability to keep track of the transformation linking the physical basis (e.g. the tight-binding free-electron orbitals) to the natural basis (the basis that diagonalizes the local density matrix computed on the single-particle Slater determinant). The use of the mixed basis gauges-away this connection, and enables us to forget about it until the end of the minimization procedure. Moreover, the introduction of a new type of Gutzwiller parameters, corresponding to the slave-boson saddle-point within the Kotliar-Ruckenstein mean-field scheme, allows to further simplify the parametrization of the variational space.

As a result, we achieved a considerable speed-up in the computation of the energy-minimum, due to the reduced problem complexity. We think that our scheme is suitable for applications to systems more complex than those dealt with in this thesis, e.g. for combining the Gutzwiller scheme with ab-initio calculations.

Acknowledgements

First of all I would like to thank my supervisor Prof. Michele Fabrizio, not only for his teachings and his support through these four years in Trieste, but also for having allowed (and sometimes forced) me to think independently, with the result of making me more autonomous.

I thank all the Condensed Matter group members, professors and colleagues, for their helpfulness. In particular, I would like to acknowledge Michel Ferrero for having supported me more than once during my Ph.D. and for his teachings during my first year at SISSA.

I thank also Prof. Adelchi Fabrocini, Prof. Michele Viviani and Prof. Giovanni Morchio, who were the inspirers of my scientific "way of thinking" during my experience in Pisa as an undergraduate.

I thank all the people that contributed to make this experience in Trieste important and unique: my group of Capoeira, my fantastic flatmate Alessia and my colleagues.

A special thank to my family, in particular to my parents and my grandparents, for being always present.

Appendix A

Resonant model out of equilibrium

In this appendix we discuss some results related with the resonant model that are necessary in order to calculate the non-equilibrium energy functional that we have introduced in chapter 5.

A.1 Equilibrium Hamiltonian and Fridel sum rule

Let us consider the resonant model Hamiltonian

$$\mathcal{H} = \sum_{\alpha k\sigma} \epsilon_k \, c^\dagger_{\alpha k\sigma} c_{\alpha k\sigma} + \sum_{\alpha k\sigma} \frac{V_k}{\sqrt{\Omega}} \left(d^\dagger_\sigma c_{\alpha k\sigma} + H.c. \right) + \sum_\sigma \epsilon_d \left(d^\dagger_\sigma d_\sigma - n_\sigma \right) \quad \text{(A.1)}$$

and its correspondent Green's function

$$G(z) = \frac{1}{z - \epsilon_d - \Delta(z)} \, . \quad \text{(A.2)}$$

We want to solve the problem to calculate the value of ϵ_d such that the ground state $|\Psi_0\rangle$ of $\mathcal{H}_0$ satisfies the condition

$$\langle \Psi_0 | \, d^\dagger_\sigma d_\sigma \, | \Psi_0 \rangle = n^0_d \, . \quad \text{(A.3)}$$

From now on we will assume that the half bandwidth W is the unit of energy and that

$$\Gamma(\epsilon) = \Gamma \sqrt{1 - \epsilon^2} \, \chi_{[-1,1]}(\epsilon) \, , \quad \text{(A.4)}$$

where $\chi_{[-1,1]}(\epsilon)$ is 1 if $\epsilon \in [-1,1]$ and is 0 otherwise; then

$$\Delta(z) \;=\; \int \frac{d\epsilon}{\pi} \frac{\Gamma(\epsilon)}{z-\epsilon'} \;=\; \Gamma\left(z - \sqrt{z^2-1}\right) . \tag{A.5}$$

The spectral function of $G(z)$ is

$$\begin{aligned} \rho_{\epsilon_d}(\epsilon) &= -\frac{1}{\pi}\mathrm{Im}\, G(\epsilon + i0^+) \\ &= \frac{1}{\pi} \frac{\Gamma\sqrt{1-\epsilon^2}\;\chi_{[-1,1]}(\epsilon)}{\left(\epsilon - \epsilon_d - \Gamma\epsilon\right)^2 + \Gamma^2(1-\epsilon^2)} \;+\; z\,\delta(\epsilon - \epsilon^*) \end{aligned} \tag{A.6}$$

where

$$\begin{aligned} \epsilon^* &= \frac{|\epsilon_d|\,(1-\Gamma)}{1-2\Gamma}\left\{-1 + \sqrt{1 - (1-2\Gamma)\frac{\epsilon_d^2+\Gamma^2}{\epsilon_d^2(1-\Gamma)^2}}\right\} \\ z &= \left(1 + \frac{\epsilon_d - \epsilon^*}{\sqrt{\epsilon^2-1}}\right) \end{aligned} \tag{A.7}$$

The value of ϵ_d such that condition (A.3) holds can be easily found numerically as the solution of the Fridel sum rule

$$n_d^0 = \int d\epsilon f(\epsilon)\rho_{\epsilon_d}(\epsilon) \tag{A.8}$$

A.2 Non-equilibrium Hamiltonian energy

The Hershfield Hamiltonian $\mathcal{H} + \Phi Y$ defined in Eq. (A.1) can be expressed in terms of the scattering operators

$$\begin{aligned} \psi^\dagger_{\alpha k\sigma} &= c^\dagger_{\alpha k\sigma} + \frac{V_k}{\sqrt{\Omega}}\, g(\epsilon_k)\, d^\dagger_\sigma \\ &\quad + \sum_{\alpha' k'} \frac{V_k V_{k'}}{\sqrt{\Omega}}\, \frac{g(\epsilon_k)}{\epsilon_k - \epsilon_{k'} + i0^+}\, c^\dagger_{\alpha' k'\sigma}\,, \end{aligned} \tag{A.9}$$

where $g(\epsilon) = G(\epsilon + i0^+)$ is the retarded Green's function of the impurity at equilibrium, as it follows:

$$\mathcal{H} + \Phi Y \;=\; \sum_{\alpha=-1,1} \sum_{k\sigma} \left(\epsilon_k + \Phi\frac{\alpha}{2}\right)\, \psi^\dagger_{\alpha k\sigma}\, \psi_{\alpha k\sigma}\,. \tag{A.10}$$

We express the Hershfield Hamiltonian (A.10) in terms of c and d operators

$$\mathcal{H}(\Phi) = \mathcal{H}_0 + \hat{V} + \Phi Y \tag{A.11}$$

where

$$\begin{aligned}
\mathcal{H}_0 &= \sum_{\alpha k\sigma} \epsilon_k \, c^\dagger_{\alpha k\sigma} c_{\alpha k\sigma} + \sum_{\sigma} \epsilon_d \, d^\dagger_\sigma d_\sigma \\
\hat{V} &= \sum_{\alpha k\sigma} \frac{V_k}{\sqrt{\Omega}} \left(d^\dagger_\sigma c_{\alpha k\sigma} + H.c. \right) \\
Y &= \sum_{\alpha k\sigma} \frac{\alpha}{2} \, c^\dagger_{\alpha k\sigma} c_{\alpha k\sigma} \\
&+ \sum_{\alpha k\sigma} \frac{\alpha}{2} \sum_{\alpha' k'} \frac{V_k V_{k'}}{\Omega} \, \frac{g(\epsilon_{k'})}{\epsilon_k - \epsilon_{k'} + i0^+} \, c^\dagger_{\alpha' k'\sigma} c_{\alpha k\sigma} + H.c. \\
&+ \sum_{\alpha k\sigma} \frac{\alpha}{2} \, \frac{V_k}{\sqrt{\Omega}} g(\epsilon_k) \, d^\dagger_\sigma c_{\alpha k\sigma} + H.c. \, .
\end{aligned} \tag{A.12}$$

In order to calculate the non-local energy functional in our approximation we need to calculate the energy gain $\delta\mathcal{E}_\Phi$ due to the presence of $\hat{V}$ and ΦY in $\mathcal{H}(\Phi)$; a problem that can be solved using the Hellmann Feynman theorem. Let us introduce the operator

$$\mathcal{H}_\lambda(\Phi) = \mathcal{H}_0 + \lambda \hat{V} + \Phi Y(\lambda) \tag{A.13}$$

where

$$\begin{aligned}
Y(\lambda) &= \sum_{\alpha k\sigma} \frac{\alpha}{2} \, c^\dagger_{\alpha k\sigma} c_{\alpha k\sigma} \\
&+ \sum_{\alpha k\sigma} \frac{\alpha}{2} \sum_{\alpha' k'} \frac{\lambda^2 V_k V_{k'}}{\Omega} \, \frac{g(\epsilon_{k'})}{\epsilon_k - \epsilon_{k'} + i0^+} \, c^\dagger_{\alpha' k'\sigma} c_{\alpha k\sigma} + H.c. \\
&+ \sum_{\alpha k\sigma} \frac{\alpha}{2} \, \frac{\lambda V_k}{\sqrt{\Omega}} \, g(\epsilon_k) \, d^\dagger_\sigma c_{\alpha k\sigma} + H.c.
\end{aligned} \tag{A.14}$$

and the correspondent minimum energy

$$\mathcal{E}(\lambda) = \langle \Psi_0(\lambda) | \, \mathcal{H}_\lambda(\Phi) \, | \Psi_0(\lambda) \rangle \tag{A.15}$$

The energy gain $\delta\mathcal{E}_\Phi$ is

$$\delta\mathcal{E}_\Phi = \int_0^1 d\lambda \, \frac{d\mathcal{E}}{d\lambda} \tag{A.16}$$

where (Hellmann Feynman theorem)

$$\begin{aligned}\frac{d\mathcal{E}}{d\lambda} &= \langle\Psi_0(\lambda)|\,\hat{V}\,|\Psi_0(\lambda)\rangle \\ &+ \Phi\,\frac{d}{d\lambda}\langle\Psi_0(\lambda)|\,Y(\lambda)\,|\Psi_0(\lambda)\rangle\,;\end{aligned} \tag{A.17}$$

so that

$$\begin{aligned}\delta\mathcal{E}_\Phi &= \int_0^1 d\lambda\,\langle\Psi_0(\lambda)|\,\hat{V}\,|\Psi_0(\lambda)\rangle \\ &+ \Phi\,\left(\,\langle\Psi_0(1)|\,Y(1)\,|\Psi_0(1)\rangle - \langle\Psi_0(0)|\,Y(0)\,|\Psi_0(0)\rangle\,\right)\,.\end{aligned} \tag{A.18}$$

The next sections of this appendix are devoted to the explicit calculation of the energy gain of the non-local energy functional out of equilibrium.

A.2.1 Non-equilibrium Green's functions

We write down here the expansion of the c and d operators in terms of scattering operators, that can be easily obtained inverting Eq. (A.9)

$$\begin{aligned}c^\dagger_{\bar\alpha\bar k\bar\sigma} &= \psi^\dagger_{\bar\alpha\bar k\bar\sigma} + \sum_{\alpha k}\frac{V_{\bar k}V_k}{\Omega}\,\frac{g^*(\epsilon_k)}{\epsilon_k-\epsilon_{\bar k}-i0^+}\,\psi^\dagger_{\alpha k\bar\sigma} \\ d^\dagger_{\bar\sigma} &= \sum_{\alpha k}\frac{V_k}{\sqrt{\Omega}}\,g^*(\epsilon_k)\,\psi^\dagger_{\alpha k\bar\sigma}\,,\end{aligned} \tag{A.19}$$

Eqs. (A.19) allows to calculate the spectral functions of any Green's function for the non-equilibrium Hamiltonian (A.10) using that

$$G^\Phi_{\psi_{\alpha k},\psi_{\alpha' k'}}(z) = \delta_{\alpha\alpha'}\delta_{kk'}\,\frac{1}{z-(\epsilon_k+\Phi\frac{\alpha}{2})}\,, \tag{A.20}$$

where $G^\Phi_{\psi_{\alpha k},\psi_{\alpha' k'}}$ is the Green's function of the scattering operators

$$G^\Phi_{\psi_{\alpha k},\psi_{\alpha' k'}}(z) = -\int_0^\beta d\tau e^{z\tau}\langle\Psi_0|\,\psi_{\alpha k\sigma}(\tau)\,\psi^\dagger_{\alpha' k'\sigma}\,|\Psi_0\rangle\,. \tag{A.21}$$

We underline that the Green's functions calculated withing the scattering operators have not any direct physical meaning, and have to be intended as a mathematical instrument that allow to calculate the average of any observable.

The impurity Green's function is

$$\begin{aligned} G^{\Phi}(z) &= \sum_{\alpha k} \frac{V_k^2}{\Omega} |g(\epsilon_k)|^2 \frac{1}{z-(\epsilon_k+\Phi\frac{\alpha}{2})} \\ &= \frac{1}{2}\sum_{\alpha} \int d\epsilon \frac{\rho(\epsilon)}{z-(\epsilon+\Phi\frac{\alpha}{2})}\,; \end{aligned} \tag{A.22}$$

while the mixed *dc* Green's functions are

$$\begin{aligned} G^{\Phi}_{\alpha k}(z) = & \frac{V_k}{\sqrt{\Omega}}\, g(\epsilon_k) \frac{1}{z-(\epsilon_k+\Phi\frac{\alpha}{2})} \\ & + \frac{V_k}{\sqrt{\Omega}} \sum_{k'\alpha'} \frac{V_{k'}^2}{\Omega} |g(\epsilon_{k'})|^2 \frac{1}{\epsilon_{k'}-\epsilon_k+i0^+} \frac{1}{z-(\epsilon_{k'}+\Phi\frac{\alpha'}{2})}\,. \end{aligned} \tag{A.23}$$

Notice that

$$\sum_{\alpha} G^{\Phi}_{\alpha k}(z) = \sum_{\alpha} G^{0}_{\alpha k}\left(z+\Phi\frac{\alpha}{2}\right)\,. \tag{A.24}$$

Let us calculate now the the *cc* Green's functions out of equilibrium. It can be easily verified that

$$\begin{aligned} G^{\Phi}_{\alpha_1 k_1,\alpha_2 k_2}(z) = & \delta_{k_1 k_2}\delta_{\alpha_1\alpha_2} \frac{1}{z-(\epsilon_{k_1}+\Phi\frac{\alpha_1}{2})} \\ & + \frac{1}{2}\sum_{\alpha} X^{0}_{\alpha_1 k_1,\alpha_2 k_2}\left(z+\Phi\frac{\alpha}{2}\right) \\ & + \alpha_1 \frac{V_k^2}{\Omega} \frac{g^*(\epsilon_{k_1})}{\epsilon_{k_1}-\epsilon_{k_2}-i0^+} \sum_{\alpha} \frac{\alpha}{2} \frac{1}{z-(\epsilon_{k_1}+\Phi\frac{\alpha}{2})} \\ & + \alpha_2 \frac{V_k^2}{\Omega} \frac{g(\epsilon_{k_2})}{\epsilon_{k_2}-\epsilon_{k_1}+i0^+} \sum_{\alpha} \frac{\alpha}{2} \frac{1}{z-(\epsilon_{k_2}+\Phi\frac{\alpha}{2})}\,, \end{aligned} \tag{A.25}$$

where

$$X^{0}_{\alpha_1 k_1,\alpha_2 k_2}(z) = \frac{1}{\Omega}\frac{V_{k_1}}{z-\epsilon_{k_1}} G^{0}(z) \frac{V_{k_2}}{z-\epsilon_{k_2}}\,. \tag{A.26}$$

When $k_1 = k_2$ and $\alpha_1 = \alpha_2$ Eq. (A.25) becomes

$$\begin{aligned} G^{\Phi}_{\alpha k,\alpha k}(z) = & \frac{1}{z-\left(\epsilon_k+\Phi\frac{\alpha}{2}\right)} \\ & + \frac{1}{2}\sum_{\alpha'} X^{0}_{\alpha k,\alpha k}\left(z+\Phi\frac{\alpha'}{2}\right) \\ & + \alpha \frac{V_k^2}{\Omega} \frac{g(\epsilon_k)-g^*(\epsilon_k)}{2i\,0^+} \sum_{\alpha'} \alpha' \frac{1}{z-(\epsilon_k+\Phi\frac{\alpha'}{2})}\,. \end{aligned} \tag{A.27}$$

that is divergent when $\Phi \neq 0$. We observe that

$$\sum_{\alpha} G^{\Phi}_{\alpha k,\alpha k}(z) = \sum_{\alpha} G^{0}_{\alpha k,\alpha k}\left(z + \Phi\frac{\alpha}{2}\right) , \tag{A.28}$$

is not divergent, while

$$\begin{aligned}\sum_{\alpha} \frac{\alpha}{2} G^{\Phi}_{\alpha k,\alpha k}(z) = &\sum_{\alpha} \frac{\alpha}{2} \frac{1}{z - (\epsilon_k + \Phi\frac{\alpha}{2})} \\ &+ \frac{V_k^2}{\Omega} \frac{g(\epsilon_k) - g^*(\epsilon_k)}{2i\,0^+} \sum_{\alpha'} \alpha' \frac{1}{z - (\epsilon_k + \Phi\frac{\alpha'}{2})} ,\end{aligned} \tag{A.29}$$

contains a divergent term proportional to $1/\Omega$, being Ω the volume of the system. In order to understand the physical meaning of the divergent term let us consider the charge difference of the two leads in the non-equilibrium steady state

$$\delta\mathcal{Q}^{\Phi} = T \sum_{\omega} e^{-i\omega 0^+} \sum_{k\alpha} \alpha\, G^{\Phi}_{\alpha k,\alpha k}(i\omega) \tag{A.30}$$

and the charge difference of the two leads at the initial time - before that the the tunnelling interaction is turned on -

$$\delta\mathcal{Q}^{0} = T \sum_{\omega} e^{-i\omega 0^+} \sum_{k\alpha} \alpha\, G^{0}_{\alpha k,\alpha k}(i\omega) . \tag{A.31}$$

The charge passed from one lead to the other during the infinite transient time necessary to reach the steady state is then

$$\delta\mathcal{Q}^{\Phi} - \delta\mathcal{Q}^{0} = 2\frac{V_k^2}{\Omega} \sum_{k\alpha} \frac{g(\epsilon_k) - g^*(\epsilon_k)}{2i\,0^+} \sum_{\alpha'} \alpha' f\left(\epsilon_k + \Phi\frac{\alpha'}{2}\right) = \infty ; \tag{A.32}$$

that is the expected result.

A.2.2 $\hat{V}$ energy gain

We calculate now the energy gain $\delta\mathcal{E}$ due to the tunnelling term out of equilibrium, namely the first term in Eq. (A.18).

Let us define

$$\mathcal{H}_{\lambda} = \sum_{\alpha k\sigma} \epsilon_k\, c^{\dagger}_{\alpha k\sigma} c_{\alpha k\sigma} + \sum_{\alpha k\sigma} \frac{\lambda V_k}{\sqrt{\Omega}} \left(d^{\dagger}_{\sigma} c_{\alpha k\sigma} + H.c.\right) + \sum_{\sigma} \epsilon_d \left(d^{\dagger}_{\sigma} d_{\sigma} - n_{\sigma}\right) . \tag{A.33}$$

We consider the Hamiltonian

$$\mathcal{H}_\lambda + \Phi Y_\lambda \;=\; \sum_{\alpha=-1,1} \sum_{k\sigma} \left(\epsilon_k + \Phi\frac{\alpha}{2}\right)\, \psi^\dagger_{\alpha k\sigma}(\lambda)\, \psi_{\alpha k\sigma}(\lambda) \tag{A.34}$$

where

$$\begin{aligned} \psi^\dagger_{\alpha k\sigma}(\lambda) \;&=\; c^\dagger_{\alpha k\sigma} + \frac{\lambda V_k}{\sqrt{\Omega}}\, g_\lambda(\epsilon_k)\, d^\dagger_\sigma \\ &+ \sum_{\alpha' k'\sigma'} \frac{\lambda^2 V_k V_{k'}}{\Omega}\, \frac{g_\lambda(\epsilon_k)}{\epsilon_k - \epsilon_{k'} + i0^+}\, c^\dagger_{\alpha' k'\sigma'}\,, \end{aligned} \tag{A.35}$$

The derivative of the average of the tunnelling term respect to the coefficient λ is, because of the Hellmann-Feynman theorem,

$$\frac{1}{2}\frac{\partial \delta\mathcal{E}_\Phi}{\partial\lambda} = 2T \sum_\omega e^{-i\omega 0^+} \sum_{k\alpha} \frac{V_k}{\sqrt{\Omega}}\, G^\alpha_{dk}(i\omega,\lambda) \;+\; c.c. \tag{A.36}$$

where

$$\begin{aligned} G^\alpha_{dk}(i\omega,\lambda) &= \frac{\lambda V_k}{\sqrt{\Omega}}\, g(\epsilon_k)\, \frac{1}{i\omega - (\epsilon_k + \Phi\frac{\alpha}{2})} \\ &+ \lambda^3 \sum_{k'\alpha'} \frac{V^2_{k'}}{\Omega}\, |g(\epsilon_{k'})|^2\, \frac{V_k}{\sqrt{\Omega}}\, \frac{1}{\epsilon_{k'} - \epsilon_k + i0^+}\, \frac{1}{i\omega - (\epsilon_{k'} + \Phi\frac{\alpha'}{2})}\,. \end{aligned} \tag{A.37}$$

It can be easily found that

$$\begin{aligned} &2T \sum_\omega e^{-i\omega 0^+} \sum_{\alpha k} \frac{V_k}{\sqrt{\Omega}}\, G^\alpha_{dk}(i\omega,\lambda) \;+\; c.c. \\ &= 2\frac{\partial}{\partial\lambda} \sum_\alpha \int \frac{d\epsilon}{2\pi}\, f\left(\epsilon + \Phi\frac{\alpha}{2}\right)\, \mathrm{Im}\left[\log\left(\epsilon - \epsilon_d - \Delta_\lambda(\epsilon)\right)\right]\,, \end{aligned} \tag{A.38}$$

where

$$\Delta_\lambda(\epsilon) = \lambda^2 \Delta(\epsilon)\,. \tag{A.39}$$

Integrating Eq. (A.36) we obtain that

$$\begin{aligned} \delta\mathcal{E}_\Phi \;&=\; \sum_\alpha \int \frac{d\epsilon}{\pi}\, f\left(\epsilon + \Phi\frac{\alpha}{2}\right)\, \mathrm{Im}\left[\log\left(\frac{\epsilon - \epsilon_d - \Delta(\epsilon)}{\epsilon - \epsilon_d}\right)\right] \\ &=\; -2T \sum_\omega \frac{1}{2} \sum_\alpha \log\left(\frac{\left(i\omega + \Phi\frac{\alpha}{2}\right) - \epsilon_d - \Delta\left(i\omega + \Phi\frac{\alpha}{2}\right)}{\left(i\omega + \Phi\frac{\alpha}{2}\right) - \epsilon_d}\right) \end{aligned} \tag{A.40}$$

Let us now consider now the energy gain due to the operator Y.

A.2.3 Y energy gain

In this section we calculate the energy gain $\delta\mathcal{E}$ due to the tunnelling term out of equilibrium, correspondent to the second term in Eq. (A.18).

Let us concentrate first on the energy of the "current" operator

$$Y_{mixed}(\lambda) = \sum_{\alpha k\sigma} \frac{\alpha}{2} \frac{\lambda V_k}{\sqrt{\Omega}} g(\epsilon_k)\, d^\dagger_\sigma c_{\alpha k\sigma} + H.c.\,. \tag{A.41}$$

We have to calculate

$$\begin{aligned} &\langle\Psi_0(1)|\, Y_{mixed}(1)\, |\Psi_0(1)\rangle - \langle\Psi_0(0)|\, Y_{mixed}(0)\, |\Psi_0(0)\rangle \\ &\quad = \sum_{\alpha k\sigma} \frac{\alpha}{2} \frac{V_k}{\sqrt{\Omega}} g(\epsilon_k)\, \langle\Psi_0(1)|\, d^\dagger_\sigma c_{\alpha k\sigma}\, |\Psi_0(1)\rangle + c.c.\,, \end{aligned} \tag{A.42}$$

that can be easily calculated using Eq.(A.23). The result is

$$\langle\Psi_0(1)|\, Y_{mixed}(1)\, |\Psi_0(1)\rangle - \langle\Psi_0(0)|\, Y_{mixed}(0)\, |\Psi_0(0)\rangle = -\int_{-\frac{\Phi}{2}}^{\frac{\Phi}{2}} d\epsilon\, \rho(\epsilon)\,, \tag{A.43}$$

where

$$\rho(\epsilon) = -\frac{1}{\pi} \operatorname{Im} g(\epsilon)\,. \tag{A.44}$$

Let us consider now the contribution of the operator

$$Y^{(1)}_{leads} = \sum_{\alpha k\sigma} \frac{\alpha}{2} c^\dagger_{\alpha k\sigma} c_{\alpha k\sigma}\,. \tag{A.45}$$

that is

$$\begin{aligned} &\langle\Psi_0(1)|\, Y^{(1)}_{leads}\, |\Psi_0(1)\rangle - \langle\Psi_0(0)|\, Y^{(1)}_{leads}\, |\Psi_0(0)\rangle \\ &\quad = \sum_{\alpha k\sigma} \frac{\alpha}{2} \langle\Psi_0(1)|\, c^\dagger_{\alpha k\sigma} c_{\alpha k\sigma}\, |\Psi_0(1)\rangle - \sum_{\alpha k\sigma} \frac{\alpha}{2} \langle\Psi_0(0)|\, c^\dagger_{\alpha k\sigma} c_{\alpha k\sigma}\, |\Psi_0(0)\rangle \\ &\quad = T \sum_\omega \sum_{k\sigma} \left(\sum_\alpha \frac{\alpha}{2} G^\Phi_{\alpha k,\alpha k}(i\omega) \right) - \sum_{\alpha k\sigma} \frac{\alpha}{2} \langle\Psi_0(1)|\, \psi^\dagger_{\alpha k\sigma} \psi_{\alpha k\sigma}\, |\Psi_0(1)\rangle \\ &\quad = T \sum_\omega \sum_{k\sigma} \frac{V_k^2}{\Omega} \frac{g(\epsilon_k) - g^*(\epsilon_k)}{2i\, 0^+} \sum_{\alpha'} \alpha' \frac{1}{z - (\epsilon_k + \Phi\frac{\alpha'}{2})}\,, \end{aligned} \tag{A.46}$$

where we have used Eq. (A.29).

Let us consider, finally, the contribution of the operator

$$Y^{(2)}_{leads} = \sum_{\alpha k\sigma} \frac{\alpha}{2} \sum_{\alpha' k'} \frac{V_k V_{k'}}{\Omega} \frac{g(\epsilon_{k'})}{\epsilon_k - \epsilon_{k'} + i0^+} c^\dagger_{\alpha' k'\sigma} c_{\alpha k\sigma} + H.c.\,. \tag{A.47}$$

Its energy contribution - in the termodinamic limit - is

$$\begin{aligned}
&\langle \Psi_0(1)|\, Y^{(2)}_{leads}\, |\Psi_0(1)\rangle - \langle \Psi_0(0)|\, Y^{(2)}_{leads}\, |\Psi_0(0)\rangle \\
&= T \sum_\omega \sum_{k\sigma} \frac{V_k^2}{\Omega} \frac{g(\epsilon_k)}{2i\,0^+} \sum_{\alpha'} \alpha' \frac{1}{z - (\epsilon_k + \Phi\frac{\alpha'}{2})} + c.c. \\
&= T \sum_\omega \sum_{k\sigma} \frac{V_k^2}{\Omega} \frac{g(\epsilon_k) - g^*(\epsilon_k)}{2i\,0^+} \sum_{\alpha'} \alpha' \frac{1}{z - (\epsilon_k + \Phi\frac{\alpha'}{2})}\,;
\end{aligned} \tag{A.48}$$

that is equal to the infinite energy contribution of $Y^{(1)}_{leads}$, and that is, explicitly,

$$\begin{aligned}
&T \sum_\omega \sum_{k\sigma} \frac{V_k^2}{\Omega} \frac{g(\epsilon_k) - g^*(\epsilon_k)}{2i\,0^+} \sum_{\alpha'} \alpha' \frac{1}{z - (\epsilon_k + \Phi\frac{\alpha'}{2})} \\
&= -\infty \int_{-\frac{\Phi}{2}}^{\frac{\Phi}{2}} d\epsilon \Gamma(\epsilon)\rho(\epsilon)
\end{aligned} \tag{A.49}$$

A.3 The current

We consider the current operator

$$\hat{I} = -i \sum_{k\sigma} \frac{V_k}{\sqrt{\Omega}} \left(d^\dagger_\sigma c_{k\sigma,-1} - H.c.\,. \right) \tag{A.50}$$

where, as usual, $\beta = -1$ is the label of the left lead. The average of $\hat{I}$ on the ground state of the Hershfield Hamiltonian $H + \Phi Y$ defined in Eq. (A.10) is

$$\begin{aligned}
I &= iT \sum_\omega e^{-i\omega 0^+} \sum_{k\sigma} \frac{V_k}{\sqrt{\Omega}} \left(G^\Phi_{-1\,k}(i\omega) - c.c. \right) \\
&= \int_{-\frac{\Phi}{2}}^{\frac{\Phi}{2}} d\epsilon\, \Gamma \sqrt{1 - \epsilon^2}\, \rho(\epsilon)\,.
\end{aligned} \tag{A.51}$$

Appendix B

Detailed calculations for the two-dots model with Gutzwiller

In chapter 5 we have studied the two-dots model within the Gutzwiller approximation. In order to simplify our calculations we have considered a variational wavefunction invariant under the action of a symmetry group G that doesn't satisfy condition (2.46), namely the condition to apply the mathematical method developed in chapter 4. For this reason a specific treatment has been necessary.

B.1 The symmetry group of the Gutzwiller wavefunction

It is well known that the two-dot system Hamiltonian Eq. (5.80) is invariant, respect to the spin rotations group of the two dots $SU(2)_{\text{spin}}$ and, provided that the two baths are particle-hole invariant, respect to the isospin rotations group $SU(2)_{\text{charge}}$, generated by the operators

$$\begin{aligned} I_z &= n_1 + n_2 - 2 \\ I^+ &= d^\dagger_{1\uparrow} d^\dagger_{2\downarrow} - d^\dagger_{1\downarrow} d^\dagger_{2\uparrow} \\ I^- &= (I^+)^\dagger . \end{aligned} \tag{B.1}$$

Nevertheless, we analyze the problem allowing the wavefunction to have a finite value of

$$\Delta = \langle d^\dagger_{1\uparrow} d^\dagger_{2\downarrow} \rangle \,, \tag{B.2}$$

partially breaking the $SU(2)_{\text{charge}}$ symmetry. Namely, we consider only variational functions invariant under the action of the group G which contains the following transformations:

- the spin rotation group $SU(2)_{\text{spin}}$,
- the symmetry under permutation of the two dots,
- the Gauge transformation

$$\begin{aligned} &d_{1\uparrow} \to d_{1\uparrow} e^{i\phi_1} \,; \;\; d_{1\downarrow} \to d_{1\downarrow} e^{i\phi_2} \\ &d_{2\downarrow} \to d_{2\downarrow} e^{-i\phi_1} \,; \;\; d_{2\uparrow} \to d_{2\uparrow} e^{-i\phi_2} \,, \end{aligned} \tag{B.3}$$

- the particle-hole transformation

$$\begin{aligned} &d^\dagger_{1\uparrow} \to d_{2\downarrow} \,; \;\; d^\dagger_{2\downarrow} \to d_{1\uparrow} \\ &d^\dagger_{1\downarrow} \to -d_{2\uparrow} \,; \;\; d^\dagger_{2\uparrow} \to -d_{1\downarrow} \,. \end{aligned} \tag{B.4}$$

Notice that the particular choice of the particle-hole symmetry (B.4) allows Δ, defined in Eq. (B.2), to be finite.

B.2 The natural basis

Let us introduce the spinor

$$\phi^\dagger = \left(d^\dagger_{1\uparrow} \, d_{2\downarrow} \, d^\dagger_{2\uparrow} \, d_{1\downarrow} \right) \,. \tag{B.5}$$

The variational density matrix

$$\mathcal{C}_{ij} = \langle \Psi_0 | \, \phi^\dagger_i \phi_j \, | \Psi_0 \rangle \tag{B.6}$$

must have, because of the assumed invariance of $|\psi_0\rangle$ respect to G, the following form

$$\mathcal{C} = \begin{pmatrix} \frac{1}{2} & \delta & 0 & 0 \\ \delta & \frac{1}{2} & 0 & 0 \\ 0 & 0 & \frac{1}{2} & \delta \\ 0 & 0 & \delta & \frac{1}{2} \,. \end{pmatrix} \tag{B.7}$$

We observe that the orthogonal transformation which diagonalizes (B.7) does not depends on the specific value of δ; namely, it does not depend on the specific variational state, provided that it is invariant under the action of G. The natural basis is

$$\begin{aligned} f^\dagger_{1\uparrow} &= \frac{d^\dagger_{1\uparrow} + d_{2\downarrow}}{\sqrt{2}}\,; \quad f^\dagger_{1\downarrow} = \frac{d^\dagger_{1\downarrow} - d_{2\uparrow}}{\sqrt{2}} \\ f^\dagger_{2\uparrow} &= \frac{d^\dagger_{2\uparrow} + d_{1\downarrow}}{\sqrt{2}}\,; \quad f^\dagger_{2\downarrow} = \frac{d^\dagger_{2\downarrow} - d_{1\uparrow}}{\sqrt{2}} \end{aligned} \tag{B.8}$$

If we introduce the spinor

$$\phi^\dagger_0 = \left(f^\dagger_{1\uparrow}\, f_{2\downarrow}\, f^\dagger_{2\uparrow}\, f_{1\downarrow} \right) \tag{B.9}$$

the correspondent variational density matrix

$$\mathcal{C}^0_{ij} = \langle \Psi_0 |\, \phi^\dagger_{0i} \phi_{0j}\, | \Psi_0 \rangle \tag{B.10}$$

is

$$\mathcal{C}^0 = \begin{pmatrix} \frac{1}{2}+\delta & 0 & 0 & 0 \\ 0 & \frac{1}{2}-\delta & 0 & 0 \\ 0 & 0 & \frac{1}{2}+\delta & 0 \\ 0 & 0 & 0 & \frac{1}{2}-\delta\,. \end{pmatrix} \tag{B.11}$$

B.3 The parametrization strategy

The Gutzwiller projector $\mathcal{P}$ must be invariant under the action of G. The parametrization of those projectors which satisfy the symmetry condition

$$[\mathcal{P}, G] = 0 \tag{B.12}$$

is very easy if we chose to represent it in the basis of states that decompose the local Hilbert space in irreducible representations of $SU(2)_{\text{spin}}$:

$$\mathcal{P}_{\mathbf{R}} = \sum_{\{\tilde{\Gamma}_\alpha\}\{\tilde{\Gamma}'_\alpha\}} \tilde{\lambda}_{\{\tilde{\Gamma}_\alpha\}\{\tilde{\Gamma}'_\alpha\}}(\mathbf{R})\, |\{\tilde{\Gamma}_\alpha\}, \mathbf{R}\rangle\langle\{\tilde{\Gamma}'_\alpha\}, \mathbf{R}|, \tag{B.13}$$

We consider the transformation V which relates the Fock original basis $|\{\Gamma_\alpha\}, \mathbf{R}\rangle$ to the correlated basis $|\{\tilde{\Gamma}_\alpha\}, \mathbf{R}\rangle$

$$V|\{\tilde{\Gamma}_\alpha\}, \mathbf{R}\rangle = |\{\Gamma_\alpha\}, \mathbf{R}\rangle \tag{B.14}$$

and the transformation U which relates the Fock natural basis $|\{n_\alpha\},\mathbf{R}\rangle$ to the Fock original basis $|\{\Gamma_\alpha\},\mathbf{R}\rangle$

$$U|\{\Gamma_\alpha\},\mathbf{R}\rangle = |\{n_\alpha\},\mathbf{R}\rangle\,. \tag{B.15}$$

Using relations (B.14) and (B.15) we can easily find that the coefficients of the natural-basis representation of the Gutzwiller projector

$$\mathcal{P}_{\mathbf{R}} = \sum_{\{n_\alpha\}\{n'_\alpha\}} \lambda_{\{n_\alpha\}\{n'_\alpha\}}(\mathbf{R})\,|\{n_\alpha\},\mathbf{R}\rangle\langle\{n'_\alpha\},\mathbf{R}|\,, \tag{B.16}$$

are related with the coefficients of the correlated-basis representation (B.13) as it follows:

$$\lambda = (VU)^\dagger\,\tilde{\lambda}\,(VU) \tag{B.17}$$

We introduce, as in chapter 2, the occupation-probability P^0 in the natural basis

$$P^0_{\{n_\alpha\}\{m_\alpha\}} \equiv \langle\Psi_0|\,|\{m_\alpha\}\rangle\langle\{n_\alpha\}|\,|\Psi_0\rangle = \delta_{\{n_\alpha\}\{m_\alpha\}}\,P^0_{\{n_\alpha\}}\,, \tag{B.18}$$

and the the matrix

$$\phi = \lambda\,\sqrt{P^0}\,. \tag{B.19}$$

In terms of $\tilde{\phi}$, the Gutzwiller constraints are

$$\begin{aligned}
\mathrm{Tr}\left(\tilde{\phi}^\dagger\,\tilde{\phi}\;\right) &= 1, && \text{(B.20)}\\
\mathrm{Tr}\left(\tilde{\phi}^\dagger\,\tilde{\phi}\;\;\tilde{f}^\dagger_\alpha\tilde{f}_\beta\right) &= \langle\Psi_0|\,f^\dagger_\alpha f_\beta\,|\Psi_0\rangle = \delta_{\alpha\beta}\,n^0_\alpha, && \text{(B.21)}\\
\mathrm{Tr}\left(\tilde{\phi}^\dagger\,\tilde{\phi}\;\;\tilde{f}^\dagger_\alpha\tilde{f}^\dagger_\beta\right) &= \langle\Psi_0|\,f^\dagger_\alpha f^\dagger_\beta\,|\Psi_0\rangle = 0, && \text{(B.22)}
\end{aligned}$$

where

$$\tilde{f}^\dagger_\alpha = (VU)^\dagger\,f^\dagger_\alpha\,(VU) \tag{B.23}$$

is the representation of the natural-basis Fock operator $f^\dagger_\alpha$ in the $|\{\Gamma_\alpha\},\mathbf{R}\rangle$ representation.

We observe that all the Gutzwiller constraints on the matrix of variatonal parameters ϕ are automatically satisfied: equations

$$\begin{aligned}
\mathrm{Tr}\left(\tilde{\phi}^\dagger\,\tilde{\phi}\;\;\tilde{f}^\dagger_{1\sigma}\tilde{f}^\dagger_{2\sigma}\right) &= 0\\
\mathrm{Tr}\left(\tilde{\phi}^\dagger\,\tilde{\phi}\;\;\tilde{f}^\dagger_{\alpha\uparrow}\tilde{f}^\dagger_{\alpha\downarrow}\right) &= 0 && \text{(B.24)}
\end{aligned}$$

are satisfied because of the invariance respect to the Gouge transformation (B.3); while the constraints

$$\begin{aligned} \mathrm{Tr}\left(\tilde{\phi}^\dagger\,\tilde{\phi}\ \ \left(\tilde{f}^\dagger_{1\uparrow}\tilde{f}^\dagger_{2\downarrow}+\tilde{f}^\dagger_{1\downarrow}\tilde{f}^\dagger_{2\uparrow}\right)\right) &= 0 \\ \mathrm{Tr}\left(\tilde{\phi}^\dagger\,\tilde{\phi}\ \ \left(\tilde{f}^\dagger_{1\uparrow}\tilde{f}^\dagger_{2\downarrow}-\tilde{f}^\dagger_{1\downarrow}\tilde{f}^\dagger_{2\uparrow}\right)\right) &= 0 \end{aligned} \tag{B.25}$$

are satisfied because of the invariance respect to $SU(2)_{\mathrm{spin}}$ and to the particle-hole transformation (B.4) respectively.

Following the parametrization strategy described in chapter 2, we consider the most general matrix $\tilde{\phi}$ invariant under the action of G and which satisfy the normalization condition (B.20) and we force the uncorrelated wavefunction $|\Psi_0\rangle$ to satisfy the Gutzwiller constraints Eqs. (B.21) and (B.22).

B.4 The non-local equilibrium energy functional

Let us consider the two-dots Hamiltonian

$$\begin{aligned} \mathcal{H} &= \sum_{\alpha=-1,1}\sum_{\beta k\sigma}\epsilon_k\, c^\dagger_{\alpha\beta k\sigma}c_{\alpha\beta k\sigma}+\sum_{\alpha=-1,1}\sum_{\beta k\sigma}\frac{V_k}{\sqrt{\Omega}}\,d^\dagger_{\sigma\beta}c_{\alpha\beta k\sigma}+H.c. \\ &+ J\,\mathcal{S}_1\mathcal{S}_2+\sum_\beta\frac{U}{2}(n_\beta-1)^2\,. \end{aligned} \tag{B.26}$$

When we calculate the average of the tunnelling operator

$$\hat{V}=\sum_{\alpha=-1,1}\sum_{\beta k\sigma}\frac{V_k}{\sqrt{\Omega}}\,d^\dagger_{\sigma\beta}c_{\alpha\beta k\sigma}+H.c. \tag{B.27}$$

on a normalized correlated wavefunction which satisfies the Gutzwiller constraints (B.21) and (B.22), the result is that

$$\langle\Psi_0|\,\mathcal{P}_d^\dagger\,\hat{V}\,\mathcal{P}_d\,|\Psi_0\rangle=\langle\Psi_0|\,\hat{V}_R\,|\Psi_0\rangle\,, \tag{B.28}$$

where the renormalized tunnelling $\hat{V}_R$ is obtained effectively transforming the impurity operators $d^\dagger_{\sigma\beta}$ as it follows:

$$d^\dagger_{\sigma\beta}\to R\,d^\dagger_{\sigma\beta}\,, \tag{B.29}$$

where

$$R = \frac{\mathrm{Tr}\left(\tilde{\phi}^{\dagger}\tilde{f}^{\dagger}_{\sigma\beta}\tilde{\phi}\ \tilde{f}_{\sigma\beta}\right)}{\sqrt{n(1-n)}}\,. \tag{B.30}$$

We have now to calculate the uncorrelated state $|\psi_0\rangle$ that minimizes the renormalized Hamiltonian

$$\mathcal{H}_R = \sum_{\alpha=-1,1}\sum_{\beta k\sigma} \epsilon_k\, c^{\dagger}_{\alpha\beta k\sigma} c_{\alpha\beta k\sigma} + \hat{V}_R \tag{B.31}$$

and satisfies the conditions (B.21) and (B.22). This state can be calculated within the Lagrange multipliers method, namely, $|\psi_0\rangle$ is the ground state of the Hamiltonian

$$\begin{aligned}\mathcal{H}_R^{Lag} &= \sum_{\alpha=-1,1}\sum_{\beta k\sigma} \epsilon_k\, c^{\dagger}_{\alpha\beta k\sigma} c_{\alpha\beta k\sigma} + \hat{V}_R \\ &\quad + \Delta\left(\frac{d^{\dagger}_{1\uparrow}d^{\dagger}_{2\downarrow} - d^{\dagger}_{1\downarrow}d^{\dagger}_{2\uparrow}}{2} + H.c. - \delta\right) \\ &\quad + \mu\sum_{\beta\sigma}\left(d^{\dagger}_{\beta\sigma}d_{\beta\sigma} - \frac{1}{2}\right)\end{aligned} \tag{B.32}$$

with Δ and μ such that

$$\begin{aligned}\langle\Psi_0|\, d^{\dagger}_{\beta\sigma}d_{\beta\sigma}\,|\Psi_0\rangle &= \frac{1}{2} \\ \langle\Psi_0|\, d^{\dagger}_{1\uparrow}d^{\dagger}_{2\downarrow} - d^{\dagger}_{1\downarrow}d^{\dagger}_{2\uparrow}\,|\Psi_0\rangle &= \delta\,.\end{aligned} \tag{B.33}$$

The problem is simplified if we assume that the two leads are particle-hole symmetric. If this condition is satisfied one can apply, as we shall prove later, a unitary transformation on the $c^{\dagger}_{\sigma\beta}$ and $d^{\dagger}_{\beta\sigma}$ operators of the Hamiltonian (B.32) that leaves unchanged the tunnelling term

$$\hat{V}_R = \sum_{\alpha=-1,1}\sum_{\beta k\sigma} \frac{R\,V_k}{\sqrt{\Omega}}\, d^{\dagger}_{\sigma\beta}c_{\alpha\beta k\sigma} + H.c. \tag{B.34}$$

and the leads Hamiltonian

$$\hat{T} = \sum_{\alpha=-1,1}\sum_{\beta k\sigma} \epsilon_k\, c^{\dagger}_{\alpha\beta k\sigma} c_{\alpha\beta k\sigma}\,, \tag{B.35}$$

and that transforms $\mathcal{H}_R^{Lag}$ in the Hamiltonian of two equal uncoupled single-dot systems

$$\begin{aligned}\mathcal{H}_R^{'Lag} &= \sum_\beta \Bigg\{ \sum_{\alpha=-1,1} \sum_{k\sigma} \epsilon_k \, c^\dagger_{\alpha\beta k\sigma} c_{\alpha\beta k\sigma} + \sum_{\alpha=-1,1} \sum_{k\sigma} \frac{R V_k}{\sqrt{\Omega}} \, d^\dagger_{\sigma\beta} c_{\alpha\beta k\sigma} + H.c. \\ &+ \sum_{\alpha=-1,1} \sum_{\sigma} \epsilon_d \, (d^\dagger_{\sigma\beta} d_{\sigma\beta} - n) \Bigg\} \equiv \sum_\beta \mathcal{H}_R^{'Lag}(\beta) \, . \end{aligned} \tag{B.36}$$

being

$$n = \frac{1}{2} + \delta \, . \tag{B.37}$$

Such operation, being unitary, doesn't change the minimum energy of the original Hamiltonian $\mathcal{H}_R^{Lag}$. The chemical potential ϵ_d can be calculated following section A.1.

B.5 The non-local non-equilibrium energy functional

Following the procedure described in chapter 5, we construct the operator Y_R from the correspondent equilibrium Hamiltonian $\mathcal{H}_R^{Lag}$ - the Hamiltonian defined in Eq. (B.32) - within the scattering operators, and we find the state that minimizes the mean value of

$$\mathcal{H}_R^*(\phi) = \mathcal{H}_R^{Lag} + \Phi \, Y_R \, . \tag{B.38}$$

The operator Y_R is formally the asintotic time evolution of the operator

$$Y_R^{(0)} = \sum_{\alpha=-1,1} \sum_{\beta k\sigma} \frac{\alpha}{2} \, c^\dagger_{\alpha\beta k\sigma} c_{\alpha\beta k\sigma} \tag{B.39}$$

generated by $\mathcal{H}_R^{Lag}$. In order to calculate

$$Y_R = e^{i\mathcal{H}_R^{Lag} T} \, Y_R^{(0)} \, e^{-i\mathcal{H}_R^{Lag} T} \tag{B.40}$$

we can perform, similarly to what we did for the equilibrium problem, a unitary transformation U on the $c^\dagger_{\sigma\beta}$ and $d^\dagger_{\beta\sigma}$ operators that leaves unchanged the

leads Hamiltonian $\hat{T}$ and the operator $Y_R^{(0)}$, and that transforms $\mathcal{H}_R^{Lag}$ in the Hamiltonian of two uncoupled Hamiltonian $\mathcal{H}_R^{'Lag}$ defined in Eq. (B.36)

$$\mathcal{H}_R^{'Lag} \equiv \sum_{\alpha=-1,1} \sum_{\beta k\sigma} \epsilon_k \, \psi'^{\dagger}_{\alpha\beta k\sigma} \psi'_{\alpha\beta k\sigma} \tag{B.41}$$

and, consequently, that transforms Y_R in

$$\begin{aligned} Y_R^{'} &= e^{i\mathcal{H}_R^{'Lag}T} \, Y_R^{(0)} \, e^{-i\mathcal{H}_R^{'Lag}T} \\ &\equiv \sum_{\alpha=-1,1} \sum_{\beta k\sigma} \frac{\alpha}{2} \, \psi'^{\dagger}_{\alpha\beta k\sigma} \psi'_{\alpha\beta k\sigma} \, , \end{aligned} \tag{B.42}$$

where

$$\begin{aligned} \psi'^{\dagger}_{\alpha\beta k\sigma} &= c^{\dagger}_{\alpha\beta k\sigma} + \frac{R\, V_k}{\sqrt{\Omega}} \, g_R^{\epsilon_d}(\epsilon_k) \, d^{\dagger}_{\beta\sigma} \\ &+ \sum_{\alpha'\beta' k'\sigma'} \frac{R^2 \, V_k V_{k'}}{\Omega} \, \frac{g_R^{\epsilon_d}(\epsilon_k)}{\epsilon_k - \epsilon_{k'} + i0^+} \, c^{\dagger}_{\alpha'\beta' k'\sigma'} \, . \end{aligned} \tag{B.43}$$

In order to calculate the non-equilibrium energy functional we have now to find the state $|\psi_0\rangle$ that minimizes the energy of

$$\mathcal{H}_R^{'*}(\Phi) = \sum_{\alpha=-1,1} \sum_{\beta k\sigma} \left(\epsilon_k + \Phi \, \frac{\alpha}{2} \right) \, \psi'^{\dagger}_{\alpha\beta k\sigma} \psi'_{\alpha\beta k\sigma} \, , \tag{B.44}$$

representing two uncoupled single-orbital Hershfield Hamiltonians, where ϵ_d is the same of Eq.(B.36).

B.5.1 Useful canonical transformation

Let us consider an impurity model coupled to a particle-hole symmetric infinite bath. The Hamiltonian is

$$\begin{aligned} H &= \sum_{a=1}^{2} \sum_{\sigma} \int_{-D}^{D} d\epsilon \left[\epsilon \, c^{\dagger}_{\epsilon a\sigma} c_{\epsilon a\sigma} + V \left(c^{\dagger}_{\epsilon a\sigma} d_{a\sigma} + H.c. \right) \right] \\ &+ \Delta \left(d^{\dagger}_{1\uparrow} d^{\dagger}_{2\downarrow} + d^{\dagger}_{2\uparrow} d^{\dagger}_{1\downarrow} + H.c. \right) . \end{aligned}$$

We can introduce the Nambu spinors

$$\begin{aligned}
\Psi_{1\epsilon} &= \begin{pmatrix} c_{\epsilon 1\uparrow} \\ -c^{\dagger}_{-\epsilon 2\downarrow} \end{pmatrix}, \\
\Psi_{2\epsilon} &= \begin{pmatrix} c_{\epsilon 2\uparrow} \\ -c^{\dagger}_{-\epsilon 1\downarrow} \end{pmatrix}, \\
D_1 &= \begin{pmatrix} d_{1\uparrow} \\ d^{\dagger}_{2\downarrow} \end{pmatrix}, \\
D_2 &= \begin{pmatrix} d_{2\uparrow} \\ d^{\dagger}_{1\downarrow} \end{pmatrix},
\end{aligned}$$

as well as their hermitean conjugate operators. In the Nambu space we introduce the Pauli matrices τ_i, $i = 0, \ldots, 3$, where τ_0 is the identity. In the Nambu language the Hamiltonian reads

$$\begin{aligned}
H &= \sum_{a=1}^{2} \int_{-D}^{D} d\epsilon \left[\epsilon \, \Psi^{\dagger}_{a\epsilon} \, \tau_0 \, \Psi^{\dagger}_{a\epsilon} + V \left(\Psi^{\dagger}_{a\epsilon} \, \tau_0 \, D_a + H.c. \right) \right] \\
&\quad + \Delta \sum_a D^{\dagger}_a \, \tau_1 \, D_a .
\end{aligned}$$

The first two terms only involve τ_0, hence are invariant under any unitary transformation in the Nambu space. In particular, we consider the transformation

$$\begin{aligned}
\Psi_{a\epsilon} &= U \, \Phi_{a\epsilon} \equiv \mathrm{e}^{-i\frac{\pi}{4}\tau_2} \, \Phi_{a\epsilon}, \\
D_a &= U \, F_a \equiv \mathrm{e}^{-i\frac{\pi}{4}\tau_2} \, F_a .
\end{aligned}$$

Since

$$\mathrm{e}^{i\frac{\pi}{4}\tau_2} \, \tau_1 \, \mathrm{e}^{-i\frac{\pi}{4}\tau_2} = \tau_3,$$

it follows that

$$\begin{aligned}
H &= \sum_{a=1}^{2} \int_{-D}^{D} d\epsilon \left[\epsilon \, \Phi^{\dagger}_{a\epsilon} \, \tau_0 \, \Phi^{\dagger}_{a\epsilon} + V \left(\Phi^{\dagger}_{a\epsilon} \, \tau_0 \, F_a + H.c. \right) \right] \\
&\quad + \Delta \sum_a F^{\dagger}_a \, \tau_3 \, F_a ,
\end{aligned}$$

which is now a diagonal Hamiltonian that describes two independent resonant level models. Note that a bath chemical potential is not invariant under the above unitary transformation. In fact

$$\begin{aligned} -\mu N &= -\mu \sum_{a=1}^{2}\sum_{\sigma}\int_{-D}^{D} d\epsilon\, c^{\dagger}_{\epsilon a\sigma}c_{\epsilon a\sigma} = -\mu \sum_{a=1}^{2}\int_{-D}^{D} d\epsilon\, \Psi^{\dagger}_{a\epsilon}\,\tau_3\,\Psi_{a\epsilon} + const. \\ &= \mu \sum_{a=1}^{2}\int_{-D}^{D} d\epsilon\, \Phi^{\dagger}_{a\epsilon}\,\tau_1\,\Phi_{a\epsilon} + const. \end{aligned}$$

Now we consider two baths $\alpha = \pm 1$ at different chemical potential. The Hamiltonian reads

$$\begin{aligned} H &= \sum_{\alpha=\pm1}\sum_{a=1}^{2}\sum_{\sigma}\int_{-D}^{D} d\epsilon \left[\epsilon\, c^{\dagger}_{\epsilon\alpha a\sigma}c_{\epsilon\alpha a\sigma} + V\left(c^{\dagger}_{\epsilon\alpha a\sigma}d_{a\sigma} + H.c.\right)\right] \\ &\quad +\Delta\left(d^{\dagger}_{1\uparrow}d^{\dagger}_{2\downarrow} + d^{\dagger}_{2\uparrow}d^{\dagger}_{1\downarrow} + H.c.\right), \end{aligned}$$

while the bias term is

$$\Phi\, Y_0 = \Phi\,\frac{1}{2}\sum_{\alpha=\pm1}\sum_{a=1}^{2}\sum_{\sigma}\int_{-D}^{D} d\epsilon\,\alpha\, c^{\dagger}_{\epsilon\alpha a\sigma}c_{\epsilon\alpha a\sigma}.$$

In this case I introduce different Nambu spinors

$$\begin{aligned} \Psi_{\alpha\,1\epsilon} &= \begin{pmatrix} c_{\epsilon\alpha 1\uparrow} \\ -c^{\dagger}_{-\epsilon-\alpha 2\downarrow} \end{pmatrix}, \\ \Psi_{\alpha\,2\epsilon} &= \begin{pmatrix} c_{\epsilon\alpha 2\uparrow} \\ -c^{\dagger}_{-\epsilon-\alpha 1\downarrow} \end{pmatrix}, \\ D_1 &= \begin{pmatrix} d_{1\uparrow} \\ d^{\dagger}_{2\downarrow} \end{pmatrix}, \\ D_2 &= \begin{pmatrix} d_{2\uparrow} \\ d^{\dagger}_{1\downarrow} \end{pmatrix}, \end{aligned}$$

through which the Hamiltonian can be rewritten as

$$\begin{aligned} H &= \sum_{\alpha=\pm1}\sum_{a=1}^{2}\int_{-D}^{D} d\epsilon \left[\epsilon\,\Psi^{\dagger}_{\alpha\,a\epsilon}\,\tau_0\,\Psi^{\dagger}_{\alpha\,a\epsilon} + V\left(\Psi^{\dagger}_{\alpha\,a\epsilon}\,\tau_0\,D_a + H.c.\right)\right] \\ &\quad +\Delta\sum_{a} D^{\dagger}_{a}\,\tau_1\,D_a, \end{aligned}$$

while the bias as

$$\Phi\, Y_0 = \frac{\Phi}{2} \sum_{\alpha=\pm 1} \sum_{a=1}^{2} \int_{-D}^{D} d\epsilon\, \alpha\, \Psi^{\dagger}_{\alpha\, a\epsilon}\, \tau_0\, \Psi_{\alpha\, a\epsilon}.$$

Under the unitary transformation

$$\begin{aligned} \Psi_{\alpha\, a\epsilon} &= U\, \Phi_{\alpha\, a\epsilon} \equiv \mathrm{e}^{-i\frac{\pi}{4}\tau_2}\, \Phi_{\alpha\, a\epsilon}, \\ D_a &= U\, F_a \equiv \mathrm{e}^{-i\frac{\pi}{4}\tau_2}\, F_a, \end{aligned}$$

the Hamiltonian becomes diagonal, i.e.

$$\begin{aligned} H &= \sum_{\alpha=\pm 1} \sum_{a=1}^{2} \int_{-D}^{D} d\epsilon \left[\epsilon\, \Phi^{\dagger}_{\alpha\, a\epsilon}\, \tau_0\, \Phi^{\dagger}_{\alpha\, a\epsilon} + V \left(\Phi^{\dagger}_{\alpha\, a\epsilon}\, \tau_0\, F_a + H.c. \right) \right] \\ &\quad + \Delta \sum_a F^{\dagger}_a\, \tau_3\, F_a, \end{aligned}$$

as well as the bias

$$\Phi\, Y_0 = \frac{\Phi}{2} \sum_{\alpha=\pm 1} \sum_{a=1}^{2} \int_{-D}^{D} d\epsilon\, \alpha\, \Phi^{\dagger}_{\alpha\, a\epsilon}\, \tau_0\, \Phi_{\alpha\, a\epsilon}.$$

This also shows that the form of the Gutzwiller projector compatible with the symmetry at equilibrium remains unaltered also out-of-equilibrium.

Bibliography

[1] A. Georges, G. Kotliar, W. Krauth, and M. J. Rozenberg. Dynamical mean-field theory of strongly correlated fermion systems and the limit of infinite dimensions. *Rev. Mod. Phys.*, 68(1):13, 1996.

[2] V. I. Anisimov, F. Aryasetiawan, and A.I. Lichtenstein. First-principles calculations of the electronic structure and spectra of strongly correlated systems: the LDA+U method. *J. Phys.: Condens. Matter*, 9:767, 1997.

[3] G. Kotliar, S. Y. Savrasov, K. Haule, V. S. Oudovenko, O. Parcollet, and C. A. Marianetti. Electronic structure calculations with dynamical mean-field theory. *Rev. Mod. Phys.*, 78(3):865, 2006.

[4] W. F. Brinkman and T. M. Rice. Application of Gutzwiller's Variational Method to the Metal-Insulator Transition. *Phys. Rev. B*, 2(10):4302–4304, 1970.

[5] Gabriel Kotliar and Jialin Liu. Superexchange mechanism and d-wave superconductivity. *Phys. Rev. B*, 38(7):5142–5145, 1988.

[6] Martin C. Gutzwiller. Effect of Correlation on the Ferromagnetism of Transition Metals. *Phys. Rev. Lett.*, 10(5):159–162, 1963.

[7] Martin C. Gutzwiller. Effect of Correlation on the Ferromagnetism of Transition Metals. *Phys. Rev.*, 134(4A):A923–A941, 1964.

[8] Martin C. Gutzwiller. Correlation of Electrons in a Narrow s Band. *Phys. Rev.*, 137(6A):A1726–A1735, 1965.

[9] G. R. Stewart. Heavy-fermion systems. *Rev. Mod. Phys.*, 56(4):755–787, 1984.

[10] G. R. Stewart. Non-Fermi-liquid behavior in d- and f-electron metals. *Rev. Mod. Phys.*, 73(4):797–855, 2001.

[11] T. M. Rice and K. Ueda. Gutzwiller method for heavy electrons. *Phys. Rev. B*, 34(9):6420–6427, 1986.

[12] B. H. Brandow. Variational theory of valence fluctuations: Ground states and quasiparticle excitations of the Anderson lattice model. *Phys. Rev. B*, 33(1):215–238, 1986.

[13] P. Fazekas and B. H.Brandow. Application of the Gutzwiller method to the periodic Anderson model. *Phys. Scr.*, 36(5):809–819, 1987.

[14] P. Fazekas and E. Müller-Hartmann. Magnetic and non-magnetic ground states of the Kondo lattice. *Z. Phys. B*, 85:285, 1991.

[15] S E Barnes. New method for the Anderson model. *J. of Phys. F: Met. Phys.*, 6(7):1375, 1976.

[16] S E Barnes. New method for the Anderson model. ii. The $U = 0$ limit. *J. of Phys. F: Met. Phys.*, 7(12):2637, 1977.

[17] Piers Coleman. $1n$ expansion for the Kondo lattice. *Phys. Rev. B*, 28(9):5255–5262, 1983.

[18] Read N. and Newns D. M. On the solution of the Coqblin-Schreiffer Hamiltonian by the large-N expansion technique. *J. Phys. C: Solid State Phys.*, 16(17):3273, 1983.

[19] Gabriel Kotliar and Andrei E. Ruckenstein. New Functional Integral Approach to Strongly Correlated Fermi Systems: The Gutzwiller Approximation as a Saddle Point. *Phys. Rev. Lett.*, 57(11):1362–1365, 1986.

[20] N Read. Role of infrared divergences in the $1/N$ expansion of the $U = \infty$ Anderson model. *J. Phys. C: Solid State Phys.*, 18(13):2651, 1985.

[21] R. Raimondi and C. Castellani. Lower and upper Hubbard bands: A slave-boson treatment. *Phys. Rev. B*, 48(15):11453–11456, 1993.

[22] R. Raimondi. Optical conductivity in the Mott-Hubbard insulator V_2O_3. *Phys. Rev. B*, 51(15):10154–10156, 1995.

[23] Masao Ogata and Hidetoshi Fukuyama. The $t - J$ model for the oxide high-T_c superconductors. *Rep. Prog. in Phys.*, 71(3):036501, 2008.

[24] B. Edegger, V. N. Muthukumar, and C. Gros. Gutzwiller RVB theory of high-temperature superconductivity: Results from renormalized mean-field theory and variational Monte Carlo calculations. *Adv. Phys.*, 56:927, 2007.

[25] X. G. Wen. Mean-field theory of spin-liquid states with finite energy gap and topological orders. *Phys. Rev. B*, 44(6):2664–2672, 1991.

[26] P. W. Anderson. The resonating valence bond state in La_2CuO_4 and superconductivity. *Science*, 235:1196, 1987.

[27] P. W. Anderson, G. Baskaran, Z. Zou, and T. Hsu. Resonating valence-bond theory of phase transitions and superconductivity in La_2CuO_4-based compounds. *Phys. Rev. Lett.*, 58(26):2790–2793, 1987.

[28] Z. Zou and P. W. Anderson. Neutral fermion, charge-e boson excitations in the resonating-valence-bond state and superconductivity in La_2CuO_4-based compounds. *Phys. Rev. B*, 37(1):627–630, 1988.

[29] Sandro Sorella. Wave function optimization in the variational Monte Carlo method. *Phys. Rev. B*, 71(24):241103, 2005.

[30] S. Sorella, G. B. Martins, F. Becca, C. Gazza, L. Capriotti, A. Parola, and E. Dagotto. Superconductivity in the Two-Dimensional $t-J$ Model. *Phys. Rev. Lett.*, 88(11):117002, 2002.

[31] Manuela Capello, Federico Becca, Michele Fabrizio, Sandro Sorella, and Erio Tosatti. Variational Description of Mott Insulators. *Phys. Rev. Lett.*, 94(2):026406, 2005.

[32] Arun Paramekanti, Mohit Randeria, and Nandini Trivedi. High- Tc superconductors: A variational theory of the superconducting state. *Phys. Rev. B*, 70(5):054504, 2004.

[33] P. W. Anderson, P. A. Lee, M. Randeria, T. M. Rice, N. Trivedi, and F. C. Zhang. The Physics Behind High-Temperature Superconducting Cuprates: The "Plain Vanilla" Version of RVB. *J. Phys.: Condens. Matter*, 16:R755, 2004.

[34] J. Bünemann, W. Weber, and F. Gebhard. Multiband gutzwiller wave functions for general on-site interactions. *Phys. Rev. B*, 57(12):6896–6916, 1998.

[35] Michele Fabrizio. Gutzwiller description of non-magnetic Mott insulators: Dimer lattice model. *Phys. Rev. B*, 76(16):165110, 2007.

[36] Frank Lechermann, Antoine Georges, Gabriel Kotliar, and Olivier Parcollet. Rotationally invariant slave-boson formalism and momentum dependence of the quasiparticle weight. *Phys. Rev. B*, 76(15):155102, 2007.

[37] Walter Metzner and Dieter Vollhardt. Ground-state properties of correlated fermions: Exact analytic results for the Gutzwiller wave function. *Phys. Rev. Lett.*, 59(1):121–124, 1987.

[38] Walter Metzner and Dieter Vollhardt. Analytic calculation of ground-state properties of correlated fermions with the Gutzwiller wave function. *Phys. Rev. B*, 37(13):7382–7399, 1988.

[39] E. Müller-Hartmann. The Hubbard model at high dimensions: some exact results and weak coupling theory. *Z. Phys. B: Condens. Matter*, 76:211, 1989.

[40] Jörg Bünemann, Florian Gebhard, and Rüdiger Thul. Landau-Gutzwiller quasiparticles. *Phys. Rev. B*, 67(7):075103, 2003.

[41] Dieter Vollhardt. Normal He_3: an almost localized Fermi liquid. *Rev. Mod. Phys.*, 56(1):99, 1984.

[42] XiaoYu Deng, Lei Wang, Xi Dai, and Zhong Fang. Local density approximation combined with Gutzwiller method for correlated electron systems: Formalism and applications. *Phys. Rev. B*, 79(7):075114, 2009.

[43] Alexander Cyril Hewson. *The Kondo Problem to Heavy Fermions*. Cambridge University Press, 1997.

[44] P. Nozières. Impuretés magnétiques et effet Kondo. *Ann. Phys. Fr.*, 10:19–35, 1985.

[45] J. M. Luttinger. Fermi Surface and Some Simple Equilibrium Properties of a System of Interacting Fermions. *Phys. Rev.*, 119(4):1153–1163, 1960.

[46] H. Aoki, S. Uji, A. K. Albessard, and Y. Ōnuki. Transition of f electron nature from itinerant to localized: Metamagnetic transition in $CeRu_2Si_2$ studied via the de Haas˘van Alphen effect. *Phys. Rev. Lett.*, 71(13):2110–2113, 1993.

[47] S. Paschen, T. Lühmann, S. Wirth, P. Gegenwart, O. Trovarelli, C. Geibel, F. Steglich, P. Coleman, and Q. Si. Hall-effect evolution across a heavy-fermion quantum critical point. *Nature*, 432:881, 2004.

[48] S. L. Bud'ko, V. Zapf, E. Morosan, and P. C. Canfield. Field-dependent Hall effect in single-crystal heavy-fermion YbAgGe below $1K$. *Phys. Rev. B*, 72(17):172413, 2005.

[49] H. Shishido, R. Settai, H. Harima, and Y. Ōnuki. A Drastic Change of the Fermi Surface at a Critical Pressure in $CeRhIn_5$: dHvA Study under Pressure. *J. Phys. Soc. Jpn.*, 74:1103, 2005.

[50] R. Daou, C. Bergemann, and S. R. Julian. Continuous Evolution of the Fermi Surface of $CeRu_2Si_2$ across the Metamagnetic Transition. *Phys. Rev. Lett.*, 96(2):026401, 2006.

[51] Hilbert v. Lohneysen, Achim Rosch, Matthias Vojta, and Peter Wolfle. Fermi-liquid instabilities at magnetic quantum phase transitions. *Rev. Mod. Phys.*, 79(3):1015, 2007.

[52] J. W. Allen and Richard M. Martin. Kondo Volume Collapse and the $\gamma \rightarrow \alpha$ Transition in Cerium. *Phys. Rev. Lett.*, 49(15):1106–1110, 1982.

[53] M. Lavagna, C. Lacroix, and M. Cyrot. Volume collapse in the Kondo lattice. *Phys. Lett. A*, 90:210, 1982.

[54] A.J. Millis. Effect of a nonzero temperature on quantum critical points in itinerant fermion systems. *Phys. Rev. B*, 48:7183, 1993.

[55] B. Johansson. Alpha-gamma transition in cerium is a Mott transition. *Phil. Mag.*, 30:469, 1974.

[56] P. Coleman, C. Pepin, Q. Si, and R. Ramazashvili. How do Fermi liquids get heavy and die? *J. Phys.: Condens. Matter*, 13:R723, 2001.

[57] Qimiao Si. Quantum Critical Metals: Beyond the Order Parameter Fluctuations. *Adv. Sol. State Phys.*, 44:253, 2004.

[58] C. Pepin. Kondo Breakdown as a Selective Mott Transition in the Anderson Lattice. *Phys. Rev. Lett.*, 98(20):206401, 2007.

[59] C. Pepin. Selective Mott transition and heavy fermions. *Phys. Rev. B*, 77(24):245129, 2008.

[60] Swee K. Goh, Johnpierre Paglione, Mike Sutherland, E. C. T. O'Farrell, C. Bergemann, T. A. Sayles, and M. B. Maple. Fermi-Surface Reconstruction in $CeRh_{1-x}Co_xIn_5$. *Phys. Rev. Lett.*, 101(5):056402, 2008.

[61] S. Friedemann, T. Westerkamp, M. Brando, N. Oeschler, S. Wirth, P. Gegenwart, C. Krellner, C. Geibel, and F. Steglich. Detaching the antiferromagnetic quantum critical point from the Fermi-surface reconstruction in $YbRh_2Si_2$. *Nat. Phys.*, 5:465, 2009.

[62] J. Flouquet, P. Haen, S. Raymond, D. Aoki, and G. Knebel. Itinerant metamagnetism of $CeRu_2Si_2$: bringing out the dead. Comparison with the new $Sr_3Ru_2O_7$ case. *Physica B*, 319:251, 2002.

[63] S. Liang, B. Doucot, and P. W. Anderson. Some New Variational Resonating-Valence-Bond-Type Wave Functions for the Spin-1/2 Antiferromagnetic Heisenberg Model on a Square Lattice. *Phys. Rev. Lett.*, 61(3):365–368, 1988.

[64] M. Capone, M. Fabrizio, C. Castellani, and E. Tosatti. Strongly correlated superconductivity and pseudogap phase near a multiband Mott insulator. *Phys. Rev. Lett.*, 93:047001, 2004.

[65] Massimo Capone, Michele Fabrizio, Claudio Castellani, and Erio Tosatti. Colloquium: Modeling the unconventional superconducting properties of expanded A_3C_{60} fullerides. *Rev. of Mod. Phys.*, 81(2):943, 2009.

[66] D. Goldhaber-Gordon, H. Shtrikman, D Mahalu, D. Abusch-Magder, U. Meirav, and M. A. Kastner. Kondo effect in a single-electron transistor. *Nature*, 391:156, 1998.

[67] Selman Hershfield. Reformulation of steady state nonequilibrium quantum statistical mechanics. *Phys. Rev. Lett.*, 70(14):2134–2137, 1993.

[68] P. Nozières. Fermi-liquid description of Kondo problem at low temperatures. *J. Low Temp. Phys.*, 17, 1974.

[69] Claudio Attaccalite and Michele Fabrizio. Properties of Gutzwiller wave functions for multiband models. *Phys. Rev. B*, 68(15):155117, 2003.

[70] Gabriel Kotliar and Andrei E. Ruckenstein. New Functional Integral Approach to Strongly Correlated Fermi Systems: The Gutzwiller Approximation as a Saddle Point. *Phys. Rev. Lett.*, 57(11):1362–1365, 1986.

[71] Nicola Lanatà, Paolo Barone, and Michele Fabrizio. Fermi-surface evolution across the magnetic phase transition in the Kondo lattice model. *Phys. Rev. B*, 78(15):155127, 2008.

[72] S. Doniach. Kondo lattice and weak antiferromagnetism. *Physica B*, 91:231, 1977.

[73] Lorenzo De Leo, Marcello Civelli, and Gabriel Kotliar. Cellular dynamical mean-field theory of the periodic Anderson model. *Phys. Rev. B*, 77:075107, 2008.

[74] Lorenzo De Leo, Marcello Civelli, and Gabriel Kotliar. $T = 0$ Heavy-Fermion Quantum Critical Point as an Orbital-Selective Mott Transition. *Phys. Rev. Lett.*, 101(25):256404, 2008.

[75] Michel Ferrero, Federico Becca, Michele Fabrizio, and Massimo Capone. Dynamical behavior across the Mott transition of two bands with different bandwidths. *Phys. Rev. B*, 72(20):205126, 2005.

[76] L. de' Medici, A. Georges, and S. Biermann. Orbital-selective Mott transition in multiband systems: Slave-spin representation and dynamical mean-field theory. *Phys. Rev. B*, 72(20):205124, 2005.

[77] Hiroshi Watanabe and Masao Ogata. Fermi-Surface Reconstruction without Breakdown of Kondo Screening at the Quantum Critical Point. *Phys. Rev. Lett.*, 99(13):136401, 2007.

[78] Hiroshi Watanabe and Masao Ogata. Fermi-Surface Reconstruction in the Periodic AndersonModel. *Phys. Soc.Jpn.*, 78(2):024715, 2009.

[79] C. M. Varma, W. Weber, and L. J. Randall. Hybridization in correlated bands studied with the Gutzwiller method: Application to fluctuating valence and heavy fermions. *Phys. Rev. B*, 33(2):1015–1019, 1986.

[80] Vladimir Z. Vulović and Elihu Abrahams. Gutzwiller approach to the Anderson lattice model with no orbital degeneracy. *Phys. Rev. B*, 36(5):2614–2625, 1987.

[81] J. Bünemann, F. Gebhard, T. Ohm, S. Weiser, and W. Weber. Gutzwiller-correlated wave functions: application to ferromagnetic nickel. In A.V. Narlikar, editor, *Frontiers in Magnetic Materials*, pages 117–151. Springer, Berlin, 2005.

[82] In a square lattice with nearest neighbor hopping t, half the bandwidth $D = 4t$, so the values of J/D in Fig. 3.1 must be multiplied by 4 to be compared with the values of J/t in Fig. 2 of Ref. [77].

[83] S. Biermann, L. de' Medici, and A. Georges. Non-Fermi-Liquid Behavior and Double-Exchange Physics in Orbital-Selective Mott Systems. *Phys. Rev. Lett.*, 95(20):206401, 2005.

[84] G. Baskaran, Z. Zou, and P. W. Anderson. The resonating valence bond state and high-tc superconductivity – a mean field theory. *Sol.State Comm.*, 63, 1987.

[85] Y. Suzumura, Y. Hasegawa, and H. Fukuyama. Mean field theory of rvb and superconductivity. *J. Phys. Soc. Jpn.*, 57:2768, 1988.

[86] A. I. Lichtenstein and M. I. Katsnelson. Antiferromagnetism and d-wave superconductivity in cuprates: A cluster dynamical mean-field theory. *Phys. Rev. B*, 62(14):R9283–R9286, Oct 2000.

[87] Dmitri A. Ivanov and Patrick A. Lee. Staggered-flux normal state in the weakly doped t-j model. *Phys. Rev. B*, 68(13):132501, Oct 2003.

[88] Patrick A. Lee, Naoto Nagaosa, and Xiao-Gang Wen. Doping a mott insulator: Physics of high-temperature superconductivity. *Rev. Mod. Phys.*, 78(1):17, 2006. and references therein.

[89] T. A. Maier, M. Jarrell, T. C. Schulthess, P. R. C. Kent, and J. B. White. Systematic study of d-wave superconductivity in the 2d repulsive hubbard model. *Physical Review Letters*, 95(23):237001, 2005.

[90] M. Capone and G. Kotliar. Competition between d-wave superconductivity and antiferromagnetism in the 2d hubbard model. *Physical Review B*, 74:054513.

[91] M. Fabrizio. Role of transverse hopping in a two-coupled-chains model. *Phys. Rev. B*, 48(21):15838–15860, 1993.

[92] Germán Sierra, Miguel Angel Martín-Delgado, Jorge Dukelsky, Steven R. White, and D. J. Scalapino. Dimer-hole-RVB state of the two-leg $t - J$ ladder: A recurrent variational ansatz. *Phys. Rev. B*, 57(18):11666–11673, 1998.

[93] Michele Fabrizio. Superconductivity from doping a spin-liquid insulator: A simple one-dimensional example. *Phys. Rev. B*, 54(14):10054–10060, 1996.

[94] Masatomo Uehara, Takashi Nagata, Jun Akimitsu, Hiroki Takahashi, Nobuo Môri, and Kyoichi Kinoshita. Superconductivity in the ladder material $sr_{0.4}ca_{13.6}cu_{24}o_{41.84}$. *Journal of the Physical Society of Japan*, 65(9):2764–2767, 1996.

[95] M. Matsukawa, Yuh Yamada, M. Chiba, H. Ogasawara, T. Shibata, A. Matsushita, and Y. Takano. Superconductivity in pr2ba4cu7o15 -

[delta] with metallic double chains. *Physica C: Superconductivity*, 411(3-4):101 – 106, 2004.

[96] Kazuhiro Sano and Yoshiaki Ōno. Superconductivity and spin gap in the zigzag-chain t–j model simulating a cuo double chain in $pr_2ba_4cu_7o_{15-\delta}$. *Journal of the Physical Society of Japan*, 76(11):113701, 2007.

[97] M. Capone, M. Fabrizio, C. Castellani, and E. Tosatti. Strongly correlated superconductivity. *Science*, 296:2364, 2002.

[98] A. W. Sandvik and D. J. Scalapino. Order-disorder transition in a two-layer quantum antiferromagnet. *Phys. Rev. Lett.*, 72(17):2777–2780, 1994.

[99] Ling Wang, K. S. D. Beach, and Anders W. Sandvik. High-precision finite-size scaling analysis of the quantum-critical point of $S = 1/2$ Heisenberg antiferromagnetic bilayers. *Phys. Rev. B*, 73(1):014431, 2006.

[100] Richard T. Scalettar, Joel W. Cannon, Douglas J. Scalapino, and Robert L. Sugar. Magnetic and pairing correlations in coupled hubbard planes. *Phys. Rev. B*, 50(18):13419–13427, Nov 1994.

[101] K. Bouadim, G. G. Batrouni, F. Hébert, and R. T. Scalettar. Magnetic and transport properties of a coupled hubbard bilayer with electron and hole doping. *Physical Review B (Condensed Matter and Materials Physics)*, 77(14):144527, 2008.

[102] S. S. Kancharla and S. Okamoto. Band insulator to Mott insulator transition in a bilayer Hubbard model, 2007.

[103] Nejat Bulut, Douglas J. Scalapino, and Richard T. Scalettar. Nodeless d-wave pairing in a two-layer hubbard model. *Phys. Rev. B*, 45(10):5577–5584, Mar 1992.

[104] Raimundo R. dos Santos. Magnetism and pairing in hubbard bilayers. *Phys. Rev. B*, 51(21):15540–15546, Jun 1995.

[105] Andreas Fuhrmann, David Heilmann, and Hartmut Monien. From Mott Insulator to Band Insulator: A DMFT Study. *Phys. Rev. B*, 73:245118, 2006.

[106] Manuela Capello, Federico Becca, Michele Fabrizio, Sandro Sorella, and Erio Tosatti. Variational Description of Mott Insulators. *Phys. Rev. Lett.*, 94(2):026406, 2005.

[107] Leon Balents and Matthew P. A. Fisher. Weak-coupling phase diagram of the two-chain hubbard model. *Phys. Rev. B*, 53(18):12133–12141, May 1996.

[108] H. J. Schulz. Metal-insulator transition in the two-chain model of correlated fermions. *Phys. Rev. B*, 59(4):R2471–R2473, Jan 1999.

[109] A. Smogunov, Andrea Dal Corso, A. Delin, R. Weht, and E. Tosatti. Colossal magnetic anisotropy of monatomic free and deposited platinum nanowires. *Nature*, 3:22, 2008.

[110] A. Smogunov, A. Dal Corso, and E. Tosatti. Ballistic conductance and magnetism in short tip suspended Ni nanowires. *Phys. Rev. B*, 73(7):075418, 2006.

[111] Alexander Smogunov, Andrea Dal Corso, and Erio Tosatti. Magnetic phenomena, spin-orbit effects, and Landauer conductance in Pt nanowire contacts: Density-functional theory calculations. *Phys. Rev. B*, 78(1):014423, 2008.

[112] Kenneth G. Wilson. *Rev. Mod. Phys.*, 47:773, 1975.

[113] Ralf Bulla, Theo A. Costi, and Thomas Pruschke. Numerical renormalization group method for quantum impurity systems. *Rev. of Mod. Phys.*, 80(2):395, 2008.

[114] Herbert Schoeller and Jürgen König. Real-Time Renormalization Group and Charge Fluctuations in Quantum Dots. *Phys. Rev. Lett.*, 84(16):3686–3689, 2000.

[115] D. Jacob, K. Haule, and G. Kotliar. Kondo Effect and Conductance of Nanocontacts with Magnetic Impurities. *Phys. Rev. Lett.*, 103(1):016803, 2009.

[116] Procolo Lucignano, Riccardo Mazzarello, Alexander Smogunov, Michele Fabrizio, and Erio Tosatti. Kondo conductance in an atomic nanocontact from first principles. *Nat. Mater.*, 8:563, 2009.

[117] Herbert Schoeller and Jürgen König. Real-Time Renormalization Group and Charge Fluctuations in Quantum Dots. *Phys. Rev. Lett.*, 84(16):3686–3689, 2000.

[118] J. E. Han and R. J. Heary. Imaginary-Time Formulation of Steady-State Nonequilibrium: Application to Strongly Correlated Transport. *Phys. Rev. Lett.*, 99(23):236808, 2007.

[119] Lothar Mühlbacher and Eran Rabani. Real-Time Path Integral Approach to Nonequilibrium Many-Body Quantum Systems. *Phys. Rev. Lett.*, 100(17):176403, 2008.

[120] Frithjof B. Anders. Steady-State Currents through Nanodevices: A Scattering-States Numerical Renormalization-Group Approach to Open Quantum Systems. *Phys. Rev. Lett.*, 101(6):066804, 2008.

[121] S. Weiss, J. Eckel, M. Thorwart, and R. Egger. Iterative real-time path integral approach to nonequilibrium quantum transport. *Phys. Rev. B*, 77(19):195316, 2008.

[122] Philipp Werner, Takashi Oka, and Andrew J. Millis. Diagrammatic Monte Carlo simulation of nonequilibrium systems. *Phys. Rev. B*, 79(3):035320, 2009.

[123] Marco Schirò and Michele Fabrizio. Real-time diagrammatic Monte Carlo for nonequilibrium quantum transport. *Phys. Rev. B*, 79(15):153302, 2009.

[124] Jörg Bünemann, Florian Gebhard, and Rüdiger Thul. Landau-Gutzwiller quasiparticles. *Phys. Rev. B*, 67(7):075103, 2003.

[125] B. A. Jones and C. M. Varma. Study of two magnetic impurities in a Fermi gas. *Phys. Rev. Lett.*, 58(9):843–846, 1987.

[126] Ian Affleck, Andreas W. W. Ludwig, and Barbara A. Jones. Conformal-field-theory approach to the two-impurity kondo problem: Comparison with numerical renormalization-group results. *Phys. Rev. B*, 52(13):9528–9546, 1995.

[127] B. A. Jones, B. G. Kotliar, and A. J. Millis. Mean-field analysis of two antiferromagnetically coupled impurities. *Phys. Rev. B*, 39(5):3415–3418, 1989.

[128] Lorenzo De Leo and Michele Fabrizio. Spectral properties of a two-orbital anderson impurity model across a non-fermi-liquid fixed point. *Phys. Rev. B*, 69(24):245114, 2004.

[129] Michel Ferrero, Lorenzo De Leo, Philippe Lecheminant, and Michele Fabrizio. Strong correlations in a nutshell. *J. Phys.: Condens. Matter*, 19(43):433201 (35pp), 2007.